Statistical Modeling of Extreme Rainfall Processes in the Context of Climate Change

By

Min Young Lee

Department of Civil Engineering and Applied Mechanics

McGill University

Montreal, Quebec, Canada

August 2012

A thesis submitted to the Graduate and Postdoctoral Studies Office in partial fulfilments of requirements of the degree of Master of Engineering

Abstract

The occurrence of extreme storms is a critical consideration in the design and management of a large number of water-resource projects. In current engineering practice, the estimation of extreme rainfalls is accomplished based on statistical frequency analysis of maximum precipitation data. The objective of this frequency analysis is hence to estimate the maximum amount of precipitation falling at a given point for a specified duration and return period. Results of precipitation frequency analysis are often summarized by “intensity-duration-frequency” (IDF) relationships for a given site. However, traditional methods in the development of IDF relations have two major limitations. Firstly, these existing methods were not able to account for the extreme rainfall characteristics over different time scales. Secondly, these traditional methods cannot take into account the potential impacts of climate variability and climate change. Therefore, the main objective of the present study is to propose an improved method for extreme rainfall estimation that could overcome these limitations. The proposed method was based on the scale-invariance GEV distribution and the statistical downscaling procedure to construct the IDF relations in the context of climate change. The Non-Central Moment method was used for the estimation of the three parameters of the GEV. Results of a numerical application using Annual Maximum Precipitation (AMP) data from a network of 14 rain-gauge stations in South Korea has indicated the feasibility and accuracy of the suggested method. In particular, the observed AMP series displayed a simple scaling behaviour. In addition, the linkages between global climate variables given by two Global Climate Models (GCMs) (one from Environment Canada and one from the UK Hadley Centre) and the local extreme rainfall characteristics have been successfully established for predicting the resulting changes of the IDF relations under different climate change scenarios A2, A1B, and B2. It was found that the IDF relations for future periods (2020’s, 2050’s, and 2080’s) showed increasing or decreasing trends depending on the GCM used and the climate scenario considered.

Résumé

La fréquence des tempêtes extrêmes est un facteur critique dans la conception et gestion d'un grand nombre de projets de ressources en eau. Dans la pratique courante, l'estimation des pluies extrêmes est réalisée en se basant sur l'analyse de fréquence statistique des données de précipitations maximales. L'objectif de cette analyse de la fréquence est donc d'estimer le montant maximal de précipitations qui tombent à un moment donné pendant une durée déterminée, ainsi que la période de retour. Les résultats de l'analyse de la fréquence des précipitations sont souvent résumés par les relations Intensité-Durée-Fréquence (IDF) pour un site donné. Toutefois, les méthodes traditionnelles dans le développement des relations IDF ont deux limites majeures. Tout d'abord, ces méthodes n'ont pas été en mesure de tenir compte des caratéristiques des précipitations extrêmes sur des différentes échelles de temps. Deuxièmement, ces méthodes traditionnelles ne tiennent pas compte des impacts potentiels de la variabilité climatique et du changement climatique. Par conséquent, l'objectif principal de cette présente étude est de proposer une méthode d'estimation des précipitations extrêmes améliorée qui pourrait surmonter ces limitations. La méthode proposée a été basée sur l'échelle d'invariance de distribution GEV et la procédure de réduction d'échelle statistique pour construire des relations IDF dans le contexte du changement climatique. La méthode des moments non-centraux a été utilisée pour l'estimation des trois paramètres de la GEV. Les résultats obtenus par une application numérique des données de Précipitations Maximales Annuelles (PMA) à partir d'un réseau de 14 stations pluviométriques en Corée de Sud ont démontré la faisabilité et la précision de la méthode proposée. La série de PMA observée a particulièrement affiché une propriété d'échelle simple. En outre, les liens entre les variables climatiques globaux donnés par les deux Modèles Climatiques Globaux (MCGs) (un en provenance d'Environnement Canada et l'autre du Centre Hadley du Royaume-Uni) et les caractéristiques des précipitations locaux extrêmes ont été établis avec succès pour prédire les changements qui résultent des relations IDF selon des différents scénarios climatiques - A2, A1B, et B2. Il a été constaté que des relations IDF pour les périodes futures (les années 2020, 2050, et 2080) ont démontré des tendances qui augmentent ou diminuent dépendemment des MCG utilisés et du scénario climatique à l'étude.

Acknowledgements

I would like to earnestly and deeply present my appreciation to my supervisor Prof. Van-Thanh-Van Nguyen for his guidance of my research work and for his encouragement and complete trust in my ability.

I also wish to enthusiastically thank to my senior Myeong-Ho Yeo who has been always ready to provide his help and cheered me up during this study. In addition, I would like to express my sincere thanks to Dr. Tan-Danh Nguyen who has readily assisted me in my study, and wish that he would be fully recovered from his current illness.

To my friends JuEun, Nadia, Ali, and Sania, I truly thank for their support.

Lastly but at most to my family, I present my love for their endless support in various aspects and being always at my side despite a long distance. I also especially acknowledged Paul for his kind support.

Table of Contents

List of Figures

List of Tables

1 Introduction

The frequency of rainfall of various magnitudes is important for a range of hydrological applications. In particular, rainfall frequency analyses have been extensively used for planning and design of engineering works that control storm runoff (e.g., dams, culverts, urban and agriculture drainage systems). This is because, in most cases, good quality flow data which has adequate length for reliable estimation of floods are generally limited or unavailable at the location of interest, while extensive precipitation records are often available. At a site where annual maximum precipitation (AMP) data series are available, frequency analysis is applied to estimate the amount of precipitation falling at a given point (or over a given area) for a specified duration and return period. Results of this analysis are often summarized by "intensity-duration-frequency" (IDF) relationships for a given site, or are usually presented in the form of a "precipitation frequency atlas", which provides rainfall accumulation depths for various durations and return periods over the region of interest. For instance, estimates of rainfall frequencies for various durations and return periods are available for Canada in the Handbook on the Principles of Hydrology (Gray, 1973).

1.1 Statement of Problems

Traditionally, to build IDF curves, a selected probability distribution is independently fitted to observed values of AMPs for various durations. This traditional IDF derivation method, however, has some limitations. Firstly, the traditional method does not take into consideration characteristics of precipitation over different time scales (time scaling problem). For instance, if the distribution is fitted to AMP data of 10-minute duration, then the results are accurate only for the 10-minute rainfall duration. Hence, the fitted model is accurate only for the specific time scale considered and cannot describe the statistical properties of the extreme rainfall processes at other time scales (Nguyen, 2004). Secondly, the traditional method uses data available at a given local site only without considering the spatial rainfall variability in the study region (spatial scaling problem). Finally, the traditional method is unable to account for the possible impacts of climate change in the future.

Recently, climate change has been recognized as having a profound impact on the hydrologic cycle at different temporal and spatial scales. For instance, some previous studies have indicated an increasing trend of extreme rainfalls in mid-latitude area including South Korea (Choi et al., 2008, 2009; Frich et al. 2002; Kim et al., 2008; Im et al., 2011; Parl et al., 2011; Jung et al., 2011). It is hence necessary to consider this climate variability in the frequency analysis of extreme rainfalls. In addition, General Circulation Models (GCMs) and Regional Climate Models (RCMs) have been recognized to be able to represent reasonably well the main features of the distribution of basic climate parameters at global and regional scales, but outputs from these models are usually at resolutions that are too coarse for many impact studies. Hence, statistical downscaling methods have been used for describing the linkage between the large-scale climate variables given by GCMs or RCMs to the observed extreme rainfall characteristics at a local site (Nguyen et al., 2006).

In summary, many previous studies have found an increase in extreme rainfall patterns in South Korea for the present time as well as for future periods (Kim et al., 2008; Kwon et al., 2009; Na, 2010). Having high population density in most urban areas in South Korea, it is necessary to develop appropriate measures to properly cope with the possible severe impacts of flooding caused by this change in extreme rainfall patterns. It is hence expected that the results of the present study will provide essential information for improving our design, planning, and management of the urban drainage systems in order to minimize the potential impacts of climate change on flooding in urban areas in South Korea.

1.2 Objectives

In view of the above-mentioned issues, the overall objective of the present study is focused on the development of an improved method for extreme rainfall frequency analysis in the context of climate variability and climate change. The feasibility of the proposed method will be assessed using extreme rainfall data available from a network of 14 raingage stations in South Korea. More specifically, this study aims at the following particular objectives:

(i) To propose a suitable method for selecting the best statistical distribution for Korean extreme rainfall data;

(ii) To propose a reliable estimation method for estimating the parameters of the selected distribution model;

(iii) To examine the scaling property of the Korean extreme rainfall processes;

(iv) To construct reliable IDF relations for South Korea for the current climate; and

(v) To develop IDF relations for South Korea for future periods in consideration of different climate change scenarios.

The current thesis is organized into five chapters. Chapter 2 presents a critical review of previous works related to the frequency analyses of extreme rainfalls in consideration of climate change. Chapter 3 presents a description of the study data and outlines the methods used in the statistical data analysis and the at-site frequency analysis of extreme rainfalls. Chapter 4 is dealing with the derivation of the IDF relations for future periods under some climate change scenarios. Finally, Chapter 5 states the major conclusions and provides some recommendations for future research.

2 Literature Review

2.1 At-Site Frequency Analysis of Extreme Rainfalls

As mentioned previously, the objective of frequency analysis of hydrologic data is to relate the magnitude of extreme events to their frequency of occurrence through the use of probability distributions (Chow et al. 1988). In particular, for extreme rainfalls, the frequency analysis is to provide an estimation of the maximum amount of precipitation falling at a given point (or over a given area) for a specified duration and return period. This analysis consists of three steps: (*i*), obtaining and screening the observed extreme rainfall data; (*ii*), selecting a representative probability distribution and estimating its parameters; (*iii*), evaluating the adequacy of the selected distribution. For the first step, two types of extreme rainfall data exist: Annual Maximum Series (AMS) and Partial Duration Series (PDS). The AMS contains the maximum rainfall amount in each complete year of record, while the PDS is a series of data selected as being above a given threshold. Arguments in favour of both types have been given in several studies, but the difference between using AMS and PDS was found to be important only for short return periods (2 to 5 years) and insignificant for long return periods (10 years or longer) (Chow 1964; Stedinger et al. 1993). Due to its simpler structure, the AMS-based method is more popular in practice.

Once the selection of the observed annual extreme rainfall series is completed, an assessment is performed to detect outliers and trends in the screening data as well as to figure out the basic statistical characteristics. Outliers which deviate markedly from other members (Grubbs 1969) may cause the distribution shape changed, hence a choice to keep the outliers for analysis is crucial. If the outliers are caused from any source of errors, they are better to be removed; otherwise they are worth to keep. For a trend analysis, various techniques can be performed to detect non-stationarity (Hirsch et al. 1993). For instance, extreme rainfall quantiles calculated for two different time periods can be compared (Gerold and Watkins Jr. 2005), and Mann-Kendal trend test is also commonly used.

The next step is the selection of a representative probability distribution. Table

2.1 shows candidate distributions generally used for frequency analyses of extreme rainfalls. Extreme Value Type Ⅰ distribution (EV1), also known as Gumbel distribution, has been broadly used for the extreme rainfall frequency analysis (Pilon et al. 1991). However, it has recently been found that EV1 theoretically and practically underestimates extreme rainfall amounts (Koutsoyiannis and Demetris 2004), particularly those at the tail of the distribution which are important in the extreme value analysis. The Generalized Extreme-Values (GEV) distribution which is inherently designed for the tail area is preferred. GEV distribution is said to be flexible because it is a generalized form of three extreme distributions: Gumbel, Weibull, and Frecher. Therefore, it generates less biased quantile estimates. Several studies have applied the GEV distribution for their frequency analysis (Fowler and Kilsby 2003; Lee and Maeng 2003; Nadarajah and Choi 2007; Nguyen 2004; Nguyen et al. 2002). Besides GEV, there are other candidate distributions, such as generalized Pareto (GPA), generalized logistic (GLO), lognormal (LN3), and Pearson type Ⅲ (PE3). The following table presents the cumulative distribution functions and the parameters of the EV1 and GEV distributions.

Table 2.1 Cumulative distribution functions (CDFs) used for frequency analyses and their parameters

Name	Cumulative Distribution Function	Parameters
EV1	$F(x) = \exp\left[-\exp\left(-\frac{x-\mu}{\sigma}\right)\right]$	μ: location σ: scale
GEV	$F(x) = \exp\left[-\exp\left\{\xi^{-1}\log\left[1-\xi\left(\frac{x-\mu}{\sigma}\right)\right]\right\}\right]$	μ: location σ: scale ξ: shape
GPA	$F(x) = 1-\exp\left\{\xi^{-1}\log\left[1-\xi\left(\frac{x-\mu}{\sigma}\right)\right]\right\}$	μ: location σ: scale ξ: shape
GLO	$F(x) = \frac{1}{1+\exp\left\{\xi^{-1}\log\left[1-\xi\left(\frac{x-\mu}{\sigma}\right)\right]\right\}}$	μ: location σ: scale ξ: shape
LN3[1]	$F(x) = \Phi\left\{\xi^{-1}\log\left[1-\xi\left(\frac{x-\mu}{\sigma}\right)\right]\right\}$	μ: location σ: scale ξ: shape
PE3[2]	$F(x) = G\left[\frac{4}{\gamma^2}, \frac{x-\left(\mu-\frac{2\sigma}{\gamma}\right)}{\frac{1}{2}\sigma\lvert\gamma\rvert}\right]/\Gamma\left(\frac{4}{\gamma^2}\right)$	μ: location σ: scale γ: shape

[1] $\Phi(.)$ is the cumulative distribution function of the standard Normal distribution.

[2] $G(\alpha, x) = \int_0^x t^{\alpha-1}e^{-t}dt$ is the incomplete gamma function, and $\Gamma(.)$ is the gamma function.

There is no single distribution that perfectly represents a data series, and therefore many tests are used to evaluate and select the best distribution. Goodness-of-fit test is the one that checks how well a selected distribution fits to the observed data. Generally, both graphical and numerical methods are used in the test. As an example of a graphical method, the probability plot illustrates how well the calculated distribution fits to the observed quantiles. The quantiles are plotted against probability, which is calculated using a plotting position formula, of which there are many kinds (e.g., Blom's for normal distribution, Gringorten's for extreme type Ⅰ distribution). Among them the Cunnane formulae is commonly used since it does not assume any distribution on data set (Cunnane 1978). For numerical methods, Chi-square test, Kolmogorov-Simirnov (K-S) test, and other tests based on L-moment statistics can be used (Hosking 1996). Besides these tests, evaluation criteria such as root mean square error (RMSE) and relative root mean square error (RRMSE) are also commonly used. In addition to numerical and graphical methods of goodness-of-fit test, characteristics of the distribution such as its number of parameters, its statistical properties, and the choice of descriptive or predictive ability should be considered (Nguyen and Nguyen 2003). Considering these three factors, GEV distribution is adequate for the frequency analysis of AMS of precipitation. About the number of distribution parameters, Wilks (1993) found that a three-parameter distribution could provide sufficient flexibility to represent extreme hydrological data.

Regarding the methods for parameter estimation, L-moment methods, maximum likelihood estimation (MLE), and non-central moment (NCM) method are currently popular. The L-moments are the combinations of order statistics, and the L-moments method is more robust than the conventional moment method in dealing with outliers in data. Also, even with a small number of samples, the L-moments method makes it possible for robust estimation. MLE method begins with building a likelihood function and then finds parameters that maximize the function, in other words, the probability. However, the MLE method suffers from the limitation that optimal solutions of the maximization problem might not be found for all distributions. When L-moments method and the MLE method were compared by Hosking (Hosking et al. 1985), the L-moments method showed better estimation results than the MLE method. Finally, the NCM method gives a formula relating NCM and GEV distribution parameters. Given the first three

NCMs, the three GEV distribution parameters are derived. The NCM method has advantages such as tractable calculation and easy interpretation. Also, the NCM method has the great advantage in applying scale-invariant properties in NCM to solve temporal scaling problems (Nguyen 2004). Therefore, the NCM method is useful for the station where rainfall data of short durations are missing.

Once a proper distribution and a parameter estimation method have been obtained, the annual maximum precipitation (AMP) quantiles for different probabilities (or return periods) can be calculated, and these quantiles can be used for the building of the intensity-duration-frequency (IDF) curves as described in the following section.

2.2 Intensity-Duration-Frequency (IDF) Relations

IDF relations provide information about how often an intensive precipitation for a given duration occurs. Therefore, they are very important for the planning, design, and management of various water resource systems. Rainfall intensities associated with different return periods, denoted by *i*, are plotted against the duration, *d*, and this relationship is plotted for every computed return period, *T*. The following figure shows an example of IDF relations.

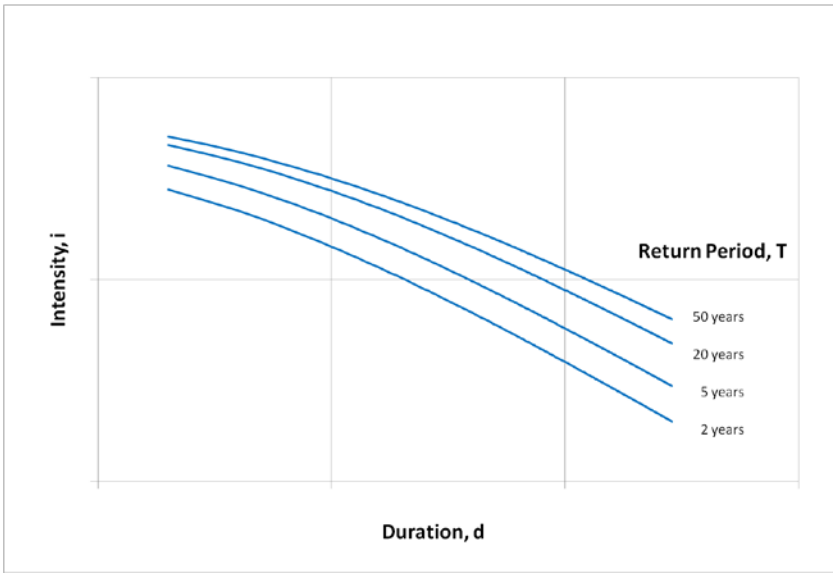

Figure 2.1 An example of IDF relations

Basically, there are two approaches to constructing IDF curves. For the first one, the IDF curves are directly estimated from the observed annual maximum data. After the annual maximum series (AMS) is sorted in descending order, a rank is assigned to its ordered values, and then the exceedance probability of each value is computed by appropriate plotting position formulae. The exceedance probability is the chance at which the rainfall amount over the corresponding data occurs. The inverse of the exceedance probability is the return period. Therefore, each value of the AMS has a specified return period. This computation is applied to AMS for all durations. The unit of AMS, which is for amount, is transformed to one for intensity. Intensities associated with specified return periods are plotted against duration to build IDF curves. This approach generates non-smooth curves, and the maximum return period is limited by the length of the observed AMS data (Langousis and Veneziano 2007)

The second approach, which is widely used in practice, is to use a parametric model for intensity (i), which can be written as $f(i) = g(T)h(d)$ (Koutsoyiannis et al. 1998). The model depends on return period (T) under the function of $g(T)$ which relies on the fact that extreme rainfall follows the extreme type distribution; on duration (d) by a function $h(d)$ which is based on the shape of IDF curves, traditionally fitted by several empirical equations. Parameters of the equations are calculated using the least-square method, and the selection of the best equation from many is done based on RMSE criteria. This approach suffers from certain weaknesses. For example, the dependence of i on T needs empirical validation, because there is no true distribution that describes perfectly the extreme data (Langousis and Veneziano 2007); and the dependence of i on d is not based on theory. Moreover, this approach requires a large number of parameter estimations and long-observed precipitation data. Actually, stations having a long period of observed data are rare, but when the scaling property is examined, valid IDF curves can be constructed even from a short length of observed data.

2.3 Scaling Property in Rainfall Process

Scale-invariant property which is used in physics has recently been applied in hydrology. It was applied first in 1990 by Gupta and Waymire to a spatial rainfall study

and by Rosso and Burlando to depth-duration-frequency (DDF) curves. After that, the scaling concept has been widely used in extreme rainfall studies such as storm hyetographs (Koutsoyiannis and Foufoula-Georgiou 1993), design storms (De Michele et al. 2001), regional estimation (Yu et al. 2004), and IDF curves (Bendjoudi et al. 1997; Nguyen et al. 1998).

Scaling concept has its root in multi-fractal theory. The theory which is originated from the study of turbulence has been progressively employed in rainfall modeling for decades. This is because of its ability to achieve, over a wide range of spatial and/or temporal scales, a strong control on the statistical moments of a given distribution of rainfall, and simulation of synthetic rainfall series preserving the scaling property observed in real rainfall series (Deidda 2000). The scaling property implies a function of scale ratio to rainfall intensity, and the function is classified as simple scaling or multi-scaling according to the type of the function. The simple scaling is an exponential form of scale ratio, and the multi-scaling is an undefined function that depends only on the scale ratio. Consequently, the scaling concept theoretically relates the change of time scale to the change of corresponding precipitation values.

The scaling property of rainfall process has been widely studied and applied to the derivation of the IDF curves by many researchers (BARA et al. 2009; Bendjoudi et al. 1997; Menabde et al. 1999; Veneziano and Furcolo 2002; Nguyen 2004;). The fact that IDF curves satisfy simple scaling relations whereas temporal rainfall has multi-fractal scale-invariance is theoretically and practically shown in many articles (Daniele Veneziano and Furcolo 2002). In addition, construction of IDF curves using the simple scaling concept could be applied to cases where the observed data of short duration rainfalls are limited. Furthermore, the scaling approach has been used for downscaling of daily rainfalls to sub-daily extreme rainfalls and for developing IDF relations under different climate change scenarios given by Global Circulation Models (GCMs) (Nguyen 2004; Nguyen et al. 2007).

2.4 Statistical Downscaling based on General Circulation Models (GCMs)

GCMs are comprehensive physical/numerical models of the atmosphere and the oceans which are accepted tools for simulating and understanding the behaviour of the climate system (Boer et al. 1992). Since the mid-1970s, GCMs have been used to study the potential impact of the increasing carbon-dioxide (CO_2) concentration on climate (Washington and Meehl 1989). Because the GCMs are numerical models, even little change in CO_2 emission rate, which is an initial condition of the model, leads to significant discrepancies in the climate change results. Hence, Intergovernmental Panel on Climate Change (IPCC) published a Special Report on emission Scenarios (SRES) in which scenarios are grouped into four families (A1, A2, B1, and B2) covering a wide range of demographic, economic, and technological driving forces and the resulting Green House Gas (GHG) emissions (IPCC 2000).

The A1 storyline assumes a world of global population peak in the middle of the century, rapid economic growth, and introduction of efficient technologies. In the storyline, three groups that describe different technological changes exist: fossil intensive (A1FI), non-fossil energy resources (A1T), and a balance across all energy sources (A1B). The A2 storyline describes a very heterogeneous world of high global population but slow economic development and slow technological change. The B2 storyline depicts a world of intermediate population and economic growth. Finally, the B1 storyline portrays a world of a population peak in the middle of the century and a rapid change in economic structures towards service and information economy (IPCC 2007).

As concerns about the impact of climate change on the earth are growing, hydrologists have been focusing on changes in rainfall-runoff and floods caused by climate change. However, there have been no available tools for the study except GCMs. But because GCMs were not primarily designed for climate-change impact studies, their spatial and temporal resolution is too coarse, and methods of downscaling have been a key challenge to hydrologists (Prudhomme et al. 2002).

Generally, GCMs generate variables at a spatial resolution of hundreds of kilometers and a temporal resolution of one day. These are very coarse and are not readily applicable in hydrology. To refine the resolution of the output variables i.e. to reduce the spatial resolution to a few kilometers and the temporal resolution to a few minutes, two

broad approaches have been developed for downscaling: dynamical downscaling (DD) and statistical downscaling (SD). While DD extracts regional scale information from dynamic modeling of regional climate process whose boundary conditions are large scale GCMs outputs, SD generates local scale weather data based on the statistical relationship between observed data and GCMs outputs. Matter of outstanding method has been argued and agreed as depending on areas and weather types, since each method has its own advantages and weaknesses (Conway et al. 1996; Gutowski et al. 2000; Kidson and Thompson 1998; Mearns et al. 1999; Murphy 1999; Pierce et al. 2012; Wilby et al. 2000; Yarnal et al. 2001). However, SD has been widely recognized as more practical over DD, especially in terms of flexible adaptation to specific study purposes and less computational requirements (Nguyen et al. 2006). SD can be classified into three groups: *Transfer Function*, *Weather Typing*, and *Stochastic Weather Generator*. The *Transfer Function* involves defining statistical relationship between large-scale upper air data and local surface climate and to define the relationship, several methods such as *Multiple Linear Regression*, *Principal Component Analysis*, and *Artificial Neural Network* can be applied. The statistical downscaling model (SDSM; Wilby et al. 2002) is a typical *Transfer Function* approach that calculates the relationship by *Multiple Linear Regression* and this has been widely applied (Chen et al. 2012; Khan et al. 2006; Wetterhall et al. 2007). The *Weather Typing* method is composed of identifying weather types and building statistical model between the types and local station data. *Stochastic Weather Generators* such as WGEN (C.W. Richardson and Wright 1981) and LARS-WG (Semenov and E.M. Barrow 1997) are numerical weather models based on the relationship between station-level weather data and area-averaged weather statistics, and recently have been extended for downscaling of GCMs (Semenov et al. 1998).

For temporal downscaling, Nguyen (2000) proposed a new method based on the “scale-invariance” concept that has been popularly practiced for modeling rainfall processes. He examined a function of the order of moments to define a simple scaling and then applied it to daily rainfall data to derive sub-daily rainfall values. This technique has been applied to the construction of IDF curves for observed rainfalls and further to rainfalls simulated by GCMs for future times with consideration of various climate change scenarios.

3 At-Site Frequency Analysis

3.1 Study Site

The Korean Peninsula is located in the northeastern edge of the Asian continent; its geographic range is 33-43°N and 124-131°E. Seventy percent of the land is covered with mountains, and most of them are in the north and east parts of the peninsula, causing a geographic slope from east to west. Climatologically, heavy precipitation mainly occurs from typhoons and the convergence zone of the monsoon front from late June through July and August over Korea. The precipitation in that period accounts for more than 40% of the annual precipitation, and the horizontal distribution of heavy rainfall amounts is roughly similar to that of the total annual precipitation (Lee et al. 1998; Park and Jung 2002).

The data used in this study is sub-daily and daily annual maximum precipitation (AMP) series obtained from the Korea Meteorological Administration (KMA) from a network of fifteen rain-gauge stations (Figure 3.1). Basic analysis was performed using the data from fourteen out of fifteen stations with whole available records (station Ullengdo was removed due to a large number of missing data). The available rainfall records for these stations are at least 30 years up to 1999, since the modern meteorological observation in Korea has been in operation since 1904 and the data is managed by the KMA (Park et al. 2011). To manage the issue of homogeneity, the KMA digitized the database for the entire period by using the same format and temporal resolution of modern observations. And it was stated that one station (Gwangju) out of the fourteen stations was relocated in 1960 (KMA, 1995), hence homogeneity test was performed on the station's data. AMP data is split into two groups; one from 1939 to 1960 (22 years) and the other from 1961 to 1982 (22 years), and then were assessed to check whether the two groups are from a same parental distribution. Mann-Whitney Test (M-W), Wald-Wolfowitz Runs Test (W-W), and Kolmogorov-Smirnov Test (K-S) were executed and results are presented in the following table. All p-values are less than 0.05, which imply that two groups of data can be reported to be extracted from the same distribution. Therefore, whole AMP data from Gwangju station is used in this study.

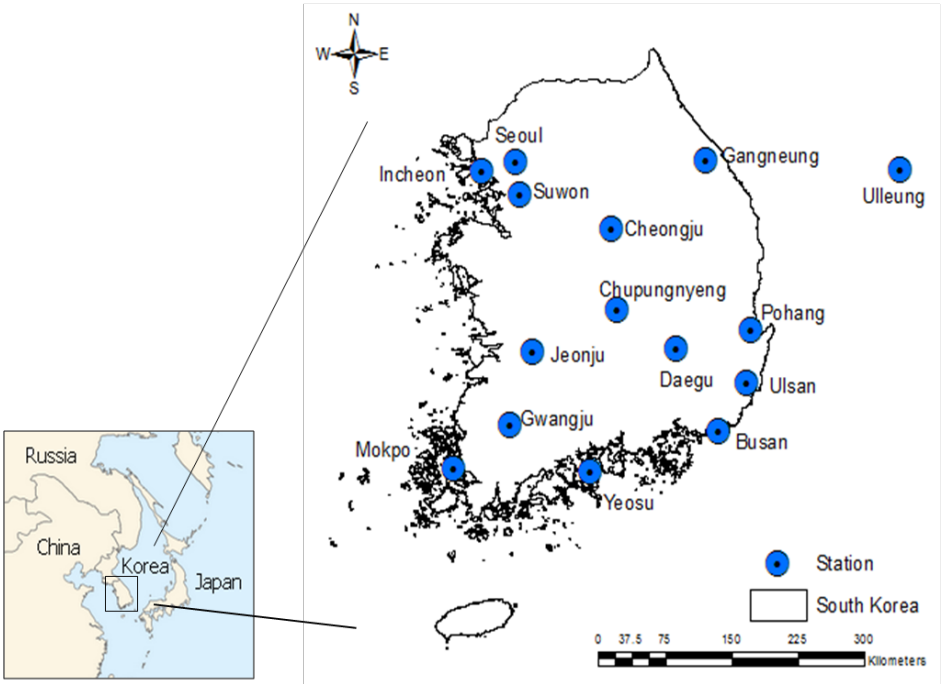

Figure 3.1 Locations of 15 stations where AMP data are obtained.

Table 3.1 Results of three homogeneity tests; Mann-Whitney (M-W), Wald-Wolfowitz Runs (W-W), and Kolmogorov-Smirnov (K-S) Tests on Gwangju station.

Duration	P-values of Homogeneity Test Statistics		
	M-W	W-W	K-S
10 min	0.185	0.500	0.215
20 min	0.108	0.500	0.215
30 min	0.270	0.915	0.860
40 min	0.348	0.439	0.621
50 min	0.453	0.439	0.860
1 hr	0.699	0.953	0.987
1.5 hr	0.673	0.915	0.860
2 hr	0.935	0.976	0.987
3 hr	0.742	0.676	0.987
4 hr	0.760	0.915	0.860
6 hr	0.496	0.857	0.621
9 hr	0.354	0.500	0.621
12 hr	0.392	0.500	0.621
15 hr	0.453	0.500	0.621
18 hr	0.366	0.857	0.387
1 day	0.324	0.953	0.860

3.2 Statistical Analysis of Data

3.2.1 Basic Statistical Data Analysis

By examining the basic descriptive statistics of data, one could identify some basic characteristics of the probability distribution of extreme rainfalls. For instance, Table 3.1 presents these basic descriptive statistics (such as mean, standard deviation, and skewness) of sixteen AMP series for durations from 10 minutes to 1 day (1440 minutes) at Seoul station. It can be observed that the skewness varies with rainfall durations. When an absolute value of skewness, a measure of symmetry, is over 1.00, it indicates highly skewed, while the value between 0.5 and 1 indicates moderately skewed. When the value is under 0.5, the data are considered a approximately symmetric. As shown in Table 3.1, most AMPs have high skewness values, indicating a highly-skewed distribution for extreme rainfalls for most rainfall durations. Similar results for other stations were presented in Appendix A (Table A.1-13).

For purposes of illustration, Figure 3.2 provides a detailed graphical analysis of the highly right-skewed distribution of daily AMPs for Seoul station. The histogram, normal Q-Q plot, and Box plot all indicate a non-symmetric distribution for these data (positive skewness of 1.584). The de-trended normal Q-Q plot also confirmed this right-skewed shape because the difference between the observed and the expected value of a normal distribution did show an upward curved pattern in both sides of the zero horizontal line, especially at the upper end.

Table 3.2 Descriptive statistics for AMP data at Seoul station for 1954-1999.

Duration	Basic Descriptive Statistics					
	Number of Data	Minimum (mm)	Maximum (mm)	Mean (mm)	Std. deviation (mm)	Skewness
10 min	46	7.00	47.20	15.98	7.12	2.08
20 min	46	9.50	60.50	24.02	10.69	1.20
30 min	46	10.40	79.00	31.55	13.94	1.27
40 min	46	10.80	96.00	38.07	17.33	1.36
50 min	46	11.20	108.00	43.63	19.78	1.14
1 hr	46	14.40	116.00	48.52	21.59	0.97
1.5 hr	46	15.50	120.00	60.44	24.40	0.37
2 hr	46	16.60	126.00	69.31	27.20	0.25
3 hr	46	17.20	157.00	82.30	31.93	0.37
4 hr	46	21.90	179.00	90.70	35.54	0.66
6 hr	46	27.90	195.00	105.92	40.79	0.58
9 hr	46	37.90	236.00	121.18	47.32	0.62
12 hr	46	52.20	265.00	130.56	52.85	0.87
15 hr	46	55.10	329.00	141.92	62.73	1.16
18 hr	46	60.80	361.00	148.83	68.49	1.27
1 day	46	62.70	445.00	161.04	79.89	1.58

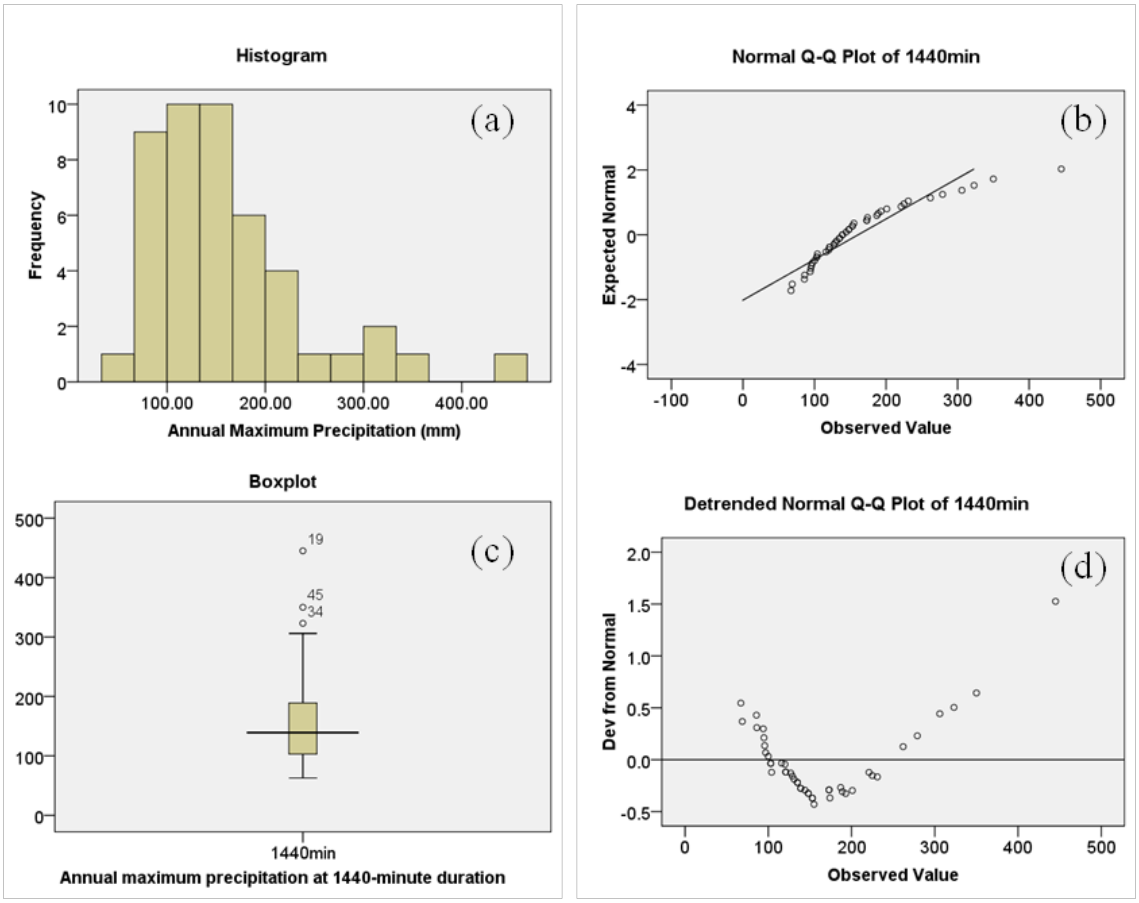

Figure 3.2 Diagnostic plots of daily (1440 minutes) AMP data of Seoul during 1954-1999 period. (a) Histogram, (b) Normal Q-Q plot, (c) Boxplot, and (d) Detrended Normal Q-Q plot clockwise from upper left.

3.2.2 Trends in AMP Data

To assess the trend in the AMP data the popular Mann-Kendall trend test was used. Table 3.2 shows the longest available AMP series without missing data at each station.

Table 3.3 The start year, end year, and data length (in years) of AMP for 14 stations

No.	Station name	Start year	End year	Data length
1	Seoul	1954	1999	46
2	Suwon	1964	1999	36
3	Incheon	1952	1999	48
4	Gangreung	1958	1999	42
6	Daegu	1916	1999	84
7	Busan	1948	1999	52
8	Gwangju	1939	1999	61
9	Jeonju	1970	1999	30
10	Mokpo	1923	1999	77
11	Pohang	1954	1999	46
12	Yeosu	1952	1999	48
13	Chupungryong	1955	1999	45
14	Ulsan	1954	1999	46
15	Cheongju	1967	1999	33

Each station has 16 AMP series of different rainfall durations, and the Mann-Kendall trend test was applied to each of these data series. In general, no significant trend was detected for most stations and for most durations, except for Gangreung (for 10, 20, 30, 40 and 50 minutes), for Daegu (for 15, 18 minutes and 24 hours), and for Gwangju (for 10 minutes) (Table 3.3). For further examination of these trends, parametric regression analysis was performed (Table 3.4). For purposes of illustration, Figure 3.3 shows the significant increasing trends of the AMP series for Gangreung station for 10-, 20-, 30-, and 40-minute durations.

Table 3.4 Results of Mann-Kendal trend test (Z values) for 16 AMP series in 14 Korean stations. Significant values (p-values are less than 0.025) are indicated in bold.

Stations	Duration (minutes)															
	10	20	30	40	50	60	90	120	180	240	360	540	720	900	1080	1440
Seoul	1.01	1.12	0.77	1.11	0.98	0.82	0.73	1.13	1.46	1.44	0.91	1.26	1.14	1.47	1.27	0.69
Suwon	0.00	-0.30	-0.08	0.22	0.00	0.08	0.22	0.30	0.33	0.61	0.49	1.14	1.19	0.98	1.06	1.43
Incheon	0.56	-0.10	-0.30	-0.04	0.38	0.30	0.74	0.54	0.28	0.00	-0.24	-0.33	-0.40	-0.55	-0.12	-0.26
Gangreung	**3.00**	**3.23**	**2.61**	**2.07**	**1.91**	1.56	1.17	1.00	1.01	1.22	1.05	1.26	1.35	0.83	0.73	1.02
Daegu	1.08	0.78	0.44	0.51	0.59	0.63	0.54	0.74	0.92	0.93	0.86	0.79	1.37	**1.83**	**1.85**	**1.78**
Busan	0.92	1.40	1.37	1.07	1.15	1.22	1.04	1.03	1.10	1.23	1.37	1.29	1.28	1.34	1.44	1.49
Gwangju	**-1.69**	-0.53	-0.27	-0.06	0.09	0.43	0.52	0.90	0.10	0.12	0.08	0.53	0.37	0.42	0.68	0.77
Jeonju	0.52	-0.07	-0.37	-0.46	-0.86	-1.07	-0.55	-0.59	-0.79	-0.86	-0.57	-1.09	-0.84	-0.91	-1.02	-0.82
Mokpo	-0.59	-0.88	-0.83	-0.34	-0.33	-0.39	-0.17	-0.82	-1.35	-1.26	-0.78	-0.27	-0.23	-0.22	-0.19	-0.43
Pohang	0.52	0.48	0.49	0.25	0.29	0.16	0.08	0.74	0.66	0.03	0.38	0.84	0.71	0.93	0.43	0.34
Yeosu	0.04	1.42	1.53	0.98	0.75	0.45	0.02	0.33	0.17	0.52	0.37	-0.21	-0.64	-0.77	-1.23	-0.99
Chupung-ryong	-0.53	-0.24	0.18	0.07	0.26	0.50	0.68	0.80	0.56	0.59	0.48	0.19	0.51	0.80	0.76	0.45
Ulsan	0.88	-0.16	-0.45	-0.14	0.09	-0.16	-0.45	-0.71	-0.78	-0.97	-0.79	-0.60	-0.85	-0.62	-0.59	-0.11
Cheongju	1.23	0.25	0.29	0.22	0.03	0.06	-0.46	-0.40	-0.48	-1.46	-1.05	-0.87	-0.28	-0.08	0.36	0.71

Table 3.5 ***Values of regression coefficients along with t-statistics and their p-values. Significant p-values (< 0.05) are indicated in bold.***

Data	Coefficient	Values	t statistics	p-value
Gangreung	intercept	-325.505	-3.538	**0.001**
10 min	slope	0.170	3.653	**0.001**
Gangreung	intercept	-494.375	-3.428	**0.001**
20 min	slope	0.258	3.539	**0.001**
Gangreung	intercept	-518.834	-2.854	**0.007**
30 min	slope	0.273	2.967	**0.005**
Gangreung	intercept	-470.540	-2.185	**0.035**
40 min	slope	0.250	2.295	**0.027**
Gangreung	intercept	-468.202	-1.869	0.069
50 min	slope	0.250	1.976	0.055
Daegu	intercept	-483.309	-1.454	0.150
1.5 hr	slope	0.294	1.732	0.087
Daegu	intercept	-547.277	-1.573	0.120
18 hr	slope	0.330	1.855	0.067
Daegu	intercept	-531.349	-0.353	0.180
1 day	slope	0.327	1.633	0.106
Gwangju	intercept	114.608	1.777	0.081
10 min	slope	-0.051	-1.560	0.124

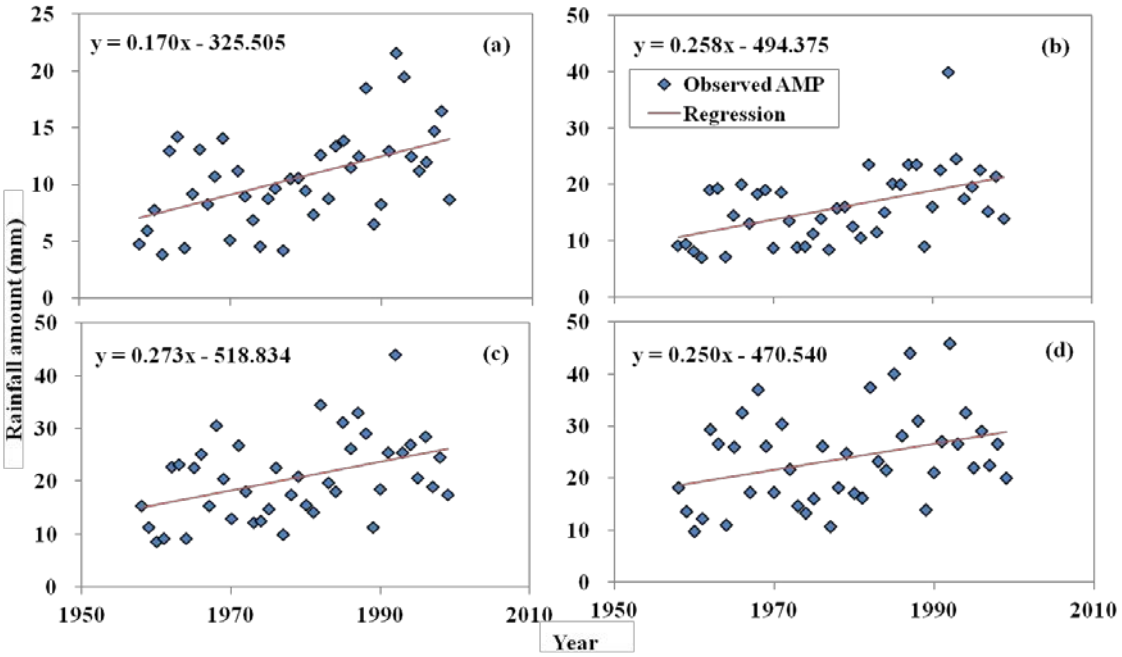

Figure 3.3 ***Plots of AMP against year together with regression lines (coefficients are calculated by SPSS, having p-values less than 0.05) for Gangreung station. (a) 10 minutes AMP, (b) 20 minutes AMP, (c) 30 minutes AMP, (d) 40 minutes AMP.***

3.3 Rainfall Frequency Analysis

3.3.1 Selection of a Statistical Probability Distribution

For extreme rainfall frequency analyses, several different probability distributions have been applied to Korean extreme precipitation data: the two-parameter Gumbel distribution (Kim et al., 2008; Kwon et al., 2009), and the four-parameter Kappa distribution (Park and Jung, 2002). The Kappa distribution was used "because several established distributions used for modeling extreme rainfalls are special cases of the K4D", including the general extreme value (GEV) distribution, generalized logistic (GLO) distribution, generalized Pareto (GPA), and Gumbel distribution. Nadarajah and Choi (2007) criticized the non-theoretical basis of the Kappa distribution and have suggested the GEV instead. Lee and Maeng (2003) used the L-moment ratio diagram to choose the appropriate distribution for daily AMP among the preselected GEV, GLO, and GPA and

found that the GEV and GLO were the most suitable. Hence, the Kolmogorov-Smirnov (K-S) test was further performed to select the GEV as the best model.

Since there is no general agreement on a representative distribution of extreme rainfall data, the one that fits well with observation and generates good estimates is to be selected. There is a graphical judgment, called 'L-moment ratio diagram', which allows a simple comparison between summary statistics, L-moment skewness and L-moment kurtosis, of sample and those of theoretical distributions. After those L-moments statistics are calculated from each of the observed AM precipitation series, they are plotted in a graph together with the theoretical L-moment ratio curve of the candidate distributions. The L-moment ratio curve is a simple expression of L-moment kurtosis in terms of L-moment skewness for commonly used distributions. The distribution whose L-moment ratio curve locates near the mean of consistently spread sample L-moment statistics is selected.

L-moments were developed by Hosking (1986) to expand the utility of probability weighted moments (PWM) which were first proposed by Greenwood et al. (1979). The PWM-driven L-moments are more robust than conventional moments because L-moments are less influenced by the effects of sampling variability (Hosking 1989). Mathematically, L-moments are linear combination of PWMs which are defined by (Hosking 1990):

$$\beta_r = \int x\{F(x)\}^r dF(x), \qquad r = 0,1,2,\dots,\mathrm{n} \tag{3.1}$$

Then, the r-th order L-moments (λ_r) are:

$$\begin{aligned}
\lambda_1 &= \beta_0 \\
\lambda_2 &= 2\beta_1 - \beta_0 \\
\lambda_3 &= 6\beta_2 - 6\beta_1 + \beta_0 \\
\lambda_4 &= 20\beta_3 - 30\beta_2 + 12\beta_1 - \beta_0
\end{aligned} \tag{3.2}$$

By dividing the higher-order L-moments by the second L-moment (λ_2), we obtain L-moment ratios (τ_r):

$$\tau_r = \frac{\lambda_r}{\lambda_2} \tag{3.3}$$

3.3.2 Estimation of Distribution Parameters and Quantiles

After selecting an appropriate distribution for extreme rainfall data, the distribution parameters are estimated using two common methods: the L-moment method and the non-central moment (NCM) method. For the generalized extreme value (GEV) distribution which is selected as appropriate for Korean extreme rainfall data, the cumulative distribution function, *F(x)* is defined as:

$$\mathrm{F}(x) = \exp\left[-\left(1 - \frac{\kappa(x-\xi)}{\alpha}\right)^{\frac{1}{\kappa}}\right], \qquad \kappa \neq 0 \tag{3.4}$$

where κ, α, ξ are shape, scale, and location parameters, respectively.

The extreme rainfall quantiles for a given return period *T* (X_T) can be calculated by the following equation:

$$X_T = \xi + \frac{\alpha}{\kappa}\{1 - [-ln(p)]^{\kappa}\} \tag{3.5}$$

where *p (=1/T)* is the exceedance probability of interest.

3.3.2.1 L-moments

The L-moment method is being considered as reliable, particularly with small samples, and is computationally tractable. Parameters of GEV distribution are obtained by substituting sample L-moments into the following equations:

$$c = \frac{2}{3+\tau_3} - \frac{\log 2}{\log 3} \tag{3.6}$$

$$\kappa \approx 7.8590c + 2.9554c^2 \tag{3.7}$$

$$\alpha = \frac{\lambda_2 \kappa}{(1-2^{-\kappa})\Gamma(1+\kappa)} \tag{3.8}$$

$$\xi = \lambda_1 + \frac{\alpha\{\Gamma(1+\kappa)-1\}}{\kappa} \tag{3.9}$$

where κ, α, ξ are shape, scale, and location parameters respectively. λ_1, λ_2 are the first and second L-moments, τ_3 is L-skewness, and $\Gamma()$ is the gamma function. The κ value on the Equation 3.7 is approximated by Hosking (1985b) and is reported to have accuracy better than 99.91% for $-0.5 \leq \tau_3 \leq 0.5$.

3.3.2.2 Non-Central Moments

Nguyen (2004) proposed another parameter estimation method that is based on the non-central moments (NCMs) especially for GEV distribution. The *k*-th order NCM, μ_k of random variable X is the mean value of *k*-times self-multiplied as shown following:

$$\mu_k = \mathrm{E}[X^k] \tag{3.10}$$

The NCM method is equating *k*-th order sample NCM to GEV parameters through the following equation (Nguyen and Pandey 1994):

$$\mu_k = \left(\xi + \frac{\alpha}{\kappa}\right)^k + (-1)^k \left(\frac{\alpha}{\kappa}\right)^k \Gamma(1+k\kappa) + k\sum_{i=1}^{k-1}(-1)^i \left(\frac{\alpha}{\kappa}\right)^i \left(\xi + \frac{\alpha}{\kappa}\right)^{k-i} \Gamma(1+i\kappa) \tag{3.11}$$

From the Equation 3.11, three GEV parameters are calculated from substituting the first three sample NCMs estimated from the extreme rainfall data.

3.3.3 Scaling Properties of Extreme Rainfall Processes

For extreme rainfall frequency analyses, conventional methods are accurate only for the selected data of a particular duration. In other words, the analysis of extreme rainfalls of the duration of interest cannot be induced from the rainfall series of different durations, even though extreme rainfall amounts of different durations occur from the same rainfall process. The scaling property, however, allows us to analyze extreme rainfalls of a given duration in consideration of properties of rainfall series of different durations, which is physically more consistent and more accurate. The scaling property in terms of intensity-duration-frequency (IDF) curves, a graphical result of extreme rainfall analysis, is mathematically proven by Pandey (1995), and practically applied to build IDF curves of Quebec by Nguyen (2004). In this study, the scaling characteristic is also used to analyze extreme rainfall data in South-Korea.

By definition, a function is scaling if $f(t)$ is proportional to its scaled function,$f(\lambda t)$, presented as:

$$f(t) = C(\lambda) f(\lambda t) \tag{3.12}$$

where $C(\lambda)$ is a function of a scaling factor, λ, which exists in a range of positive values, and *t* is the duration of rainfall. Inspired from the Equation 3.12, the Equation 3.13 can be proven (Nguyen, 2004).

$$C(\lambda) = \lambda^{-\beta} \tag{3.13}$$

where β is a constant, and the Equation 3.14 is also proven.

$$f(t) = t^{\beta} f(1) \tag{3.14}$$

From Equations 3.13 and 3.14, the *k*-th order NCM, $\mu_k(t)$, of duration *t* can be defined as follows:

$$\mu_k(t) = E\{f^k(t)\} = \alpha(k) t^{\beta(k)} \quad in\ which \quad \alpha(k) = E\{f^k(1)\} \tag{3.15}$$

The rainfall process has a simple scaling behaviour if $\beta(k) = \beta k$. Otherwise, the process will be multi-scaling (Nguyen et al. 2002). Hence, the multi-scaling function will display a non-linear form when it is plotted in log-log scale, while the simple scaling

function shows a straight line in this plot. The slope of the straight line is the scaling exponent, β, which is proportional to the order of the NCM. It should be noted that if the slope β has two different values, then the rainfall process exhibits two different scaling behaviours in two different ranges of duration, and the dividing point is called a 'break point'.

$$\begin{cases} \forall t \in [t_1 : t_2] & f(t) = \left(\frac{t}{t_2}\right)^{\beta_1} f(t_2) \\ \forall t \in [t_2 : t_3] & f(t) = \left(\frac{t}{t_3}\right)^{\beta_2} f(t_3) \end{cases} \tag{3.16}$$

where t_2 is the time point that the break occurs, and in each interval scaling exponent has different values, β_1, β_2.

On the basis of Equation 3.15, the sample estimates of the first three NCMs were used to assess the simple scaling behaviour of the AMPs from daily (the longest duration) to all sub-daily durations. As shown by Equation 3.11, for the GEV distribution, the first three NCMs can be computed using the following expressions:

$$\mu_1 = \left(\xi + \frac{\alpha}{\kappa}\right) - \left(\frac{\alpha}{\kappa}\right)\Gamma(1+\kappa) \tag{3.17}$$

$$\mu_2 = \left(\xi + \frac{\alpha}{\kappa}\right)^2 + \left(\frac{\alpha}{\kappa}\right)^2 \Gamma(1+2\kappa) - 2\left(\frac{\alpha}{\kappa}\right)\left(\xi + \frac{\alpha}{\kappa}\right)\Gamma(1+\kappa) \tag{3.18}$$

$$\mu_3 = \left(\xi + \frac{\alpha}{\kappa}\right)^3 - \left(\frac{\alpha}{\kappa}\right)^3 \Gamma(1+3\kappa) + 3\left(\frac{\alpha}{\kappa}\right)^2 \left(\xi + \frac{\alpha}{\kappa}\right)\Gamma(1+2\kappa) - 3\left(\frac{\alpha}{\kappa}\right)\left(\xi + \frac{\alpha}{\kappa}\right)^2 \Gamma(1+\kappa) \tag{3.19}$$

Hence, replacing the sample estimates of the first three NCMs into Equations (3.17), (3.18) and (3.19), the three GEV parameters can be estimated by solving this system of three equations. Once the parameters are determined, the quantiles corresponding to each return period can be calculated based on Equation 3.5.

3.3.4 Construction of IDF Curves

To construct IDF curves (Figure 2.1), empirical and theoretical probabilities of

AMPs for each given duration are needed. The empirical probabilities are computed from the observed AMP data using a “plotting-position” formula (Nguyen et al., 1989), and the theoretical probabilities are computed using the fitted scaling GEV distribution. In the present study, the empirical probabilities of AMPs were computed using the Cunnane’s formula (Cunnane, 1978):

$$p = \frac{i - 0.4}{n + 0.2} \tag{3.20}$$

where p is the exceedance probability, which can be further converted into the return period by $T = 1/p$, and i is the rank of each AMP value in the ordered data series from the largest to the smallest value. The computation of the theoretical probabilities using the scaling GEV distribution was carried out using the procedure described in Section 3.3.3. The comparison of the estimated empirical and theoretical extreme rainfall quantiles will be compared using both numerical and graphical criteria as described in the following section.

3.3.5 Performance Criteria

To assess the accuracy of the proposed methods, estimated values are compared with the empirical values given by the observed data using both graphical comparison and numerical assessment indices.

3.3.5.1 Graphical Assessment

Dalgaard (2008) and Klein Tank et al. (2009) have suggested several forms of graphs as tools to assess the goodness of fit of the theoretical distribution to the data such as histograms, Q-Q plots, and probability plots. In particular, the Q-Q plot represents the agreement between estimated and observed quantiles and is commonly used to assess the accuracy of the fitted theoretical distribution. In addition, the probability plot can also be used to assess the goodness of fit of the theoretical distribution by displaying the agreement between the cumulative distribution function and the empirical probabilities estimated from the data using a plotting-position formula. Attention should be paid to the

selection of a suitable plotting-position formula for the computation of the empirical probabilities since different formulas were available for different underlying distributions of the data. In this study, the Cunnane's formula was used since it is a compromise formula that does not require any assumption of a specific distribution of the data.

3.3.5.2 Numerical Assessment

In this study, two numerical assessment indices were used: the root-mean-square-error (RMSE) and the relative-root-mean-square-error (RRMSE):

$$RMSE = \sqrt{\frac{1}{n}\sum_{i=1}^{n}\left(X_{Obs,i} - X_{Est,i}\right)^2} \tag{3.21}$$

in which $X_{Obs,i}$ is the i^{th} observed data point, $X_{Est,i}$ is the i^{th} estimated value, and n is the number of data points; and

$$RRMSE = \sqrt{\frac{1}{n}\sum_{i=1}^{n}\left(\frac{X_{Obs,i} - X_{Est,i}}{\overline{X_{Obs}}}\right)^2} \tag{3.22}$$

where $\bar{X}_{Osb}$is the mean value of observed data.

The smaller the values of RMSE or RRMSE are the better the fit of the assumed distribution will be. In addition, the outliers could have a higher impact on the RMSE values than the RRMSE ones (Tao 2001).

3.4 Results and Discussion

3.4.1 Choice of the Best-Fit distribution

In current engineering practice, there is no general agreement regarding what is the "best" distribution to represent the distribution of sample extreme rainfall data. For instance, several distributions have been used for extreme rainfalls in Korea such as the Generalized Pareto (GPA), Generalized Extreme Value (GEV), Generalized Logistic

(GLO), Log-Normal (LN3), and Pearson Type 3 (PE3) (Daniell and Tabios 2008). Hence, in the present study, the common L-moment ratio diagram method was used to identify the most suitable model for the AMP data considered. For purposes of illustration, Figure 3.4 shows the L-moment diagram for the daily AMP series at 14 stations in Korea. It can be seen that the average location of these 14 points is quite close to the GEV curve. Similar results were found for other durations as well (see Appendix B). Therefore, the GEV distribution can be selected as the most appropriate distribution for the AMP data in Korea.

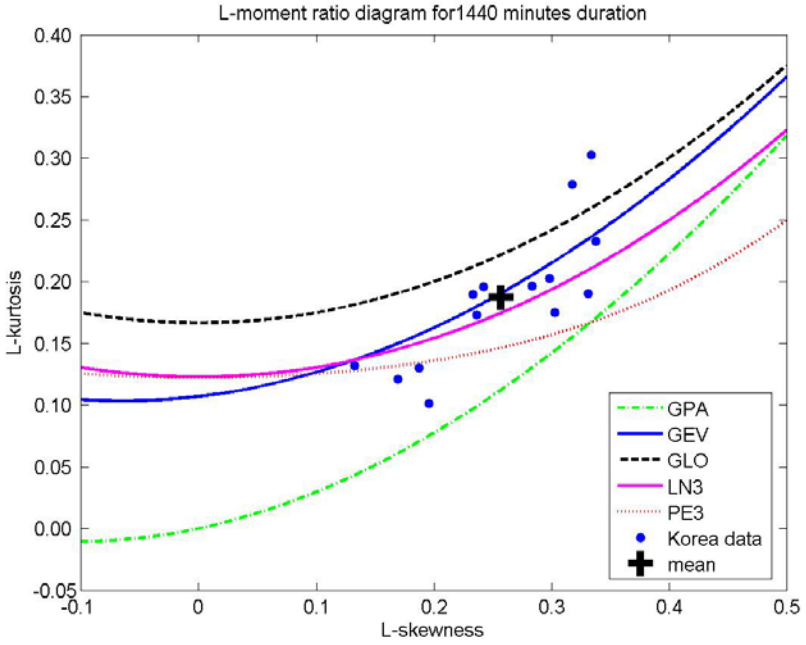

Figure 3.4 L-moment ratio diagram for 1440 minutes annual maximum precipitation in Korea

3.4.2 Estimation of Distribution Parameters and Quantiles

The L-moment method has been commonly applied to the estimation of the parameters of the GEV distribution. In addition, Nguyen et al. (2002) have suggested the use of the NCM procedure for estimating the GEV parameters because of the scale-invariance property of the NCMs. In the present study, for comparison purposes both L-moment and NCM methods were used for the GEV parameter estimation using the AMP data in Korea. This section shows the application results of these methods to the AMP

series (1957-1999) of Seoul station. The proposed method can be applied to other stations in Korea.

For purposes of illustration, Tables 3.6 and 3.7 present the estimated GEV parameters and estimated extreme rainfall quantiles obtained from the L-moment and NCM methods respectively for the Seoul station. In general, it can be seen that both methods have provided comparable estimates. In addition, Figures 3.5, 3.6 and 3.7 show the good agreement of the fitted GEV distributions with the empirical quantiles for AMPs for 10-minute, 60-minute, and 1-day durations respectively. Quantile plots for other durations are presented in Appendix C (Figure C.1-16). Furthermore, Table 3.8 shows the RMSE and RRMSE values of the two estimation methods for different rainfall durations. It was found that the accuracy of these two estimation methods was quite similar as well. In summary, based on the graphical and numerical comparisons, both L-moment and NCM methods can provide comparable results and hence these procedures can be used for estimating the parameters of the GEV distribution. The NCM method however was selected in the present study since the scale-invariance property of the NCMs is useful in the estimation of the sub-daily extreme rainfalls from the rainfall data of longer durations as indicated by Nguyen et al. (2002).

Table 3.6 GEV quantiles and parameters estimated by L-moment method for Seoul station.

Duration	GEV parameters			Quantile estimates for T year of return period					
	κ	α	ξ	2 yrs	5 yrs	10 yrs	25 yrs	50 yrs	100 yrs
10 min	0.17	5.04	13.29	15.08	19.96	22.72	25.73	27.67	29.38
20 min	0.06	8.03	19.35	22.26	30.87	36.25	42.72	47.29	51.63
30 min	0.13	10.95	25.87	29.79	40.75	47.15	54.37	59.17	63.50
40 min	0.16	13.65	31.32	36.17	49.49	57.05	65.38	70.79	75.57
50 min	0.18	16.33	36.08	41.87	57.51	66.22	75.65	81.67	86.93
1 hr	0.15	18.10	39.84	46.29	64.08	74.26	85.54	92.91	99.48
1.5 hr	0.26	23.17	51.40	59.50	80.18	90.86	101.70	108.18	113.53
2 hr	0.23	26.17	58.77	67.96	91.89	104.58	117.75	125.80	132.58
3 hr	0.15	29.40	68.79	79.27	108.22	124.82	143.27	155.33	166.10
4 hr	0.05	29.74	74.36	85.17	117.37	137.73	162.40	179.98	196.85
6 hr	0.05	34.77	87.05	99.67	137.16	160.75	189.23	209.44	228.76
9 hr	0.02	39.62	98.65	113.11	157.11	185.65	221.04	246.82	272.02
12 hr	-0.04	41.15	104.50	119.69	168.12	201.42	244.96	278.35	312.45
15 hr	-0.14	42.76	109.91	126.00	181.47	223.49	283.48	333.57	388.56
18 hr	-0.17	45.30	113.72	130.84	190.83	237.20	304.64	361.96	425.84
1 day	-0.21	48.87	120.51	139.12	206.42	260.48	341.91	413.50	495.61

Table 3.7 GEV quantiles and parameters estimated by NCM method for Seoul station.

Duration	GEV parameters			Quantile estimates for T year of return period					
	κ	α	ξ	2 yrs	5 yrs	10 yrs	25 yrs	50 yrs	100 yrs
10 min	0.10	4.72	13.18	14.88	19.73	22.64	26.01	28.31	30.42
20 min	0.10	8.06	19.62	22.52	30.84	35.84	41.64	45.59	49.25
30 min	0.08	10.30	25.68	29.40	40.28	46.98	54.92	60.44	65.65
40 min	0.04	12.28	30.61	35.08	48.55	57.18	67.76	75.38	82.76
50 min	0.05	14.63	35.18	40.50	56.36	66.41	78.60	87.29	95.64
1 hr	0.07	16.71	39.29	45.34	63.10	74.13	87.26	96.47	105.17
1.5 hr	0.22	22.12	51.25	59.03	79.42	90.33	101.73	108.75	114.71
2 hr	0.24	25.40	59.14	68.06	91.19	103.41	116.04	123.73	130.20
3 hr	0.18	29.36	69.47	79.88	108.01	123.69	140.68	151.51	160.98
4 hr	0.10	30.65	75.20	86.23	117.94	137.07	159.31	174.51	188.60
6 hr	0.12	35.94	88.34	101.24	137.83	159.55	184.43	201.20	216.55
9 hr	0.10	41.44	100.66	115.56	158.21	183.80	213.40	233.55	252.14
12 hr	0.05	43.97	106.74	122.70	170.17	200.09	236.26	261.95	286.54
15 hr	$5.10E^{-04}$	49.22	113.22	131.26	187.02	223.91	270.51	305.07	339.36
18 hr	$7.91E^{-06}$	53.85	117.55	137.29	198.32	238.73	289.78	327.65	365.25
1 day	$7.58E^{-06}$	63.08	124.70	147.82	219.32	266.65	326.46	370.83	414.87

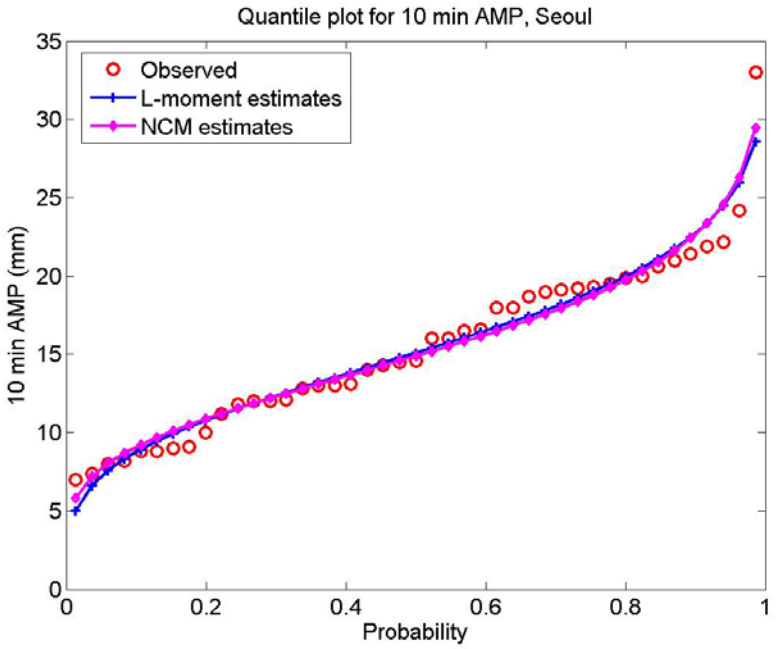

Figure 3.5 Quantile plot of 10 minutes AMP, estimated by two parameter estimation methods and observed, at Seoul for 1957-1999 period.

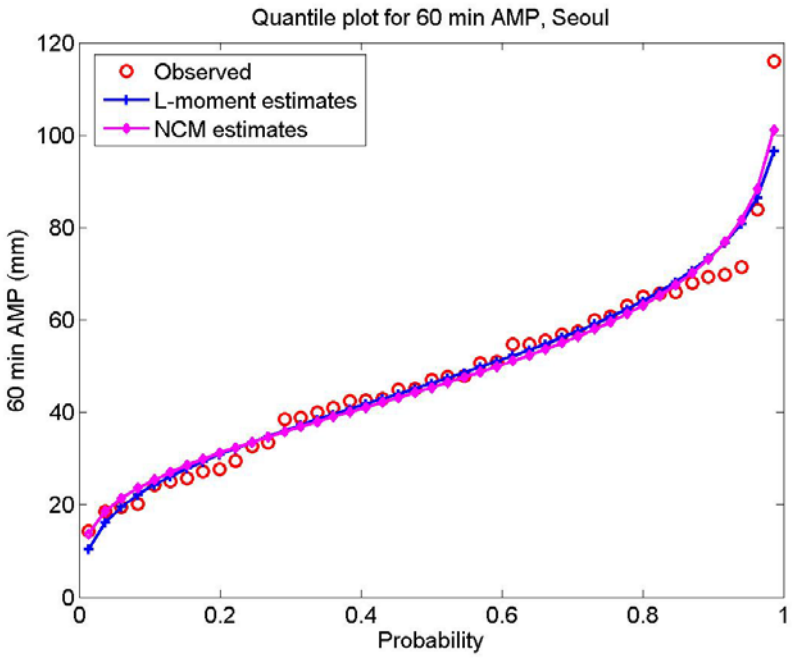

Figure 3.6 Quantile plot of 60 minutes AMP, estimated by two parameter estimation methods and observed, at Seoul for 1957-1999 period.

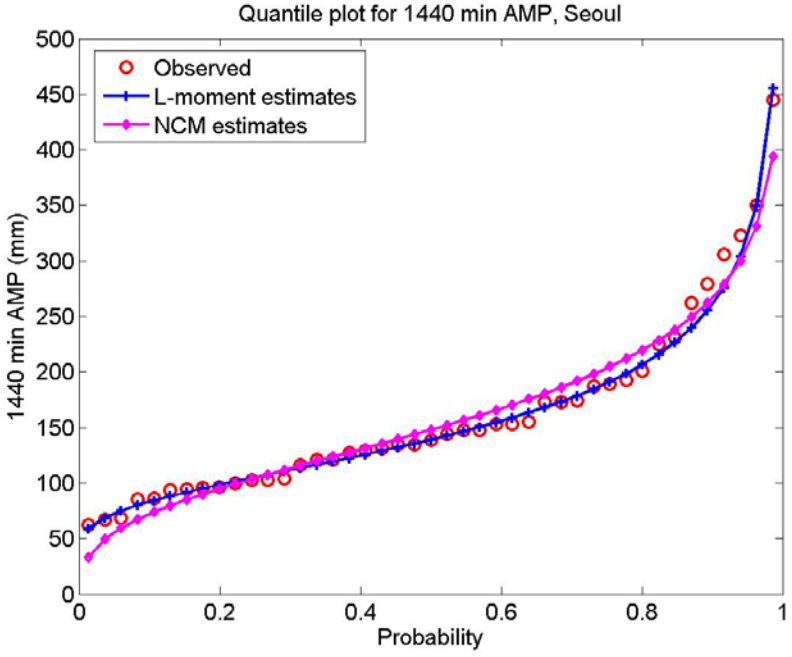

Figure 3.7 Quantile plot of daily (1440 minutes) AMP, estimated by two parameter estimation methods and observed, at Seoul for 1957-1999 period.

Table 3.8 RMSE and RRMSE values of estimated AMP quantiles by two parameter estimation methods: L-moment method and NCM method. Values in bold indicate smaller errors of the estimates compared to their counterparts.

Duration	RMSE		RRMSE	
	L-moment	NCM	L-moment	NCM
10 min	1.071	**1.034**	0.069	**0.067**
20 min	**0.926**	0.982	**0.039**	0.042
30 min	1.897	**1.757**	0.061	**0.057**
40 min	3.628	**3.313**	0.097	**0.089**
50 min	4.322	**4.012**	0.101	**0.093**
1 hr	3.850	**3.589**	0.080	**0.075**
1.5 hr	3.250	3.231	0.054	0.054
2 hr	2.379	2.400	0.035	0.035
3 hr	2.667	2.734	0.033	0.033
4 hr	**5.040**	5.108	**0.056**	0.057
6 hr	6.914	**6.659**	0.066	**0.063**
9 hr	6.161	**5.866**	0.051	**0.049**
12 hr	7.480	7.484	0.058	0.058
15 hr	**9.130**	9.574	**0.064**	0.068
18 hr	**8.897**	10.512	**0.060**	0.071
1 day	**8.430**	15.179	**0.052**	0.094

3.4.3 Evaluation of the Scaling Properties of Extreme Rainfalls

In this section, the scale-invariance (or scaling) property of the NCMs of AMPs is examined using the available observed AMP data at Seoul station for the period from 1957 to 1999. Figure 3.8 shows the plot of the relations between the first three NCMs of AMPs and rainfall durations in log-log scale. It can be observed that two log-linear relations were identified for two different portions of rainfall durations: from 10 minutes to 60 minutes and from 60 minutes to one day; indicating two different scaling behaviours of the AMP processes.

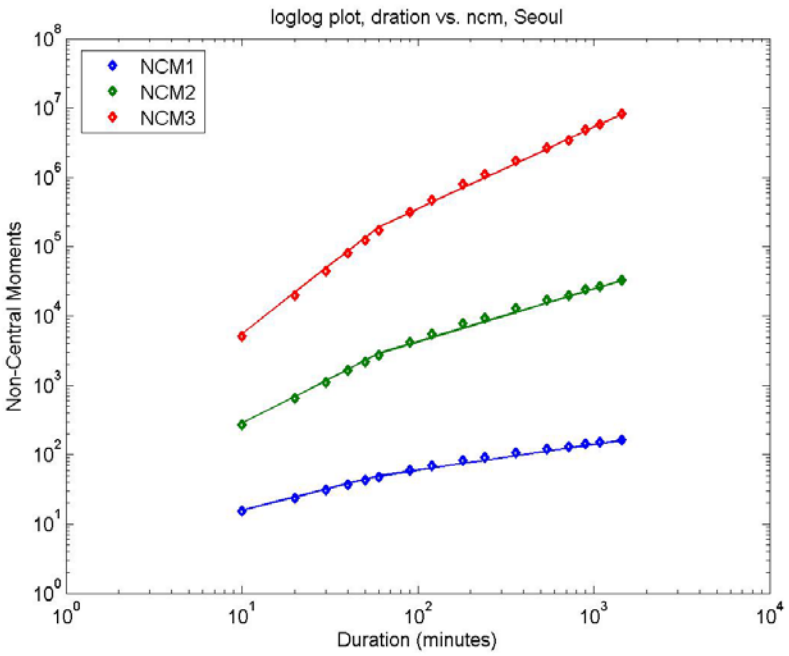

Figure 3.8 The 1st, 2nd, and 3rd NCMs against rainfall durations in log-log scale, Seoul station, 1957-1999 data period.

According to Equation 3.15, the slopes of the fitted regression lines of the NCM-rainfall duration relations provide the values of the scaling exponent $\beta(k)$ as shown in Table 3.9. Figure 3.9 shows the strong linear relationship between the values of the scaling exponent β and the order k of the NCMs. Indeed, the coefficients of determination (R^2) of the fitted linear regression lines are 0.9999 and 0.9996 respectively for the 10 to 60 minutes interval and the 60 minutes to 1 day interval. This linear relationship $\beta(k) = \beta k$ indicated the simple scaling behaviour of the AMPs as presented in Section 3.3.3.

Table 3.9 Scaling exponent values for time intervals of 10 – 60 minutes and 60 – 1440 minutes, Seoul station, 1957-1999 data period.

Interval of duration	Order of NCM		
	1	2	3
10 min – 1 hr	0.636	1.296	1.976
1 hr – 1 day	0.371	0.762	1.180

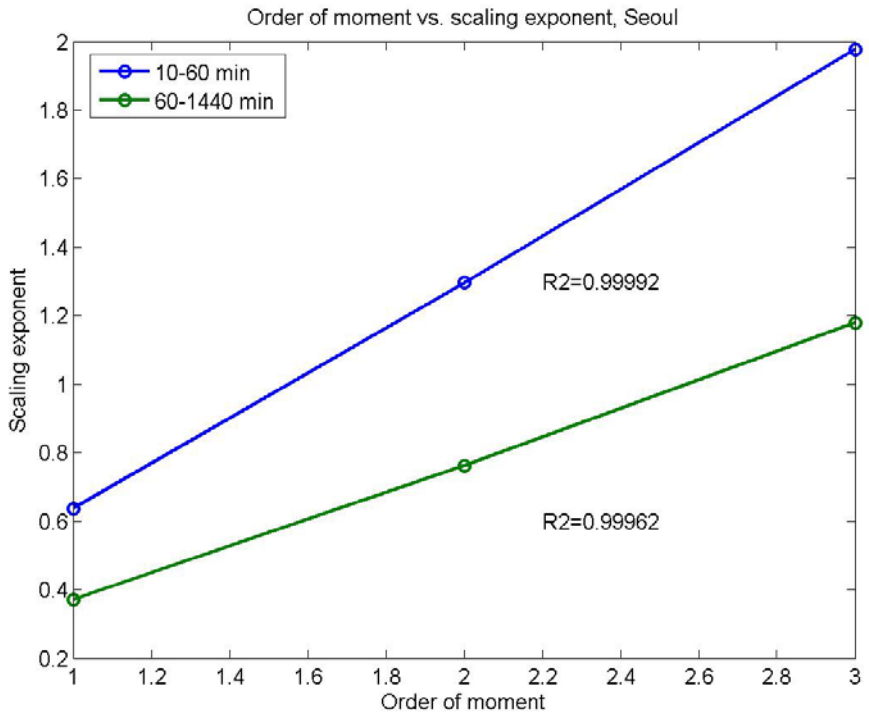

Figure 3.9 Plot of scaling exponent, $\beta(k)$ against the order of NCM, k, Seoul station, 1957-1999 data period.

Table 3.10 presents the results of the scaling behaviour of the AMPs for all 14 stations. It can be observed that some stations (Seoul, Busan, Gwangju, Jeonju, and Chupungryong) have a similar scaling behaviour (the break point of the log-linear relationship as shown in Figure 3.8 is located at the 60-minute duration), but other stations have a different scaling regime. However, the simple scaling property was observed for the AMP processes at all 14 stations as indicated by the very high R^2 values (close to 1) of the fitted regression lines. Consequently, on the basis of the observed simple scaling behaviour the sub-daily extreme rainfall statistical properties can be derived from the properties of extreme rainfalls of longer durations.

Table 3.10 Scaling exponent and R^2 values in each interval of duration for the 14 Korean stations.

Station	Data Period (year)	Duration Interval	Order of NCM, *k*			R^2
			1	2	3	
Seoul	1961-1999	10 min – 1 hr	0.636	1.296	1.976	1.000
		1 hr – 1 day	0.371	0.762	1.180	1.000
Suwon	1964-1999	10 min – 3 hr	0.547	1.120	1.721	1.000
		3 hr – 1 day	0.388	0.799	1.251	0.999
Incheon	1961-1999	10 min – 1.5 hr	0.602	1.218	1.850	1.000
		1.5 hr – 1 day	0.356	0.754	1.189	0.999
Gangreung	1961-1999	10 min – 6 hr	0.563	1.139	1.743	1.000
		6 hr – 1 day	0.479	0.960	1.406	1.000
Daegu	1961-1999	10 min – 9 hr	0.438	0.871	1.290	1.000
		9 hr – 1 day	0.362	0.703	1.012	0.999
Busan	1961-1999	10 min – 1 hr	0.641	1.286	1.905	1.000
		1 hr – 1 day	0.427	0.861	1.318	1.000
Gwangju	1961-1999	10 min – 1 hr	0.598	1.200	1.801	1.000
		1 hr – 1 day	0.398	0.806	1.238	1.000
Jeonju	1970-1999	10 min – 1 hr	0.651	1.311	1.980	1.000
		1 hr - 1440	0.399	0.798	1.202	1.000
Mokpo	1961-1999	10 min – 9 hr	0.493	0.994	1.513	1.000
		9 hr – 1 day	0.316	0.664	1.083	0.997
Pohang	1961-1999	10 min - 50 min	0.563	1.116	1.657	1.000
		50 min – 1 day	0.455	0.928	1.427	1.000
Yeosu	1961-1999	10 min – 2 hr	0.562	1.145	1.746	1.000
		2 hr – 1 day	0.408	0.819	1.233	1.000
Chupungryong	1961-1999	10 min – 1 hr	0.543	1.093	1.655	1.000
		1 hr – 1 day	0.432	0.865	1.298	1.000
Ulsan	1961-1999	10 min – 4 hr	0.554	1.137	1.744	1.000
		4 hr – 1 day	0.410	0.853	1.356	0.999
Cheongju	1967-1999	10 min - 40 min	0.536	1.073	1.603	1.000
		40 min – 1 day	0.396	0.807	1.245	1.000

In the present study, the accuracy of the estimation of extreme rainfall quantiles for all 16 durations using the scaling property of the NCMs (referred to as the "scaling NCM method") was compared to the quantiles estimated by the "traditional NCM method". Here, the traditional NCM method refers to the calculation of the quantiles by fitting the GEV distribution to the extreme rainfall data set of each duration independently, while the scaling NCM method allows deriving the sub-daily quantiles from the estimated GEV quantiles of longer durations based on the scaling property of the extreme rainfall NCMs. For purposes of illustration, Figures 3.10 and 3.11 show the comparison between the observed quantiles and the quantiles estimated by the traditional NCM method and the scaling NCM procedure for 10-minute and 60-minute duration respectively. In addition, the RMSE, RRMSE, and R^2 values of the estimated quantiles by both methods for all durations for Seoul station are presented in Table 3.11. It can be seen that except for some noted difference in the RMSE and RRMSE values for the durations from 120 minutes to 720 minutes the quantiles estimated by both methods are comparable. Furthermore, both estimation methods are accurate as indicated by the high R^2 values ($R^2 > 0.90$). Similar results were found for other durations as shown in Appendix D (Figures D.1-16). In summary, the scaling NCM method can provide extreme rainfall quantiles as comparable as those given by the traditional method and it is more suitable for the downscaling of extreme rainfalls from daily scale to sub-daily scales.

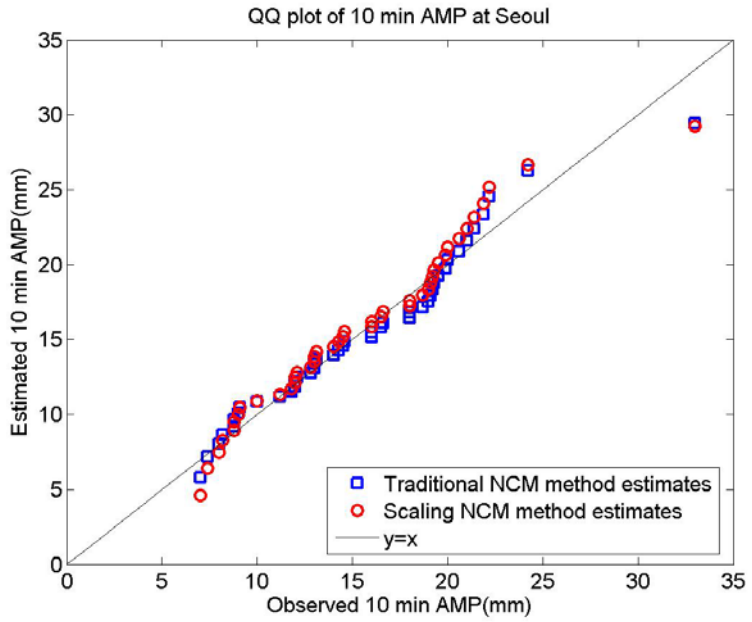

Figure 3.10 Q-Q plot of estimated quantiles versus observed quantiles for 10-minute extreme rainfalls for Seoul station. (Blue squares: quantiles estimated by traditional NCM method, red circles: quantiles estimated by scaling NCM method)

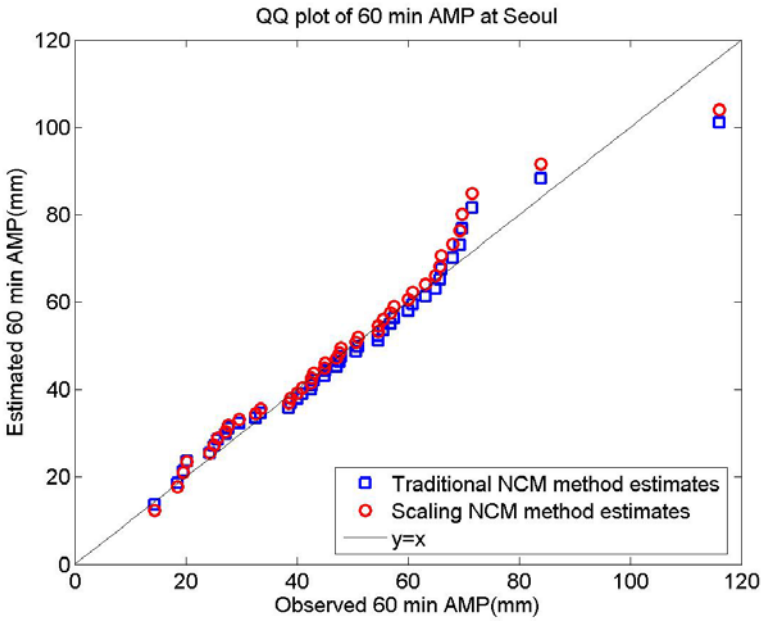

Figure 3.11 Q-Q plot of estimated quantiles versus observed quantiles for 60-minute extreme rainfalls for Seoul station.

Table 3.11 RMSE and RRMSE values of estimated quantiles by traditional NCM method and scaling NCM method for Seoul station.

Duration	RMSE (mm)		RRMSE		R^2	
	NCM	Scaling NCM	NCM	Scaling NCM	NCM	Scaling NCM
10 min	1.034	1.191	0.067	0.075	0.963	0.951
20 min	0.982	1.523	0.042	0.062	0.989	0.973
30 min	1.757	2.113	0.057	0.066	0.979	0.969
40 min	3.313	3.590	0.089	0.094	0.952	0.943
50 min	4.012	4.219	0.094	0.096	0.949	0.943
1 hr	3.589	4.005	0.075	0.081	0.967	0.959
1.5 hr	3.231	5.231	0.054	0.091	0.980	0.948
2 hr	2.400	7.024	0.035	0.110	0.992	0.927
3 hr	2.734	8.969	0.033	0.121	0.992	0.918
4 hr	5.108	9.404	0.057	0.114	0.979	0.928
6 hr	6.659	12.573	0.063	0.131	0.973	0.904
9 hr	5.866	12.065	0.049	0.108	0.985	0.935
12 hr	7.484	10.581	0.058	0.085	0.980	0.960
15 hr	9.574	11.605	0.068	0.086	0.977	0.966
18 hr	10.512	11.153	0.071	0.077	0.977	0.974
1 day	15.179	15.179	0.095	0.095	0.965	0.965

3.4.4 IDF Relations

In the above sections, it has been demonstrated that the AMP processes in South Korea displayed a simple scaling behaviour and that the NCM scaling method can be used to estimate the GEV distribution parameters and the extreme rainfall quantiles for different durations. Consequently, this “scaling GEV” method can be used to construct the IDF relations at a study site where the AMP data for different durations are available. For instance, Figure 3.16 shows the IDF curves for Seoul station for six different return periods – 2, 5, 10, 25, 50, 100 years constructed by the scaling GEV method, and Figure 3.17 shows the good agreement of the theoretical IDF curves with the observed empirical quantiles. Similar results were found for the IDF curves for other stations as presented in

Appendix E. For a close investigation of the accuracy of the scaling GEV method, Figure 3.18 (a) – (p) show the good fit of the estimated scaling GEV distribution to the observed empirical AMP quantiles for each rainfall duration separately. Therefore, the scaling GEV method can be used as a suitable model for extreme rainfall frequency analysis and for the construction of the IDF relations at a given site.

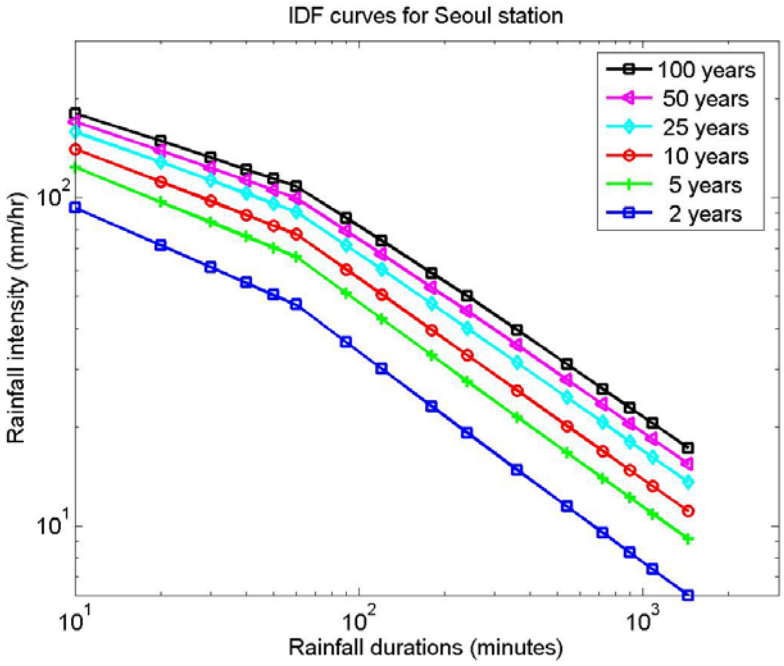

Figure 3.12 Intensity-Duration-Frequency (IDF) curves drawn by scaling GEV method for Seoul station.

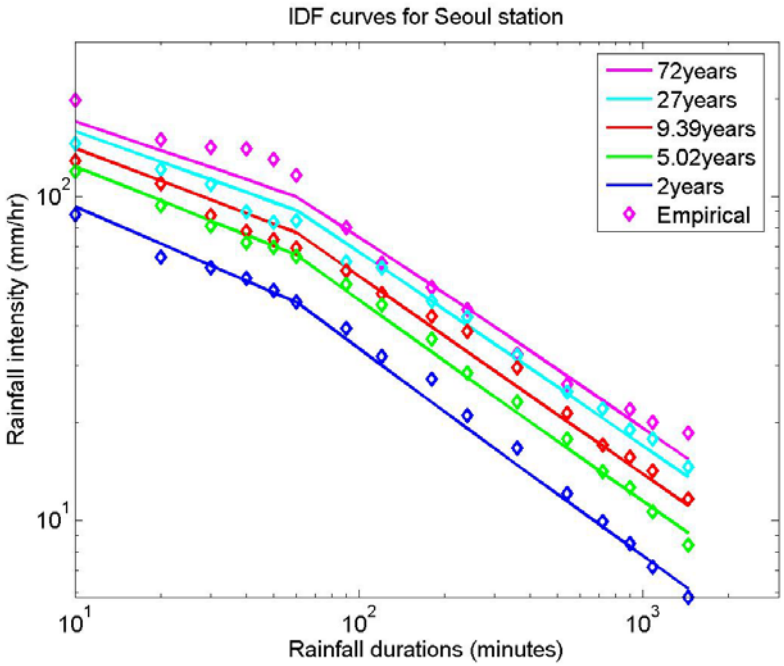

Figure 3.13 Estimated IDF curves and observed quantiles for Seoul station.

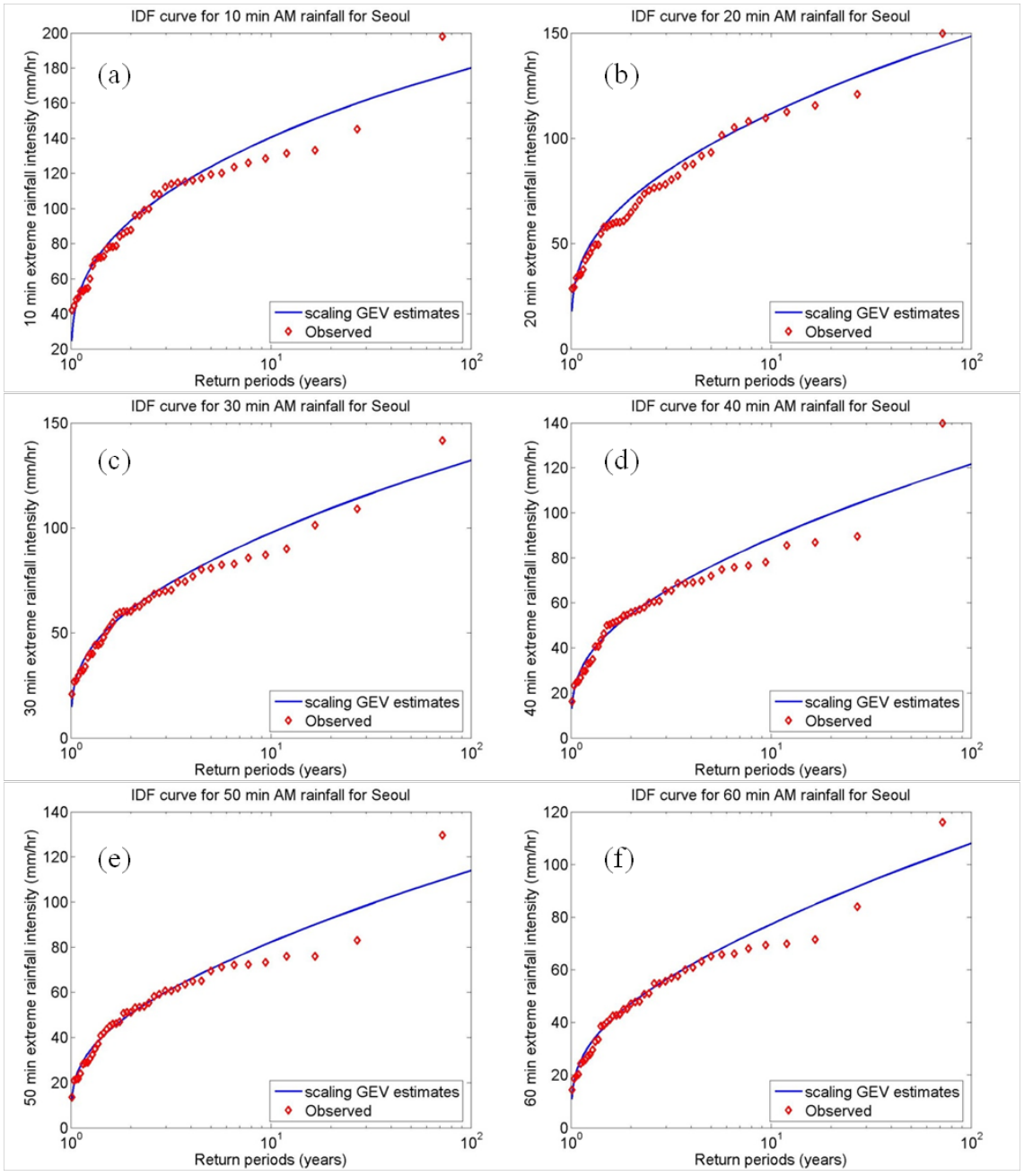
IDF curve for 10 min AM rainfall for Seoul
(a)
10 min extreme rainfall intensity (mm/hr)
Return periods (years)
scaling GEV estimates
Observed
IDF curve for 20 min AM rainfall for Seoul
(b)
20 min extreme rainfall intensity (mm/hr)
Return periods (years)
scaling GEV estimates
Observed
IDF curve for 30 min AM rainfall for Seoul
(c)
30 min extreme rainfall intensity (mm/hr)
Return periods (years)
scaling GEV estimates
Observed
IDF curve for 40 min AM rainfall for Seoul
(d)
40 min extreme rainfall intensity (mm/hr)
Return periods (years)
scaling GEV estimates
Observed
IDF curve for 50 min AM rainfall for Seoul
(e)
50 min extreme rainfall intensity (mm/hr)
Return periods (years)
scaling GEV estimates
Observed
IDF curve for 60 min AM rainfall for Seoul
(f)
60 min extreme rainfall intensity (mm/hr)
Return periods (years)
scaling GEV estimates
Observed

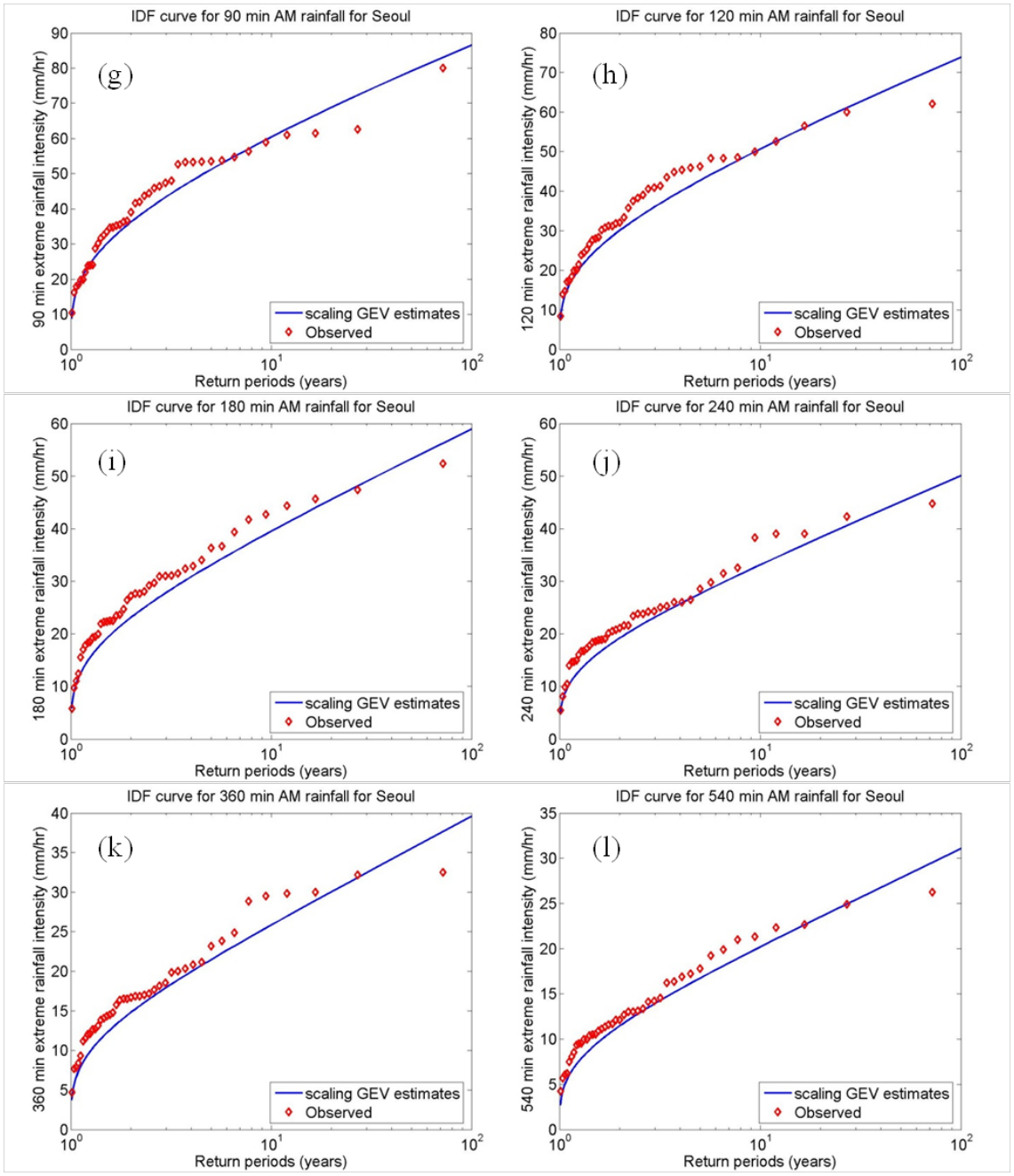
IDF curve for 90 min AM rainfall for Seoul
(g)
90 min extreme rainfall intensity (mm/hr)
Return periods (years)
scaling GEV estimates
Observed
IDF curve for 120 min AM rainfall for Seoul
(h)
120 min extreme rainfall intensity (mm/hr)
Return periods (years)
scaling GEV estimates
Observed
IDF curve for 180 min AM rainfall for Seoul
(i)
180 min extreme rainfall intensity (mm/hr)
Return periods (years)
scaling GEV estimates
Observed
IDF curve for 240 min AM rainfall for Seoul
(j)
240 min extreme rainfall intensity (mm/hr)
Return periods (years)
scaling GEV estimates
Observed
IDF curve for 360 min AM rainfall for Seoul
(k)
360 min extreme rainfall intensity (mm/hr)
Return periods (years)
scaling GEV estimates
Observed
IDF curve for 540 min AM rainfall for Seoul
(l)
540 min extreme rainfall intensity (mm/hr)
Return periods (years)
scaling GEV estimates
Observed

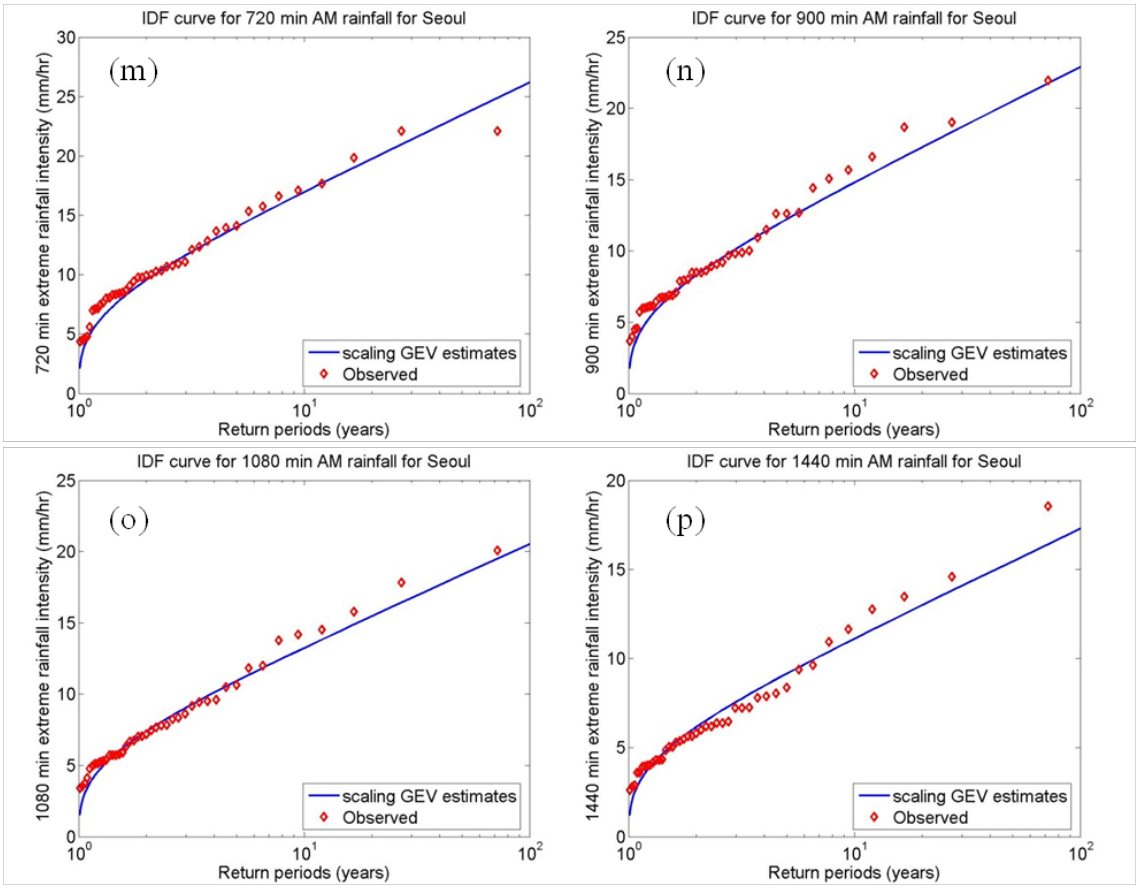

Figure 3.18 The agreement between the estimated scaling GEV distributions with the observed empirical AMP quantiles for duration of (a) 10 min, (b) 20 min, (c) 30 min, (d) 40 min, (e) 50 min, (f) 60 min, (g) 90 min, (h) 120 min, (i) 180 min, (j) 240 min, (k) 360 min, (l) 540 min, (m) 720 min, (n) 900 min, (o) 1080 min, and (p) 1440 min at Seoul station.

4 Construction of Future IDF Curves Considering Climate Change

4.1 Data

As described in the previous chapter, it is feasible to construct the IDF relations by the proposed scaling GEV method for the current climate using the available AMP data at Seoul station for the present (1961-1999) period. The present chapter deals with the constructions of these relations in consideration of different climate change scenarios using the spatial-temporal downscaling method suggested by Nguyen et al. (2007). This downscaling method is a combination of a spatial downscaling of daily precipitation process for describing the linkage between global climate predictors and the daily rainfall process at a local site and a temporal downscaling of daily AMPs to sub-daily AMPs at the study site. Further detail of this spatial-temporal downscaling procedure can be found in the paper by Nguyen et al. (2007)

In the present study, climate scenarios given by two popular Global Circulation Models were selected in this study: the scenarios A2 and A1B given by the Canadian GCM version 3 (denoted by CGCM3A2 and CGCM3A1B, respectively), and the A2 and B2 scenarios given by the UK Hadley Centre's GCM model (denoted by HadCM3A2 and HadCM3B2, respectively). In addition, the spatial downscaling of the daily AMPs was performed using the Statistical Downscaling Model (SDSM) proposed by Wilby et al. (2002) for Seoul station. More specifically, a dataset of 100 simulations of daily precipitation time series have been produced for Seoul station for the current (1961-1999) period as well as for future periods for different selected climate scenarios: 2020's (2010-2039), 2050's (2040-2069), and 2080's (2070-2099). The daily AMP data were then extracted from each of these 100 simulations, and the median values of the extracted 100 daily AMP series represent the downscaled daily AMP given by each given climate scenario of the two selected GCMs.

4.2 Application of the Spatial-Temporal Downscaling Method

As described by Nguyen et al. (2007), it is expected that the spatially downscaled AMPs at a local site using the SDSM are biased as shown for instance by Figure 4.1 for

Seoul station (the observed daily AMPs lie far above the spread of the 100 spatially downscaled AMP time series from the HadCM3). It is hence necessary to perform a bias-correction of these spatially downscaled AMPs in order to obtain a good agreement with the observed daily AMPs at a given site. Therefore, the downscaled AMPs will be adjusted by adding an amount called the "residual" that represents the difference between the downscaled and observed daily AMPs. The residual is computed by the following equation:

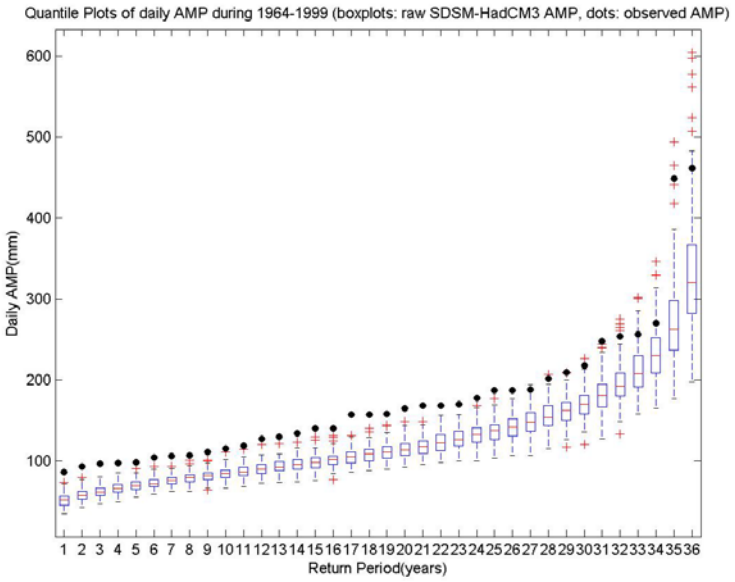

Figure 4.1 ***Box-plots of 100 HadCM3 simulations compared with observed values (black points) for 1964-1999. The tops and bottoms of each "box" are the 25th and 75th percentiles of the data, respectively. The distances between the tops and bottoms are the interquartile ranges, and the line in the middle of each box is the median. The whiskers are lines extending above and below each box, and the red + signs are outliers. Both simulated and observed data are sorted in ascending order before plotted.***

$$e_\tau = x_\tau - \hat{y}_\tau \tag{4.1}$$

where e_τ is the residual, x_τ is the observed data, and $\hat{y}_\tau$ is the downscaled GCMs for the same return period τ. According to Nguyen et al. (2007), the residual can be estimated

from a second order polynomial relation as follows:

$$e_\tau = m_0 + m_1 \hat{y}_\tau + m_2 \hat{y}_\tau^{\,2} + \varepsilon \quad (4.2)$$

where m_0, m_1, and m_2 are parameters of the regression function, and ε is the resulting error term. After the residual is estimated, downscaled GCMs are adjusted by adding the residual to themselves as

$$y_\tau = \hat{y}_\tau + e_\tau \quad (4.3)$$

4.3 Results and Discussion

Figure 4.2 shows the difference (residual) between the spatially-downscaled annual maximum daily precipitations (AMDPs) from the HadCM3 and the observed values for Seoul station. A correction of this difference is hence necessary. Figure 4.3 shows the best fit of the 2nd order nonlinear regression curve to the residuals (Equation 4.2) with very high values of coefficient of determination (R^2) for CGCM3, HadCM3A2, and HadCM3B2 ($R^2 > 0.872$). After making the adjustment of the bias using this second-order function, the adjusted downscaled AMDPs did agree very well to the observed AMDPs as shown in Figure 4.4. Finally, Figure 4.5 shows the distributions of the downscaled AMDPs before and after adjustment as compared with the empirical distribution of the observed AMDPs. It can be seen that the adjustment (or bias correction) has provided a better agreement between the downscaled and observed AMDPs.

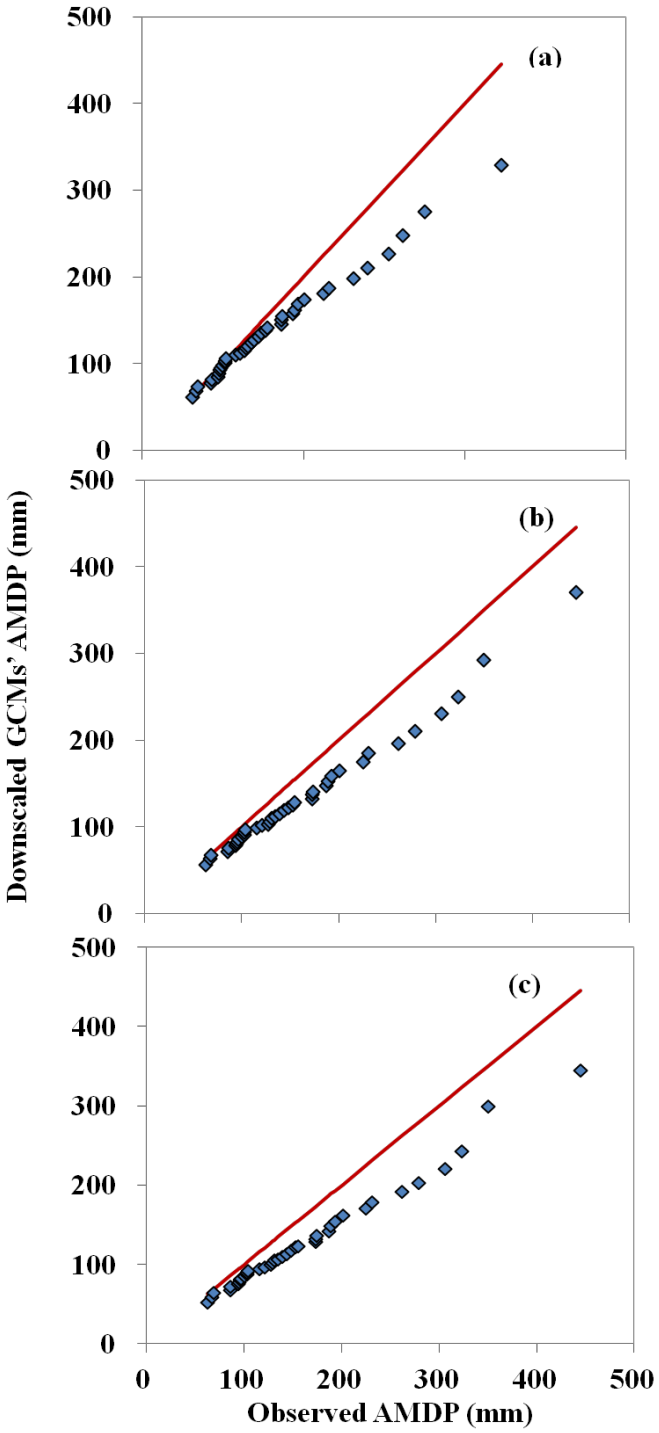

Figure 4.2 ***Q-Q plots of SDSM-downscaled GCM annual maximum daily precipitation (AMDP) vs. observed AMDP, respectively for CGCM3(a), HadCM3A2(b), and HadCM3B2(c), Seoul station, 1961-1999 data period***

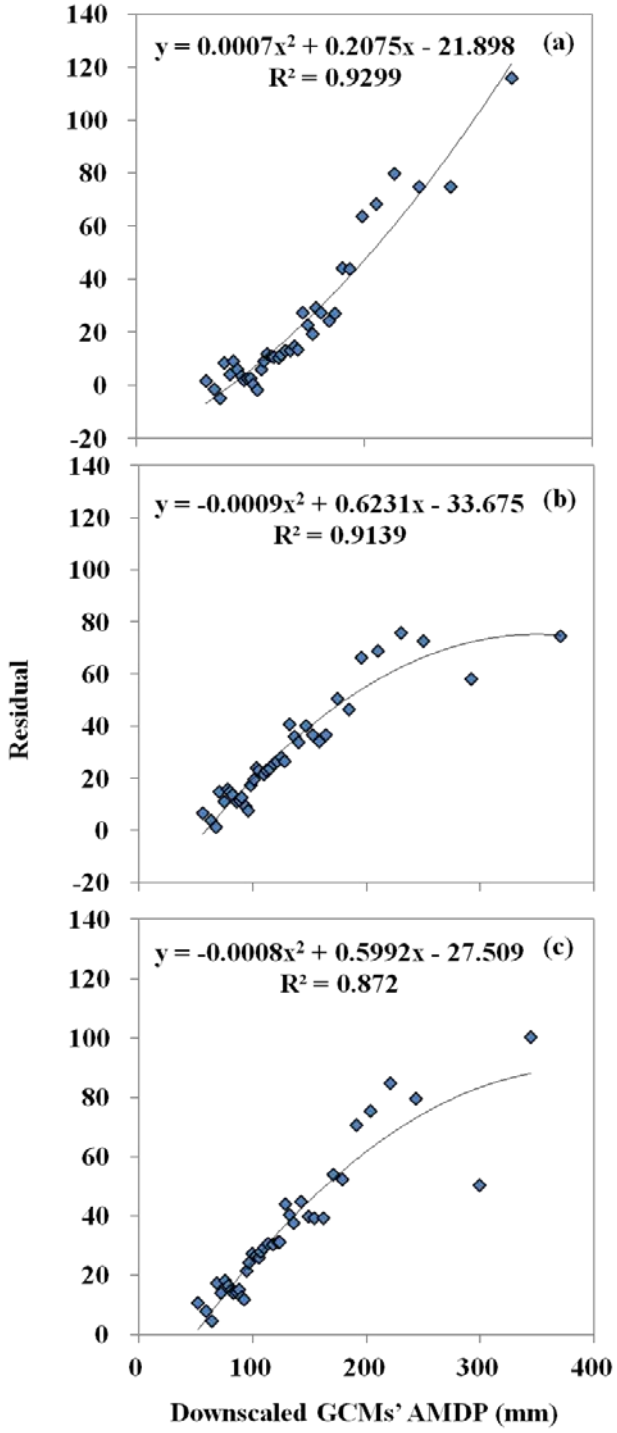

Figure 4.3 Plots of residual vs. downscaled GCM AMDP, along with 2nd-order nonlinear regression curve, for CGCM3(a), HadCM3A2(b), and HadCM3B2(c), Seoul, 1961-1999.

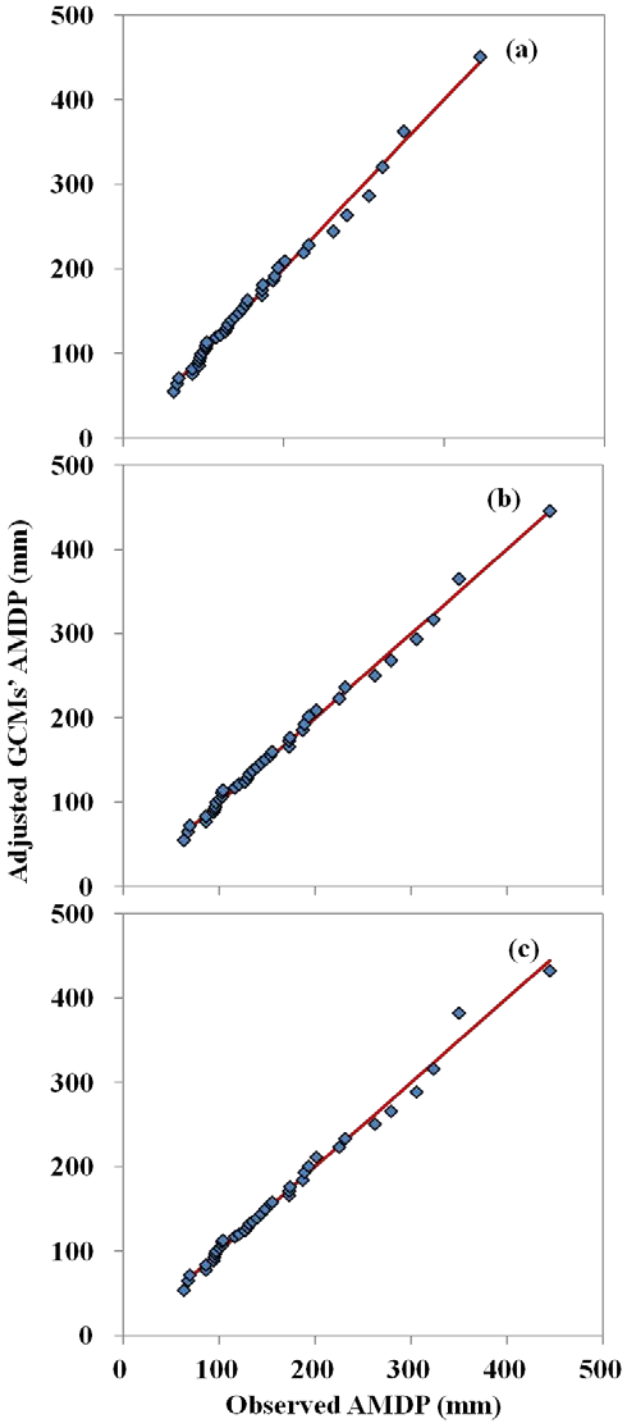

Figure 4.4 Q-Q plots of adjusted GCM annual maximum daily precipitation (AMDP) vs. observed AMDP, respectively for CGCM3(a), HadCM3A2(b), and HadCM3B2(c), Seoul station, 1961-1999 data period.

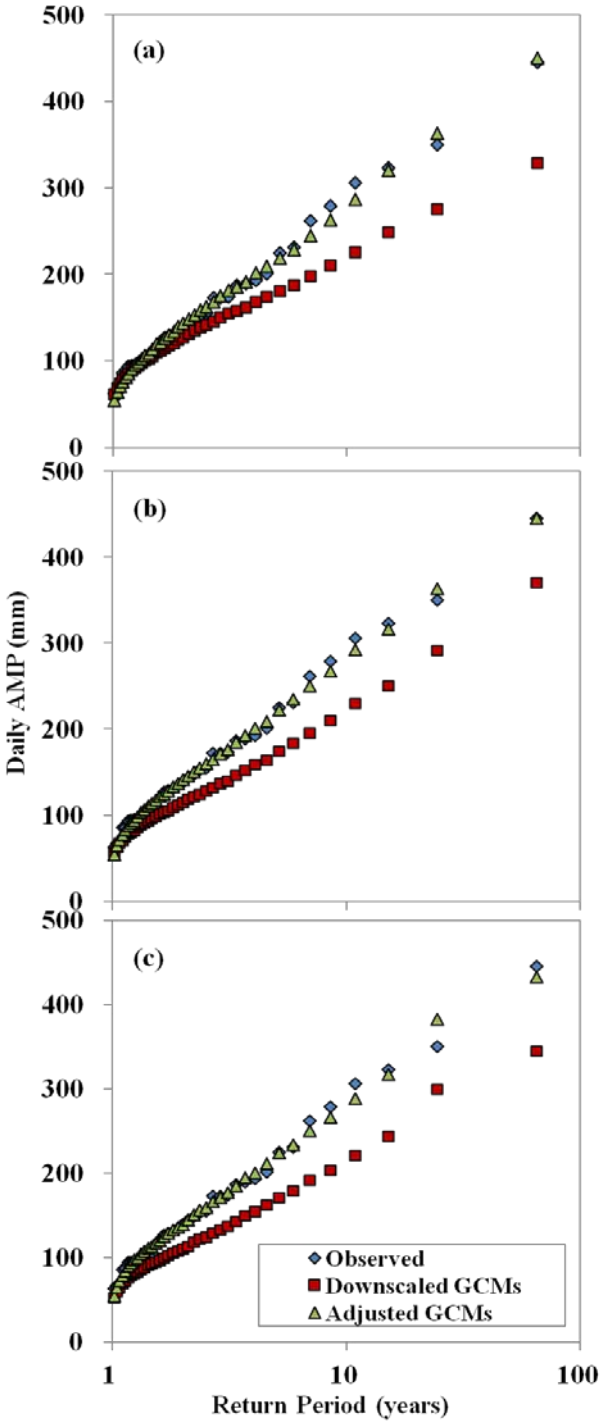

Figure 4.5 Distribution of AMDP, before and after adjustment, together with observed AMDP, CGCM3(a), HadCM3A2(b), and HadCM3B2(c), Seoul station, 1961-1999 data period.

In the previous section, the bias-correction method has contributed to an

improvement in the goodness-of-fit between the downscaled and observed AMDPs. However, the validity of the bias-correction for the current period should be tested for making the appropriate correction of the AMDPs for future periods. More specifically, for the first step, the observed AMP for the 1961-1999 period for Seoul station was split into two series: one from 1961 to 1986 (26 years) for calibration and the other from 1987 to 1999 (13 years) for validation. The fitted 2^{nd} order correction function for the calibration period will then be applied to the data of the validation period for making necessary adjustment. Finally, the improvement in the agreement between adjusted AMPs and observed AMPs for the validation period will be assessed.

As described above, using the fitted second-order correction function for the 1961-1986 calibration period (Figure 4.6) at Seoul station a significant improvement of the agreement between downscaled and observed AMDPs has been achieved as shown in Figure 4.7. Similar improvements have been found for other stations as presented in Table 4.1.

The fitted correction function for the calibration period is now used to make correction of bias of the downscaled AMDPs for the 1987-1999 validation period as shown in Figure 4.8. In general, it can be seen that the correction function estimated for the calibration period did improve the agreement between the downscaled and observed AMDPs for the validation period. However, as expected this improvement is less significant than the improvement achieved for the calibration period. Similar results were found for most of the 14 Korean stations considered (Table 4.2). In summary, the bias correction is necessary to improve the good match between the downscaled AMPs and the observed values at a local site for both calibration and validation periods.

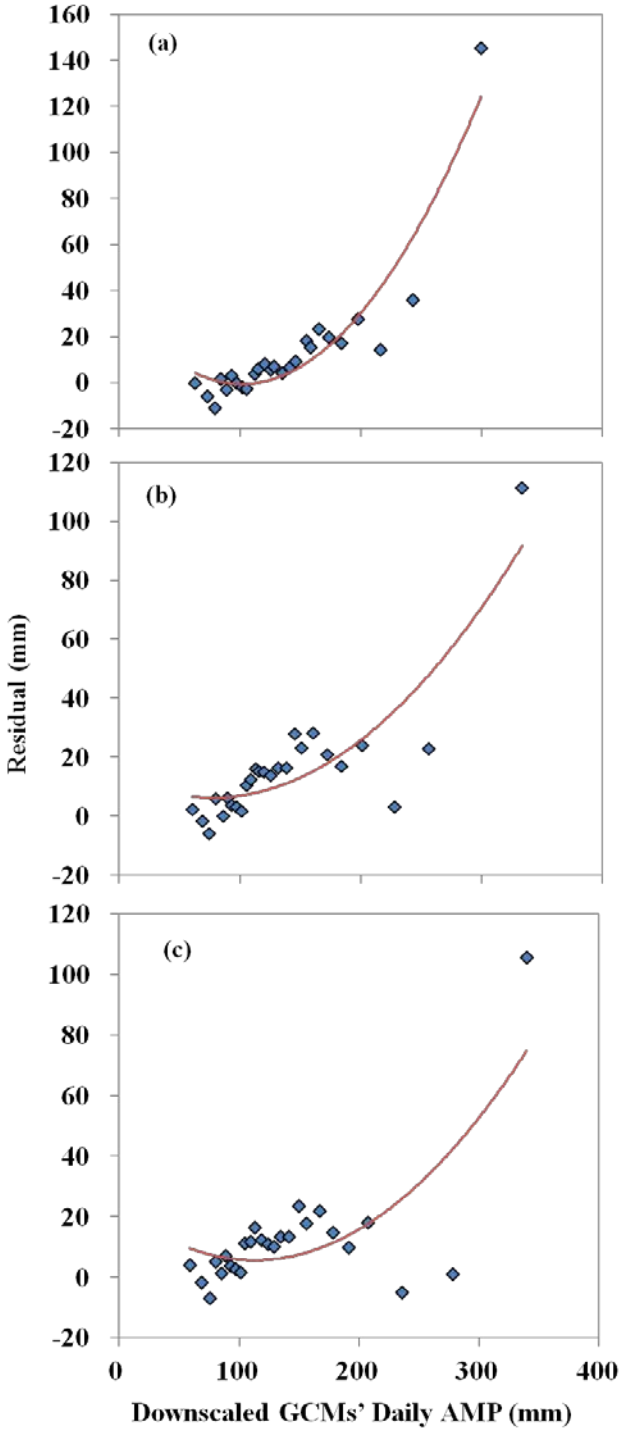

Figure 4.6 Residuals of GCM downscaled annual maximum daily precipitation (AMDP) from observed AMDP, plotted against AMDP estimated by CGCM3A2(a), HadCM3A2(b), and HadCM3B2(c).

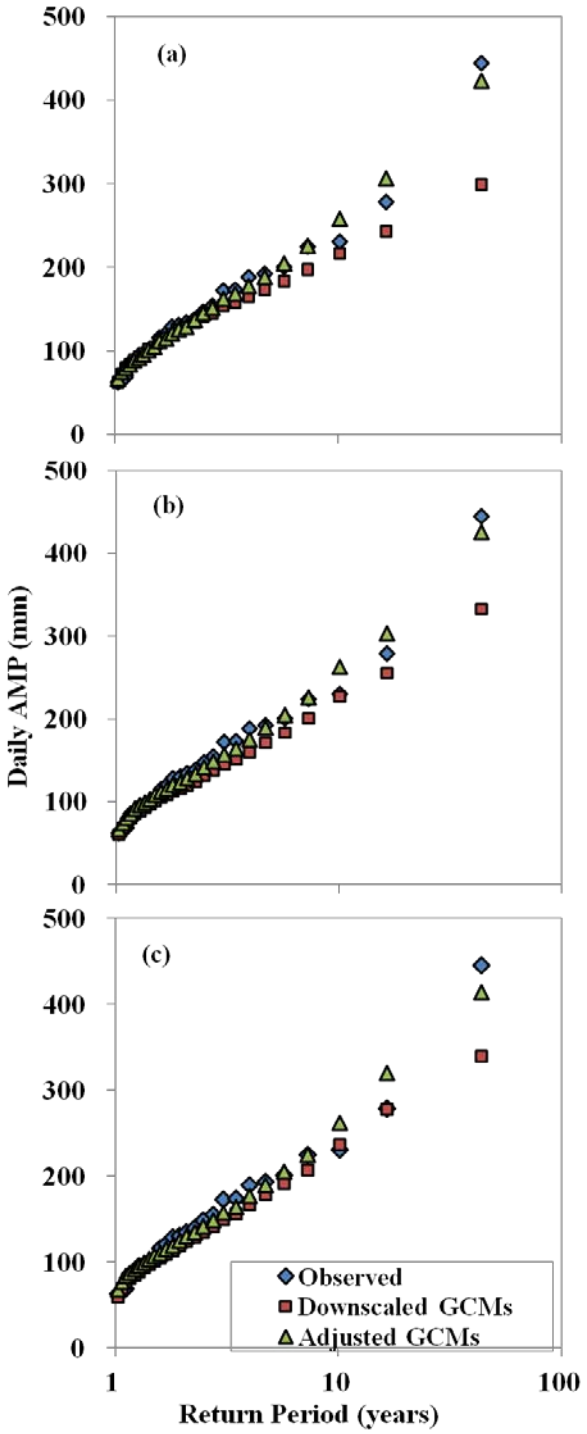

Figure 4.7 ***Distribution of downscaled GCM AMDP before and after adjustment, along with observed AMDP for calibration period (1961-1986) of Seoul, CGCM3A2(a), HadCM3A2(b), and HadCM3B2(c).***

Table 4.1 ***RRMSE values of AMDP estimates without and with bias-correction for 14 Korean stations during the calibration period (1961-1986). Bold values indicate smaller errors.***

Station	C3A2		C3A1B		H3A2		H3B2	
	before correction	after correction	before correction	after correction	before correction	after correction	before correction	after correction
Seoul	0.098	**0.061**	0.092	**0.071**	0.104	**0.069**	0.090	**0.079**
Suwon*	0.335	**0.058**	0.335	**0.058**	0.322	**0.060**	0.319	**0.059**
Incheon	0.205	**0.066**	0.205	**0.066**	0.332	**0.058**	0.335	**0.066**
Gangreung	0.306	**0.071**	0.306	**0.071**	0.142	**0.073**	0.142	**0.074**
Daegu	0.145	**0.055**	0.145	**0.055**	0.373	**0.057**	0.384	**0.051**
Busan	0.353	**0.085**	0.353	**0.085**	0.147	**0.074**	0.139	**0.066**
Gwangju	0.075	**0.039**	0.078	**0.040**	0.162	**0.040**	0.152	**0.044**
Jeonju**	0.250	**0.051**	0.256	**0.051**	0.333	**0.063**	0.329	**0.063**
Mokpo	0.214	**0.110**	0.214	**0.110**	0.324	**0.090**	0.343	**0.093**
Pohang	0.197	**0.071**	0.197	**0.071**	0.300	**0.072**	0.306	**0.078**
Yeosu	0.429	**0.076**	0.429	**0.076**	0.248	**0.061**	0.255	**0.064**
Chupungryong	0.086	**0.058**	0.086	**0.058**	0.205	**0.054**	0.190	**0.052**
Ulsan	0.384	**0.111**	0.384	**0.111**	0.251	**0.113**	0.257	**0.111**
Choengju***	0.061	**0.043**	0.064	**0.041**	0.249	**0.041**	0.240	**0.042**

* Calibration period for Suwon is 1964-1987.

** Calibration period for Jeonju is 1970-1989.

*** Calibration period for Cheongju is 1967-1988.

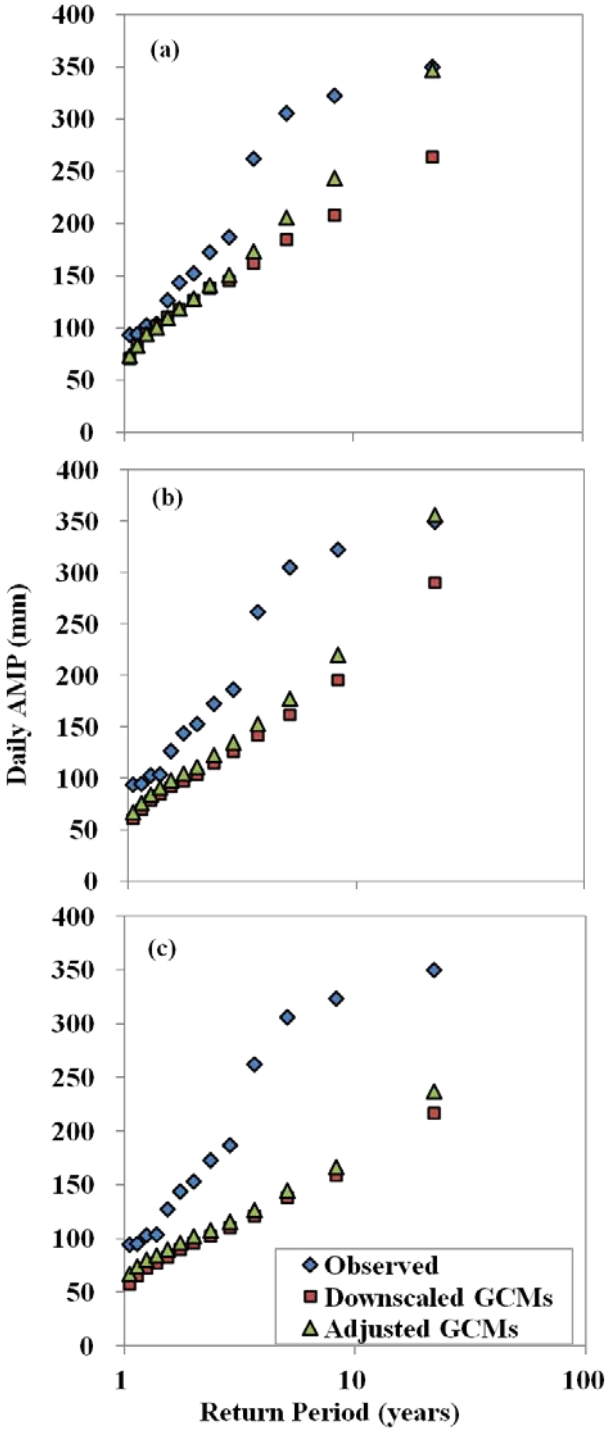

Figure 4.8 Distribution of downscaled GCM AMDP before and after adjustment, along with observed AMDP for validation period (1987-1999) of Seoul, CGCM3A2(a), HadCM3A2(b), and HadCM3B2(c).

Table 4.2 ***RRMSE values of AMDP estimates without and with bias-correction for 14 Korean stations during the validation period (1987-1999). Bold values present less errors of estimated AMDP to the observed AMDP.***

Station	C3A2		C3A1B		H3A2		H3B2	
	before correction	after correction	before correction	after correction	before correction	after correction	before correction	after correction
Seoul	0.238	**0.195**	0.256	**0.234**	0.328	**0.273**	0.406	**0.362**
Suwon*	0.458	**0.203**	0.458	**0.203**	0.435	**0.185**	0.438	**0.195**
Incheon	0.298	**0.156**	0.298	**0.156**	0.487	**0.278**	0.507	**0.316**
Gangreung	0.380	**0.149**	0.380	**0.149**	0.133	**0.085**	0.136	**0.058**
Daegu	0.116	0.124	0.116	0.124	0.359	**0.113**	0.366	**0.118**
Busan	0.294	**0.244**	0.294	**0.244**	0.114	0.170	0.131	0.155
Gwangju	0.144	**0.118**	0.158	**0.128**	0.162	**0.102**	0.169	**0.119**
Jeonju**	0.113	0.279	0.130	0.326	0.134	0.408	0.146	0.385
Mokpo	0.198	0.207	0.198	0.207	0.426	**0.227**	0.432	**0.229**
Pohang	0.274	**0.156**	0.274	**0.156**	0.395	**0.165**	0.354	**0.138**
Yeosu	0.296	0.314	0.296	0.314	0.254	0.344	0.207	0.269
Chupungryong	0.162	**0.184**	0.162	**0.184**	0.368	**0.182**	0.354	**0.201**
Ulsan	0.361	**0.194**	0.361	**0.194**	0.335	0.495	0.265	0.442
Choengju***	0.209	0.225	0.236	0.260	0.489	**0.315**	0.492	**0.325**

* Validation period for Suwon is 1988-1999.

** Validation period for Jeonju is 1990-1999.

*** Validation period for Cheongju is 1989-1999.

4.3.1 Distributions of Annual Maximum Daily Precipitations in the Context of Climate Change

As mentioned previously, the AMDPs were extracted from the 100 downscaled daily precipitation time series for Seoul station for the current (1961-1999) period as well as for future periods for different selected climate scenarios (CGCM3A2, CGCM3A1B, HadCM3A2, and HadCM3B2). The median values of the extracted 100 daily AMP series represent the downscaled daily AMP at Seoul station for each given climate scenario. For the present study, the future period is divided into 3 phases: 2010-2039 (2020's), 2040-2079 (2050's), and 2080-2099 (2080's) so that changes in the precipitation pattern caused by climate variability can be studied and compared among these periods.

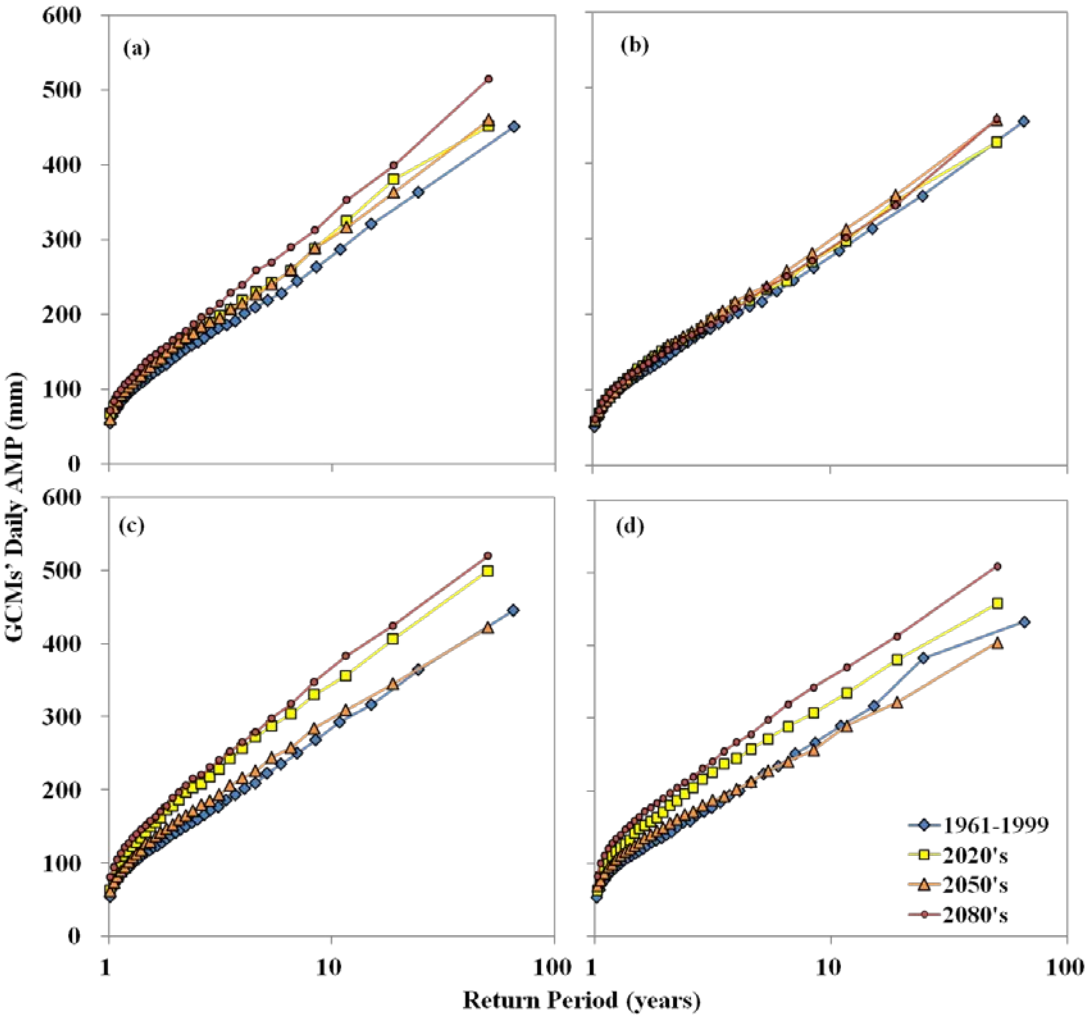

Figure 4.9 Distributions of AMDPs for current period and for future periods: 2020's, 2050's, and 2080's estimated by CGCM3A2 (a), CGCM3A1B (b), HadCM3A2 (c), and HadCM3B2 (d).

Figure 4.9 illustrates the changing distributions of AMDPs, estimated from two GCMs and three scenarios. Firstly, different GCMs generate different patterns; (a) and (b) derived from CGCM3 show narrower gaps among the distributions, while (c) and (d) from HadCM3 show broader gaps among the distributions. However, one common feature of all models is the increase of AMDP in the future and the highest amount in the 2080's. Specifically with the CGCM3A2 projection, the AMDP amount increases in the 2020's, stays the same in the 2050's, and further increases in the 2080's. For the CGCM3A1B projection, the AMDP amount gradually increases from the current level. The HadCM3 projection (Figure 4.9 (c) and (d)) shows an increase in the 2020's, a

decrease in the 2050's, followed by a relatively big increase in the 2080's for both A2 and B2 scenarios. Especially in the HadCM3B2 case, the AMDP amount in the 2050's becomes similar to the current amount in high return periods. Consequently, the GCMs give different projection results, but agree on a gradual increase of AMDPs at Seoul under climate change.

4.3.2 Temporal Downscaling of Daily AMP to Sub-Daily Durations

Once the future daily AMP series is provided, the scaling property, discussed in section 2.3.4, allows deriving sub-daily AMPs, which can then be used to construct IDF relations in consideration of climate change for future periods. To examine the scaling property from the current period (1961-1999), the observed AMP data over 16 rainfall durations is used. Figure 4.10 shows the log-log plot of the first three computed NCMs against rainfall durations. Graphically, two linear relationships are displayed; the first one for shorter durations and the second one for longer durations. Table 4.3 presents the values of scaling exponents and their quantities in relation to the order of the moments that are used to determine the type of scaling property – simple scaling or multi-scaling. For this purpose, the scaling exponents are plotted against the order of moment as shown in Figure 4.11, and the relationship is almost perfectly linear, showing high value of the coefficients of determination – 0.9999 and 0.9996. Hence, the AMP series at Seoul station has a simple scaling property.

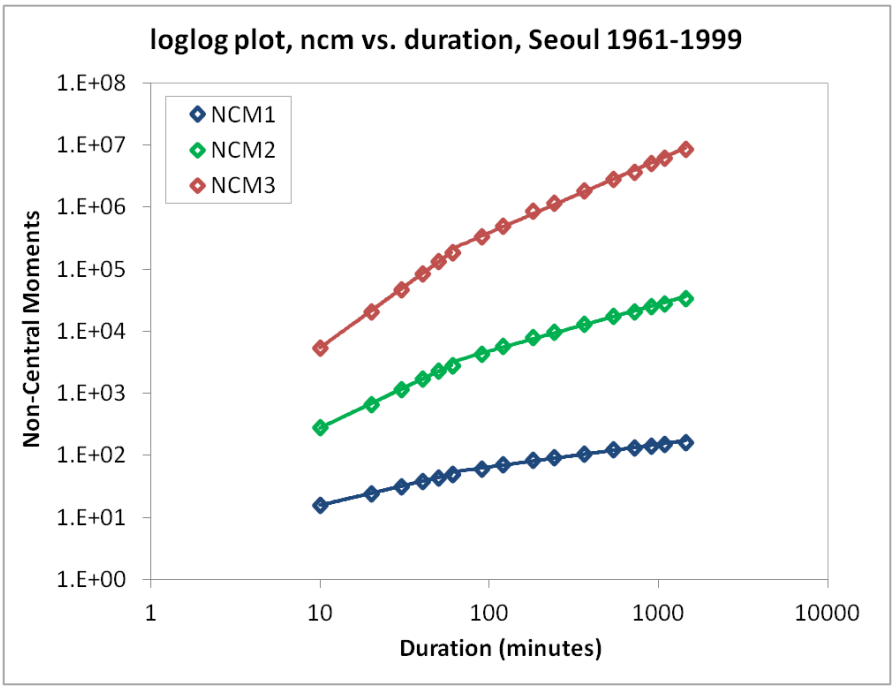

Figure 4.10 Log-log plot of the first three NCMs against rainfall durations, Seoul stations for 1961-1999 period.

Table 4.3 Scaling exponent values corresponding to order of NCM and duration intervals, Seoul stations for 1961-1999 period.

Interval of duration (minutes)	Order of NCM		
	1	2	3
10 - 60	0.642	1.301	1.980
60 - 1440	0.366	0.758	1.178

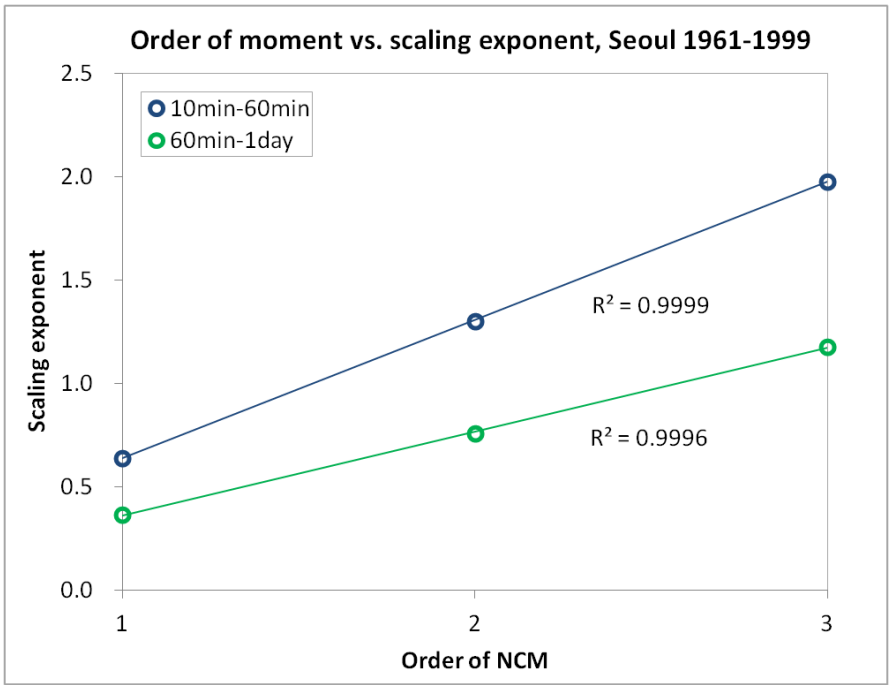

Figure 4.11 Plot of scaling exponent vs. order of NCM in two duration intervals, Seoul station, 1961-1999 period.

Using the simple scaling property explained above, future sub-daily AMPs are derived from the future daily AMP series in order to construct IDF curves for the periods 2010-2039 (2020's), 2040-2069 (2050's), 2070-2099 (2080's) as well as the current period. In Figure 4.12, IDF curves of the 4 periods are plotted in one graph so that one can easily examine its evolution. A measure of frequency – return periods – are selected as happening once in every 2 and 50 years to avoid confusion that arises from a large number of points in a graph. These graphs are provided to show the change of AMPs rather than to give an exact estimation of AMP. Similar to the previous section's result, the AMPs over all durations increases from the current level and shows the highest level in the 2080's. Also, CGCM3 estimates (Figure 4.12 (a) and (b)) show less evolution than HadCM3 estimates (Figure 4.12 (c) and (d)). IDF curves of a 2-year return period show similar evolution behaviour over the four models – though the rates are different. AMP intensity increases in the 2020's, decreases in the 2050's, followed by a large increase in the 2080's. IDF curves of a 50-year return period, however, show different evolution patterns throughout the four models. For more exact comparison, future IDF quantiles are presented in Table 4.4 (a) and (b). Generally, HadCM3 projects more intense AMPs

compared to CGCM3, even though they project under the same A2 scenario. However, similar evolution procedures are detected throughout the 4 model projections, which is an "increase then decrease followed by another increase" behaviour. One interesting point is the greater evolution of the less extreme AMP – as return period years decrease, evolution rates become greater.

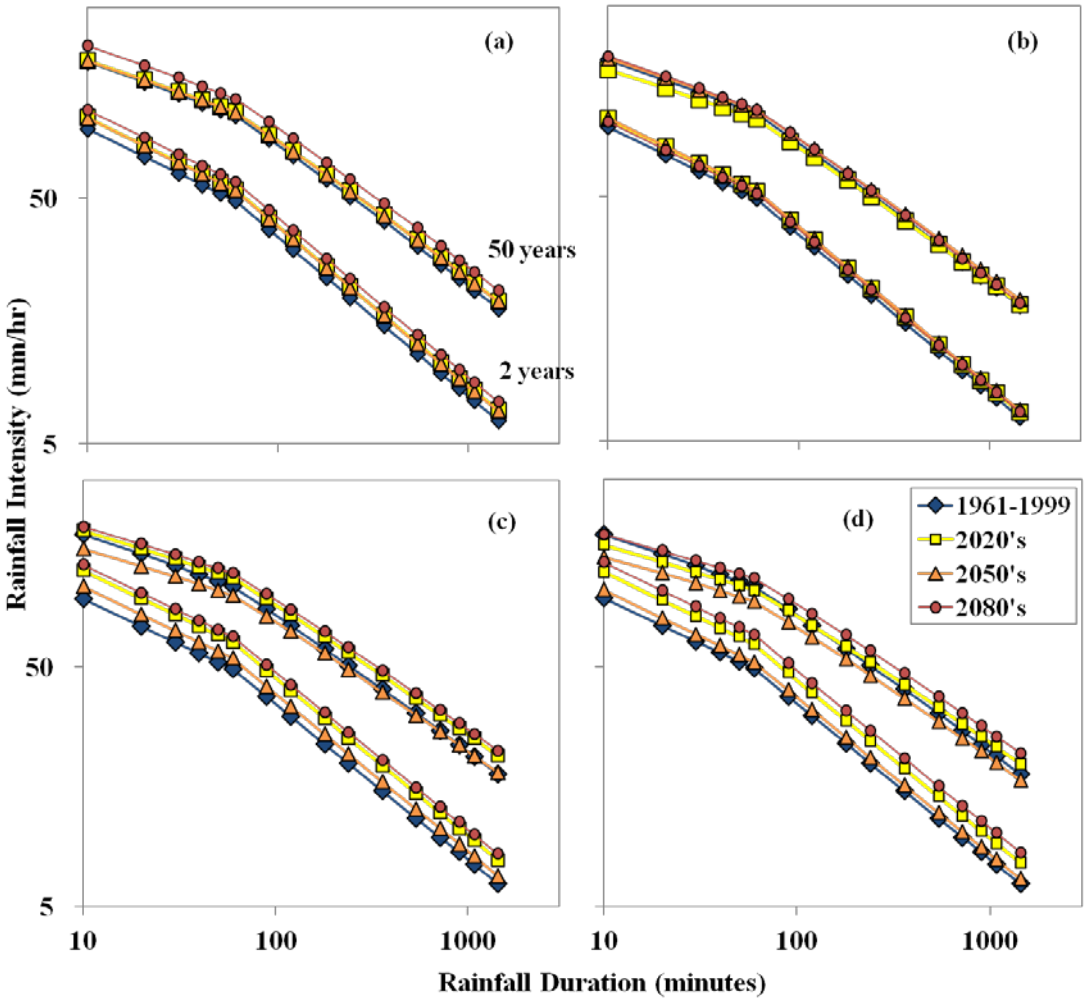

Figure 4.12 IDF curves (50-year and 2-year return periods) of four periods for Seoul station estimated by CGCM3A2 (a), CGCM3A1B (b), HadCM3A2 (c), and HadCM3B2 (d).

Table 4.4 AMP quantiles for Seoul station estimated by (a) CGCM3A2.

GCMs	Periods	Return years	Rainfall Duration (minutes)															
			10	20	30	40	50	60	90	120	180	240	360	540	720	900	1080	1440
CGCM3 A2	1961 -1999	50	171.1	140.1	124.2	114.0	106.5	100.8	80.3	68.3	54.2	45.9	36.3	28.6	24.1	21.1	18.9	15.9
		25	160.8	130.1	114.6	104.7	97.6	92.1	72.8	61.5	48.5	40.9	32.2	25.2	21.2	18.6	16.6	14.0
		5	127.3	99.9	86.6	78.3	72.4	67.8	52.6	43.9	34.0	28.4	22.0	17.1	14.3	12.5	11.1	9.3
		2	95.9	73.8	63.3	56.8	52.3	48.8	37.4	31.0	23.8	19.7	15.1	11.7	9.7	8.4	7.5	6.2
	2020's	50	175.4	144.9	129.1	118.8	111.3	105.4	84.5	72.0	57.3	48.7	38.6	30.6	25.9	22.7	20.3	17.1
		25	167.5	136.6	120.8	110.6	103.2	97.5	77.4	65.6	51.8	43.8	34.5	27.1	22.8	20.0	17.9	15.1
		5	138.4	108.8	94.5	85.4	79.0	74.1	57.4	47.9	37.2	31.0	24.0	18.6	15.5	13.5	12.1	10.1
		2	107.2	82.2	70.5	63.2	58.1	54.2	41.5	34.3	26.3	21.8	16.7	12.8	10.7	9.2	8.2	6.8
	2050's	50	175.0	144.5	128.7	118.4	110.9	105.1	84.1	71.7	57.1	48.5	38.4	30.4	25.7	22.5	20.2	17.0
		25	166.9	136.0	120.3	110.1	102.7	97.1	77.0	65.2	51.5	43.5	34.3	27.0	22.7	19.9	17.8	15.0
		5	137.5	108.1	93.8	84.8	78.4	73.5	57.0	47.6	36.9	30.8	23.9	18.5	15.4	13.5	12.0	10.1
		2	106.4	81.6	70.0	62.8	57.7	53.9	41.2	34.1	26.1	21.7	16.6	12.8	10.6	9.2	8.2	6.8
	2080's	50	199.9	164.1	145.8	133.8	125.2	118.5	94.6	80.5	63.9	54.2	42.9	33.9	28.6	25.0	22.4	18.9
		25	188.9	153.1	135.1	123.5	115.1	108.7	86.0	72.8	57.4	48.4	38.1	29.9	25.2	22.0	19.7	16.6
		5	151.5	118.9	103.2	93.2	86.2	80.8	62.6	52.3	40.5	33.8	26.2	20.3	17.0	14.8	13.2	11.1
		2	115.0	88.4	75.8	68.0	62.5	58.4	44.7	37.0	28.4	23.5	18.1	13.9	11.6	10.0	8.9	7.4

Table 4.4 AMP quantiles for Seoul station estimated by (b) CGCM3A1B.

GCMs	Periods	Return years	Rainfall Duration (minutes)															
			10	20	30	40	50	60	90	120	180	240	360	540	720	900	1080	1440
CGCM3 A1B	1961 -1999	50	171.0	140.0	124.2	113.9	106.5	100.8	80.3	68.3	54.2	45.9	36.3	28.6	24.1	21.1	18.9	15.9
		25	160.7	130.0	114.6	104.7	97.5	92.0	72.8	61.5	48.5	40.9	32.2	25.2	21.2	18.6	16.6	14.0
		5	127.3	99.9	86.6	78.2	72.3	67.8	52.6	43.9	34.0	28.4	22.0	17.1	14.3	12.5	11.1	9.3
		2	95.9	73.8	63.3	56.8	52.3	48.8	37.4	31.0	23.8	19.7	15.1	11.7	9.7	8.4	7.5	6.2
	2020's	50	159.5	132.6	118.6	109.3	102.6	97.3	78.2	66.8	53.4	45.4	36.1	28.6	24.2	21.3	19.1	16.1
		25	153.9	126.2	112.0	102.7	96.0	90.7	72.2	61.3	48.5	41.0	32.4	25.5	21.5	18.8	16.9	14.2
		5	130.9	103.2	89.6	81.1	75.0	70.3	54.6	45.6	35.3	29.5	22.8	17.7	14.8	12.8	11.5	9.6
		2	103.5	79.3	67.9	60.8	55.9	52.2	39.9	33.0	25.3	20.9	16.0	12.3	10.2	8.8	7.8	6.5
	2050's	50	175.2	144.3	128.5	118.1	110.6	104.7	83.8	71.4	56.8	48.2	38.2	30.2	25.6	22.4	20.1	16.9
		25	166.7	135.6	119.8	109.6	102.3	96.6	76.6	64.8	51.2	43.2	34.0	26.8	22.5	19.7	17.7	14.9
		5	136.2	107.0	92.8	83.9	77.6	72.8	56.4	47.1	36.5	30.4	23.6	18.3	15.3	13.3	11.9	9.9
		2	104.3	80.1	68.6	61.6	56.6	52.8	40.4	33.5	25.7	21.3	16.3	12.5	10.4	9.0	8.0	6.7
	2080's	50	176.9	144.9	128.6	117.9	110.2	104.3	83.1	70.7	56.1	47.5	37.6	29.5	24.9	21.8	19.5	16.4
		25	166.1	134.4	118.5	108.2	100.9	95.2	75.2	63.6	50.1	42.3	33.3	26.1	21.9	19.2	17.2	14.5
		5	131.8	103.4	89.7	81.1	75.0	70.3	54.5	45.5	35.3	29.5	22.9	17.8	14.9	13.0	11.6	9.7
		2	100.4	77.3	66.3	59.6	54.8	51.2	39.2	32.5	25.0	20.7	15.9	12.3	10.2	8.9	7.9	6.6

Table 4.4 AMP quantiles for Seoul station estimated by (c) HadCM3A2.

GCMs	Periods	Return years	Rainfall Duration (minutes)															
			10	20	30	40	50	60	90	120	180	240	360	540	720	900	1080	1440
HadCM3 A2	1961 -1999	50	170.2	139.5	123.8	113.6	106.2	100.5	80.2	68.2	54.1	45.9	36.3	28.6	24.1	21.1	18.9	15.9
		25	160.3	129.8	114.4	104.5	97.4	91.9	72.7	61.5	48.5	40.9	32.2	25.3	21.2	18.6	16.6	14.0
		5	127.6	100.1	86.8	78.4	72.5	68.0	52.7	44.0	34.1	28.4	22.0	17.1	14.3	12.5	11.1	9.3
		2	96.2	74.0	63.5	57.0	52.4	48.9	37.5	31.0	23.8	19.7	15.2	11.7	9.7	8.4	7.5	6.2
	2020's	50	182.2	152.0	136.3	125.9	118.4	112.5	90.8	77.8	62.4	53.2	42.4	33.7	28.6	25.1	22.6	19.2
		25	177.8	146.5	130.3	119.8	112.1	106.2	84.9	72.2	57.3	48.6	38.4	30.3	25.6	22.4	20.1	16.9
		5	156.4	123.8	107.7	97.5	90.3	84.7	65.8	54.9	42.6	35.6	27.5	21.3	17.8	15.5	13.8	11.5
		2	126.1	96.5	82.6	73.9	67.9	63.3	48.3	39.9	30.5	25.2	19.3	14.8	12.3	10.6	9.4	7.8
	2050's	50	153.3	128.3	115.2	106.6	100.2	95.2	77.0	66.0	52.9	45.1	36.0	28.6	24.2	21.3	19.2	16.2
		25	149.8	123.7	110.2	101.4	94.9	89.9	71.9	61.2	48.6	41.2	32.5	25.7	21.7	19.0	17.0	14.4
		5	132.7	105.1	91.5	82.8	76.6	71.9	55.9	46.7	36.2	30.2	23.4	18.1	15.1	13.2	11.7	9.8
		2	108.2	82.7	70.8	63.4	58.2	54.3	41.4	34.2	26.1	21.6	16.6	12.7	10.5	9.1	8.1	6.7
	2080's	50	188.9	158.3	142.1	131.5	123.6	117.5	95.0	81.4	65.2	55.6	44.3	35.2	29.8	26.2	23.6	20.0
		25	184.4	152.4	135.8	124.9	117.0	110.8	88.5	75.3	59.8	50.7	40.0	31.6	26.6	23.4	21.0	17.7
		5	163.2	129.2	112.4	101.8	94.2	88.4	68.6	57.3	44.5	37.1	28.8	22.3	18.6	16.2	14.4	12.0
		2	133.2	101.9	87.1	78.0	71.6	66.8	51.0	42.1	32.2	26.7	20.4	15.7	13.0	11.2	10.0	8.3

Table 4.4 AMP quantiles for Seoul station estimated by (d) HadCM3B2.

GCMs	Periods	Return years	Rainfall Duration (minutes)															
			10	20	30	40	50	60	90	120	180	240	360	540	720	900	1080	1440
HadCM3 B2	1961 -1999	50	169.1	138.7	123.2	113.1	105.7	100.1	79.9	67.9	53.9	45.7	36.2	28.6	24.1	21.1	18.9	15.9
		25	159.6	129.3	114.0	104.2	97.1	91.7	72.6	61.4	48.4	40.8	32.1	25.2	21.2	18.6	16.6	14.0
		5	127.6	100.1	86.8	78.5	72.5	68.0	52.7	44.0	34.1	28.5	22.0	17.1	14.3	12.5	11.1	9.3
		2	96.5	74.1	63.6	57.1	52.5	49.0	37.5	31.1	23.8	19.8	15.2	11.7	9.7	8.4	7.5	6.2
	2020's	50	159.4	134.0	120.8	112.1	105.7	100.7	81.9	70.6	56.9	48.7	38.9	31.0	26.4	23.2	20.9	17.7
		25	157.4	130.9	117.2	108.2	101.5	96.4	77.5	66.2	52.8	44.9	35.6	28.1	23.8	20.9	18.7	15.8
		5	145.5	116.1	101.4	92.0	85.2	80.1	62.3	52.1	40.4	33.8	26.2	20.3	16.9	14.7	13.1	10.9
		2	123.6	94.6	80.9	72.4	66.4	61.9	47.1	38.9	29.7	24.5	18.8	14.4	11.9	10.3	9.1	7.6
	2050's	50	140.7	119.0	107.3	99.5	93.6	89.1	72.1	61.9	49.6	42.3	33.7	26.8	22.7	20.0	17.9	15.1
		25	137.9	114.9	102.7	94.5	88.6	84.0	67.2	57.2	45.4	38.5	30.4	24.0	20.3	17.8	15.9	13.4
		5	124.1	98.5	85.8	77.7	71.9	67.5	52.4	43.8	34.0	28.4	22.0	17.1	14.3	12.4	11.1	9.3
		2	104.1	79.5	68.0	60.9	55.9	52.2	39.8	32.9	25.2	20.9	16.0	12.3	10.2	8.8	7.8	6.5
	2080's	50	176.0	148.9	134.5	124.9	117.7	112.1	91.2	78.4	63.1	53.9	43.0	34.2	29.1	25.6	23.0	19.5
		25	173.5	144.9	129.8	119.8	112.4	106.6	85.6	73.0	58.1	49.3	39.1	30.8	26.1	22.9	20.5	17.3
		5	159.4	127.1	110.9	100.5	93.1	87.4	68.0	56.8	44.1	36.8	28.5	22.1	18.5	16.1	14.3	12.0
		2	135.7	103.7	88.6	79.3	72.8	67.8	51.7	42.7	32.6	27.0	20.7	15.9	13.2	11.4	10.1	8.4

4.3.3 Time-Changing Trends of AMP Simulated by GCMs Scenarios

Future projection of daily AMPs by four different GCMs scenarios shows distinct trend in their periods as shown in Figure 4.13 for the 50-year AMDP. At Seoul station, CGCM3 estimates future precipitation to be gradually increase, but it is emission scenario that differentiates trend in 2080's. While CGCM3A2 shows a continuous increase, CGCM3A1B shows a decrease. On the other hand, HadCM3 projection somewhat fluctuates, and time-changing trends are similar between two different emission scenarios – A2 and B2 as indicated in Figure 4. 13. The 50-year AMDPs for other stations are presented in Table 4.5.

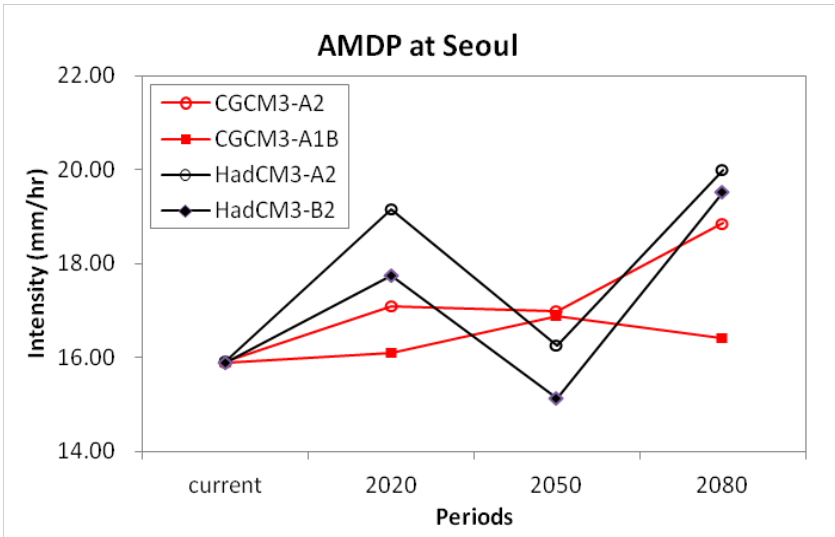

Figure 4.13 Trends of the 50-year AMDPs given by CGCM3A2, CGCMA1B, HadCM3A2, and HadCM3B2 scenarios for current, 2020's, 2050's, and 2080's for Seoul station.

Table 4.5 The 50-year return period daily AMP intensity simulated by CGCM3-A2, CGCM3-A1B, HadCM3-A2, and HadCM3-B2 for periods of current, 2020's, 2050's, and 2080's.

	CGCM3-A2				CGCM3-A1B			
Station	Current	2020's	2050's	2080's	Current	2020's	2050's	2080's
Seoul	15.90	17.10	16.99	18.86	15.90	16.10	16.88	16.42
Suwon	16.18	20.60	24.72	53.29	16.18	20.32	25.22	33.67
Incheon	14.42	15.47	16.81	18.93	14.42	15.74	16.53	17.26
Gangreung	13.62	15.41	14.74	15.44	13.62	14.80	15.48	15.18
Daegu	9.27	9.66	10.55	10.79	9.27	9.14	10.54	10.33
Busan	15.27	17.06	19.34	21.17	15.27	17.52	17.85	19.41
Gwangju	11.41	12.64	13.45	14.95	11.41	11.81	12.10	13.22
Jeonju	11.58	12.09	12.44	13.02	11.58	12.19	12.83	13.03
Mokpo	11.61	12.50	13.48	17.30	11.61	13.39	15.17	16.50
Pohang	10.98	12.28	12.33	12.47	10.98	11.60	10.97	11.33
Yeosu	13.24	15.78	15.04	17.47	13.24	16.84	15.43	18.62
Chupungryong	9.81	9.61	10.14	9.67	9.81	9.75	9.30	9.77
Ulsan	15.02	15.64	17.03	19.21	15.02	15.07	16.81	17.06
Cheongju	10.74	10.57	11.36	11.79	10.74	10.31	11.35	11.63
	HadCM3-A2				HadCM3-B2			
Station	Current	2020's	2050's	2080's	Current	2020's	2050's	2080's
Seoul	15.91	19.15	16.25	19.99	15.90	17.74	15.13	19.52
Suwon	16.16	19.20	19.02	21.50	16.17	18.65	17.46	18.26
Incheon	14.45	22.09	14.13	21.19	14.41	21.68	12.40	21.35
Gangreung	13.65	12.51	14.54	13.13	13.66	13.59	14.11	14.02
Daegu	9.29	10.54	9.25	10.89	9.29	10.84	9.26	10.77
Busan	15.34	15.51	17.24	18.88	15.31	16.17	17.42	20.25
Gwangju	11.40	10.97	11.43	12.71	11.39	12.50	11.34	13.36
Jeonju	11.59	11.50	12.22	12.94	11.59	13.37	11.42	13.42
Mokpo	11.65	16.55	12.06	16.13	11.67	18.95	12.38	17.20
Pohang	11.00	13.45	15.65	16.45	10.97	13.77	12.87	18.86
Yeosu	13.18	12.90	12.94	15.11	13.19	14.83	14.00	15.76
Chupungryong	9.81	7.95	9.52	9.44	9.81	8.71	11.05	9.69
Ulsan	14.99	8.65	12.46	10.41	15.05	9.29	15.02	10.96
Cheongju	10.74	13.52	11.11	13.27	10.75	13.59	10.65	14.00

5 Conclusion and Recommendations

5.1 Conclusions

The following main conclusions can be drawn from the present research:

Selection of the Best-fit Distribution

(1) By the method of L-moment ratio diagram, the GEV distribution was found to be the most suitable distribution to represent the distribution of AMPs for all 14 raingage stations in South Korea as compared to the GPA, GLO, LN3, and PE3.

Parameter and Quantile Estimation

(2) Both non-central moment (NCM) and L-moment methods provided comparable estimates of GEV parameters and quantiles. However, the NCM method was selected in the present study since the scale-invariance property of the NCMs is useful in the estimation of the sub-daily extreme rainfalls from the rainfall data of longer durations for downscaling purposes..

Scaling Property of Extreme Rainfall Processes

(3) The AMP processes at 14 stations in South Korea displayed a simple scaling behaviour. However, some stations (Seoul, Busan, Gwangju, Jeonju, and Chupungryong) have a similar scaling property (the break point of the log-linear relationship is located at the 60-minute duration), but other stations have a different scaling regime.

(4) On the basis of this simple scaling behaviour the sub-daily extreme rainfall statistical properties can be derived from the properties of extreme rainfalls of longer durations.

Construction of Intensity-Duration-Frequency (IDF) Curves

(5) It has been demonstrated that the scaling GEV method can be used to construct the IDF relations for a given location where AMP data for different durations are

available.

(6) It has been shown that the spatial-temporal downscaling method can be used to construct the IDF relations for current and future periods under different climate change scenarios.

(7) It was found that the second-order non-linear function can be used to make appropriate bias correction to improve the agreement between the spatially downscaled AMDPs and the observed empirical AMDPs a given local site for both calibration and validation periods.

(8) Spatially downscaled then bias-adjusted AMDPs have provided reasonable projection of future daily extreme rainfall patterns, indicating different trends depending on different climate change scenarios. In general, with AMP data from South Korean stations, HadCM3 showed fluctuating trends, while CGCM3 indicated a general increasing trend. Furthermore, the different projection results of AMP trends for future periods from different GCMs for the same climate scenario has indicated the high uncertainty of these models.

5.2 Recommendations for Future Study

(1) When scaling property was examined for the selected 14 Korean stations, a simple scaling behaviour of two different time intervals was detected, but some of these stations showed different scaling regimes. Considering the physical reason to explain the different scaling behaviours in terms of the rainfall dynamics and climatic conditions might be useful to delineate homogeneous regions for rainfall regional analyses, especially for the estimation of extreme rainfalls at locations with limited or without rainfall data.

(2) In this study, the scaling property of extreme rainfall processes was successfully integrated into the GEV distribution and the associated NCM parameter estimation method for the estimation of rainfall extremes over different durations. It is hence useful to consider more general statistical and stochastic models (such

as the peak-over-threshold models) that could take into account the properties of hydrologic processes at different time and spatial scales.

(3) The scaling-GEV technique can be categorized as a statistical temporal downscaling method, because it derives precipitation amounts in shorter temporal scales from the one in longer time scale based mainly on the statistical properties of the rainfall process. But, there are other dynamic downscaling methods that are strongly relying on the physical properties of the underlying rainfall process. The development of a combined statistical-dynamical downscaling method could be useful in this case.

(4) IDF curves are of practical use in hydrology field for the design of various hydraulic structures that require runoff estimation. Hence, from the constructed IDF curves for current and future climates, it is necessary to develop the linkage between the extreme rainfalls and the runoff characteristics (e.g., runoff peaks and volumes) in order to be able to propose appropriate design procedures in the context of climate variability and climate change.

(5) In the present study, the statistical properties of the annual maximum rainfall series have been considered as stationary (i.e., constant over time). However, due to climate change these properties might vary with time. It is hence necessary to develop an improved method for modeling and estimating extreme rainfalls in the context of nonstationarity.

References

BARA, M., KOHNOVÁ, S., GAÁL, L., SZOLGAY, J., and HLAVČOVÁ, K. (2009). "Estimation of IDF curves of extreme rainfall by simple scaling in Slovakia." *Contributions to Geophysics and Geodesy*, 39(3), 187-206.

Bendjoudi, H., Hubert, P., and Schertzer, D. (1997). "Interphation multifractale des prkipitations Multifractal curves." *Sciences-New York*, 323-326.

Boer, G. J., Arpe, K., Blackburn, M., Qui, M. D. I., Gates, W. L., Hart, T. L., Treut, H. L. E., Roeckner, E., Sheinin, D. A., Simmonds, I., Wetherald, R. T., and Williamson, D. (1992). "Some Results From an Intercomparison of the Climates Simulated by 14 Atmospheric General Circulation Models." *Journal of Geophysical Research*, 97(D12), 12771-12786.

Chen, H., Xu, C.-Y., and Guo, S. (2012). "Comparison and evaluation of multiple GCMs, statistical downscaling and hydrological models in the study of climate change impacts on runoff." *Journal of Hydrology*, 434-435, 36-45.

Choi, G., Collins, D., Ren, G., Trewin, B., Baldi, M., Fukuda, Y., Afzaal, M., Pianmana, T., and Gomboluudev, P. (2009). "Changes in means and extreme events of temperature and precipitation in the Asia-Pacific Network region, 1955 – 2007." *International Journal of Climatology*, 29, 1906-1925.

Choi, G., Kwon, W.-tae, Boo, K.-on, and Cha, Y.-M. (2008). "Recent Spatial and Temporal Changes in Means and Extreme Events of Temperature and Precipitation across the Republic of Korea." *Journal of the Korean Geographical society*, 43(5), 681-700.

Chow, V. T. (1964). *Handbook of applied hydrology; a compendium of water-resources technology*. McGraw-Hill, New York.

Chow, V. T., Maidment, D. R., and Mays, L. W. (1988). *Applied hydrology*. McGraw-Hill, New York.

Conway, D., Wilby, R. L., and Jones, P. D. (1996). “Precipitation and air flow indices over the British Isles.” *Climate Research*, 7, 169-183.

Cunnane, C. (1978). “Unbiased plotting positions — A review.” *Journal of Hydrology*, 37(3–4), 205-222.

Dalgaard, P. (2008). *Introductory statistics with R.* Springer.

Daniell, T. M., and Tabios, Q. Q. (Eds.). (2008). “Rainfall Intensity Duration Frequency (IDF) Analysis for the Asia Pacific Region.” *Asian Pacific FRIEND*, Jakarta.

Fowler, H. J., and Kilsby, C. G. (2003). “A regional frequency analysis of United Kingdom extreme rainfall from 1961 to 2000.” *International Journal of Climatology*, 23(11), 1313-1334.

Frich, P., Alexander, L. V., Gleason, B., Haylock, M., Tank, A. M. G. K., and Peterson, T. (2002). “Observed coherent changes in climatic extremes during the second half of the twentieth century.” *Climate Research*, 19, 193-212.

Gerold, L. A., and Watkins Jr., D. W. (2005). “Short Duration Rainfall Frequency Analysis in Michigan Using Scale-Invariance Assumptions.” *Water Resources*, (December), 450-457.

Gray, D. M. (1973). *Handbook on the principles of hydrology: With special emphasis directed to Canadian conditions in the discussions, applications, and presentation of data*. Water Information Center, inc.

Greenwood, J. A., Landwehr, J. M., Matalas, N. C., and Wallis, J R. (1979). “Probability weighted moments: Definition and relation to parameters of several distributions expressable in inverse form.” *Water Resour. Res.*, AGU, 15(5), 1049-1054.

Grubbs, F. E. (1969). “Procedures for Detecting Outlying Observations in Samples.” *Technometrics*, American Statistical Association and American Society for Quality, 11(1), 1-21.

Gutowski, W. J., Wilby, R. L., Hay, L. E., Anderson, C. J., Arritt, R. W., Clark, M. P., Leavesley, G. H., Pan, Z., Da Silva, R., and Takle, E. S. (2000). "Statistical and Dynamical Downscaling of Global Model Output for US National Assessment Hydrological Analyses." *11th Symposium on Global Change Studies*, Long Beach, CA.

Hirsch, R. M., Helsel, D. R., Cohn, T. A., and Gilroy, E. J. (1993). "Statistical Analysis of Hydrological Data." *Handbook of Hydrology*, David R Maidment, ed., McGraw-Hill.

Hosking, J. R. M. (1986). *The theory of probability weighted moments.* Yorktown Heights, NY.

Hosking, J. R. M. (1989). *Some theoretical results concerning L-moments*. Yorktown Heights, NY, 1-9.

Hosking, J. R. M. (1990). "L-Moments: Analysis and Estimation of Distributions Using Linear Combinations of Order Statistics." *Journal of the Royal Statistical Society. Series B (Methodological),* Blackwell Publishing for the Royal Statistical Society, 52(1), 105-124.

Hosking, J. R. M., Wallis, J.R., and Wood, E. F. (1985). "Estimation of the Generalized Extreme-Value Distribution by the Method of Probability-Weighted Moments." *Technometrics*, American Statistical Association and American Society for Quality, 27(3), 251-261.

IPCC. (2000). *Emissions Scenarios*. *Group*, pp 570.

IPCC. (2007). *Climate Change 2007: Synthesis Report*. *Change*, 12-17.

Khan, M. S., Coulibaly, P., and Dibike, Y. (2006). "Uncertainty analysis of statistical downscaling methods." *Journal of Hydrology*, 319, 357-382.

Kidson, J. W., and Thompson, C. S. (1998). “Comparison of statistical and model-based downscaling techniques for estimating local climate variations.” *Journal of Climate1*, 11, 735-753.

Kim, B. S., Kim, B. K., Kyung, M. S., and Kim, H. S. (2008). “Evaluation on Effects of Climate Change on Extreme Rainfall and I-D-F Analysis.” Journal of Korea Water Resources Association, 41(4), 379–394.(in Korean)

Klein Tank, A. M. G., Zwiers, F. W., and Zhang, X. (2009). “Guidelines on Analysis of extremes in a changing climate in support of informed decisions for adaptation.” *Climate Data and Monitoring*, World Meteorological Organization (WMO), 72.

Koutsoyiannis, D., Kozonis, D., and Manetas, A. (1998). “intensity-duration-frequency relationships.” *Science*, 206, 118-135.

Kwon, H. H., Kim, B. S., Kim, B. K., and Yun, S. Y. (2009). “Analysis of Changes in Temporal and Spatial Properties of Extreme Rainfall in Terms of Climate Change.” Conference Proceeding of Korea Water Resources Association, 1152–1155.(in Korean)

Langousis, A., and Veneziano, D. (2007). “Intensity-duration-frequency curves from scaling representations of rainfall.” *Water Resources Research*, 43(2).

Lee, D.-K., Kim, H.-R., and Hong, S.-Y. (1998). “Heavy Rainfall over Korea during 1980~1990.” *Korean Journal of the Atmospheric Sciences*, Korean Meteorological Society, 1(1), 32-50.

Lee, S. H., and Maeng, S. J. (2003). “FREQUENCY ANALYSIS OF EXTREME RAINFALL USING L-MOMENT y.” *Irrigation and Drainage*, 52, 219-230.

Mearns, L. O., Bogardi, L., Giorgi, F., Matyasovszky, I., and Palecki, M. (1999). “Comparison of climate change scenarios generated from regional climate model experiments and statistical downscaling.” *Journal of Geophysical Research*, 104, 6603-6621.

Menabde, M., Seed, A., and Pegram, G. (1999). “A simple scaling model for extreme rainfall.” *Water Resources Research*, 35(1), 335-339.

Na, Y. S. (2010). “Study of Design Storm and Flood Changes in Terms of Climate Change.” SeJong University.(in Korean)

De Michele, C., Kottegoda, N. T., and Rosso, R. (2001). “The derivation of areal reduction factor of storm rainfall from its scaling properties.” *Water Resour. Res.*, AGU, 37(12), 3247-3252.

Murphy, J. (1999). “An evaluation of statistical and dynamical techniques for downscaling local climate.” *Journal of Climate*, 12, 2256-2284.

Nadarajah, S., and Choi, D. (2007). “Maximum daily rainfall in South Korea.” *Journal of Earth System Science*, 116(4), 311-320.

Nguyen, T.D. (2004). “Regional Estimation of Extreme Rainfall Events.” McGill University.

Nguyen, V. T. V., Nguyen, T D, and Wang, H. (1998). “Regional estimation of short duration rainfall extremes.” *Water Science and Technology*, 37(11), 15-19.

Nguyen, V.-T.-V., Nguyen, T.D., and Ashkar, F. (2002). “Regional frequency analysis of extreme rainfalls.” *Water Science and Technology*.

Nguyen, V.-T.-V., Nguyen, T.-D., and Gacon, P. (2006). “On the linkage of large-scale climate variability with local characteristics of extremes: an evaluation of statistcal downscaling methods.” *Advances in Geosciences*, 4(16), 1-9.

Nguyen, V.-T.-V., Nguyen, T.D., and Cung, A. (2007). “A statistical approach to downscaling of sub-daily extreme rainfall processes for climate-related impact studies in urban areas.” *Water Science and Technology: Water Supply*.

Nguyen, V.-T.-V., and Pandey, G. R. (1994). “Estimation of Short-Duration Rainfall Distribution Using Data Measured at Longer Time Scales.” *Water Science and Technology*, 29(1-2), 39-45.

Park, J., and Jung, H. (2002). “Modelling Korean extreme rainfall using a Kappa distribution and maximum likelihood estimate.” *Theoretical and Applied Climatology*, 64, 55-64.

Park, J.-S., Kang, H.-S., Lee, Y. S., and Kim, M.-K. (2011). “Changes in the extreme daily rainfall in South Korea.” *International Journal of Climatology*, 31, 2290-2299.

Pierce, D., Das, T., Cayan, D., Maurer, E., Miller, N., Bao, Y., Kanamitsu, M., Yoshimura, K., Snyder, M., Sloan, L., Franco, G., and Tyree, M. (2012). “Probabilistic estimates of future changes in California temperature and precipitation using statistical and dynamical downscaling.” *Climate Dynamics*, Springer Berlin / Heidelberg, 1-18.

Pilon, P., Adamowski, K., and Alila, Y. (1991). “Regional analysis of annual maxima precipitation using L-moments.” *Atmospheric Research*, 27(1-3), 81-92.

Prudhomme, C., Reynard, N., and Crooks, S. (2002). “Downscaling of global climate models for flood frequency analysis: where are we now?” *Hydrological Processes*, 16(6), 1137-1150.

Richardson, C.W., and Wright, D. A. (1981). *WGEN: A model for generating daily weather variables*. U.S. Dept. of Agriculture, Agricultural Research Service.

Semenov, M. A., Brooks, R. J., Barrow, Elaine M., and Richardson, Clarence W. (1998). “Comparison of the WGEN and LARS-WG stochastic weather generators for diverse climates.” *Climate Research*, 10, 95-107.

Semenov, M. A., and Barrow, E.M. (1997). “Use of Stochastic Weather Generator in the Development of regional climate change impacts.” *Climatic Change*, 35, 397-414.

Stedinger, J. R., Vogel, R. M., and Foufoula-Georgiou, E. (1993). “Frequency analysis of extreme events.” *Handbook of Hydrology*, McGraw-Hill, New York.

Tao, Q. (2001). “Statistical Modelling of Extreme Precipitation in Southern Quebec.” McGill University.

Veneziano, Daniele, and Furcolo, P. (2002). “Multifractality of rainfall and scaling of intensity- duration-frequency curves.” *Water Resources Research*, 38(12), 1-12.

Washington, W. M., and Meehl, G. A. (1989). “Climate sensitivity due to increased CO2: experiments with a coupled atmosphere and ocean general circulation model.” *Climate Dynamics*, 4, 1-38.

Wetterhall, F., Bárdossy, A., Chen, D., S., H., and C., X. (2007). “Daily precipitation-downscaling techniques in three Chinese regions.” *Water Resources Research*, 42.

Wilby, R. L., Dawson, C. W., and Barrow, E.M. (2002). “SDSM - a decision support tool for the assessment of regional climate chagne impacts.” *Environmetnal Modeling & Sofrware*, 17, 147-159.

Wilby, R., Hay, L., Gutowski, W., Takle, E., Pan, ZT, Leavesley, G., and Clark, M. (2000). “Hydrological responses to dynamically and statistically downscaled climate model output.” *Geophysical Research Letters*, 27, 1199-1202.

Yarnal, B., Comrie, A. C., Frakes, B., and Brown, D. P. (2001). “Developmetns and Prospects in Synoptic Climatology.” *International Journal of Climatology*, 21, 1923-1950.

Yu, P., Yang, T., and Lin, C. (2004). “Regional rainfall intensity formulas based on scaling property of rainfall.” *Journal of Hydrology*, 295(1-4), 108-123.

Appendix A

Table A. 1 Descriptive statistics for AMP data at Suwon station for 1964-1999

Duration	Basic Descriptive Statistics					
	Number of Data	Minimum (mm)	Maximum (mm)	Mean (mm)	Std. deviation (mm)	Skewness
10 min	36	6.40	27.50	15.58	4.78	0.49
20 min	36	10.80	36.60	23.97	6.68	0.28
30 min	36	14.00	47.00	30.74	8.47	0.26
40 min	36	18.00	57.00	35.91	9.47	0.40
50 min	36	20.00	65.00	39.73	10.61	0.43
1 hr	36	23.80	80.00	44.51	13.46	0.70
1.5 hr	36	29.20	94.00	53.73	17.86	0.60
2 hr	36	33.60	131.00	63.40	24.65	0.98
3 hr	36	37.40	171.00	76.82	32.05	1.27
4 hr	36	42.60	200.00	87.80	37.70	1.36
6 hr	36	49.70	220.00	103.09	43.09	1.22
9 hr	36	63.00	308.00	123.03	52.76	1.73
12 hr	36	72.20	341.00	135.99	60.78	1.96
15 hr	36	73.30	378.00	147.04	67.70	2.05
18 hr	36	74.20	395.00	153.78	70.94	2.07
1 day	36	85.80	462.00	173.76	85.58	2.07

Table A. 2 Descriptive statistics for AMP data at Incheon station for 1952-1999

Duration	Basic Descriptive Statistics					
	Number of Data	Minimum (mm)	Maximum (mm)	Mean (mm)	Std. deviation (mm)	Skewness
10 min	48	6.00	24.30	14.28	4.73	0.34
20 min	48	8.00	43.30	22.32	8.26	0.65
30 min	48	10.50	56.80	28.43	11.39	0.81
40 min	48	12.00	70.40	33.75	13.55	0.88
50 min	48	13.00	82.00	38.23	15.48	0.91
1 hr	48	13.50	103.00	42.65	17.77	1.18
1.5 hr	48	15.00	123.00	52.77	22.73	1.17
2 hr	48	16.50	139.00	61.36	28.06	1.17
3 hr	48	17.50	164.00	71.47	32.98	1.28
4 hr	48	24.00	204.00	80.47	36.63	1.45
6 hr	48	28.50	258.00	94.32	44.02	1.60
9 hr	48	31.50	297.00	108.41	52.19	1.54
12 hr	48	51.50	338.00	119.61	58.95	1.61
15 hr	48	53.90	349.00	126.00	63.18	1.59
18 hr	48	56.30	353.00	132.06	64.98	1.51
1 day	48	57.40	372.00	141.93	72.85	1.67

Table A. 3 Descriptive statistics for AMP data at Gangreung station for 1958-1999

Duration	Basic Descriptive Statistics					
	Number of Data	Minimum (mm)	Maximum (mm)	Mean (mm)	Std. deviation (mm)	Skewness
10 min	42	3.90	21.60	10.54	4.17	0.51
20 min	42	7.00	40.00	15.97	6.48	1.14
30 min	42	8.50	44.00	20.58	7.87	0.61
40 min	42	9.70	45.80	23.74	8.99	0.57
50 min	42	10.90	54.00	26.78	10.29	0.62
1 hr	42	12.40	62.00	29.53	11.37	0.75
1.5 hr	42	15.10	86.00	36.25	14.51	1.25
2 hr	42	18.00	105.00	42.72	18.37	1.60
3 hr	42	24.40	142.00	55.72	24.03	1.72
4 hr	42	29.00	165.00	65.72	28.03	1.90
6 hr	42	34.20	207.00	81.50	35.93	1.81
9 hr	42	35.20	245.00	99.91	45.26	1.41
12 hr	42	39.70	260.00	115.10	52.45	1.17
15 hr	42	42.90	270.00	129.59	58.15	0.91
18 hr	42	46.90	286.00	141.04	62.22	0.84
1 day	42	48.20	328.00	158.28	69.99	0.83

Table A. 4 Descriptive statistics for AMP data at Daegu station for 1916-1999

Duration	Basic Descriptive Statistics					
	Number of Data	Minimum (mm)	Maximum (mm)	Mean (mm)	Std. deviation (mm)	Skewness
10 min	84	4.60	44.40	12.67	5.79	2.20
20 min	84	7.10	44.40	19.63	8.44	0.93
30 min	84	10.50	56.70	24.71	10.14	0.89
40 min	84	12.50	66.90	28.95	11.43	0.98
50 min	84	14.60	79.20	32.16	12.66	1.22
1 hr	84	14.70	80.90	34.94	13.84	1.17
1.5 hr	84	19.70	99.90	41.83	16.71	1.21
2 hr	84	21.90	111.90	46.89	17.97	1.07
3 hr	84	24.60	121.00	54.53	20.98	0.86
4 hr	84	27.00	130.00	60.09	23.28	0.89
6 hr	84	29.50	140.50	68.87	27.02	0.93
9 hr	84	30.00	182.40	78.49	32.29	1.18
12 hr	84	35.50	194.30	86.04	35.50	1.13
15 hr	84	38.00	212.10	92.47	38.19	1.01
18 hr	84	41.50	220.80	98.16	40.08	0.94
1 day	84	43.80	249.70	109.58	45.01	0.82

Table A. 5 Descriptive statistics for AMP data at Busan station for 1948-1999

Duration	Basic Descriptive Statistics					
	Number of Data	Minimum (mm)	Maximum (mm)	Mean (mm)	Std. deviation (mm)	Skewness
10 min	52	4.10	40.00	14.33	6.22	1.32
20 min	52	4.30	51.00	21.58	9.60	0.85
30 min	52	4.30	56.10	27.99	12.47	0.68
40 min	52	4.30	71.10	34.23	16.09	0.66
50 min	52	4.30	80.00	38.80	17.93	0.53
1 hr	52	4.30	88.50	43.37	20.10	0.48
1.5 hr	52	5.50	103.00	53.01	23.78	0.32
2 hr	52	5.60	114.00	60.73	26.35	0.21
3 hr	52	5.60	160.00	75.29	32.64	0.31
4 hr	52	9.70	174.00	86.55	37.39	0.25
6 hr	52	11.50	213.00	103.63	44.60	0.35
9 hr	52	12.20	304.00	121.32	55.30	0.74
12 hr	52	12.20	370.00	133.15	62.82	1.20
15 hr	52	12.20	406.00	143.32	68.43	1.25
18 hr	52	12.20	439.00	150.10	73.26	1.31
1 day	52	43.40	444.00	158.12	75.63	1.28

Table A. 6 Descriptive statistics for AMP data at Gwangju station for 1939-1999

Duration	Basic Descriptive Statistics					
	Number of Data	Minimum (mm)	Maximum (mm)	Mean (mm)	Std. deviation (mm)	Skewness
10 min	61	5.50	23.00	13.99	4.56	0.22
20 min	61	9.10	39.00	21.39	6.99	0.56
30 min	61	10.00	50.00	27.56	8.86	0.35
40 min	61	12.40	60.00	32.10	10.94	0.54
50 min	61	14.20	67.00	35.63	12.30	0.53
1 hr	61	15.30	68.50	38.62	13.37	0.45
1.5 hr	61	18.90	94.20	46.17	16.13	0.84
2 hr	61	20.80	103.00	51.77	18.59	0.86
3 hr	61	24.00	141.00	61.31	22.37	1.16
4 hr	61	28.70	183.00	69.30	25.49	1.73
6 hr	61	34.20	219.00	83.41	31.56	1.73
9 hr	61	38.20	244.00	96.99	37.11	1.53
12 hr	61	40.10	276.00	105.97	41.50	1.63
15 hr	61	51.20	301.00	112.39	44.88	1.77
18 hr	61	54.70	327.00	118.95	48.35	1.86
1 day	61	55.60	336.00	129.94	52.09	1.43

Table A. 7 Descriptive statistics for AMP data at Jeonju station for 1970-1999

Duration	Basic Descriptive Statistics					
	Number of Data	Minimum (mm)	Maximum (mm)	Mean (mm)	Std. deviation (mm)	Skewness
10 min	30	6.60	21.00	13.91	4.13	0.02
20 min	30	11.20	36.00	21.78	6.49	0.29
30 min	30	12.00	49.50	29.23	9.67	0.28
40 min	30	18.20	59.00	35.47	11.31	0.35
50 min	30	20.70	64.50	39.91	12.44	0.19
1 hr	30	22.00	75.70	43.78	14.36	0.39
1.5 hr	30	24.00	91.50	53.40	17.86	0.30
2 hr	30	25.30	99.10	60.94	20.07	0.34
3 hr	30	31.40	133.00	72.14	24.46	0.66
4 hr	30	39.10	157.00	83.00	28.95	0.85
6 hr	30	46.00	197.00	98.98	34.42	1.02
9 hr	30	61.00	223.00	114.47	38.80	0.99
12 hr	30	71.00	250.00	127.24	41.82	0.96
15 hr	30	77.00	261.00	135.03	44.80	0.87
18 hr	30	77.00	277.00	141.64	48.11	0.90
1 day	30	77.00	291.00	154.21	51.56	0.80

Table A. 8 Descriptive statistics for AMP data at Mokpo station for 1923-1999

Duration	Basic Descriptive Statistics					
	Number of Data	Minimum (mm)	Maximum (mm)	Mean (mm)	Std. deviation (mm)	Skewness
10 min	77	4.80	22.00	12.78	4.19	0.17
20 min	77	7.30	33.50	19.38	6.43	0.33
30 min	77	8.90	42.70	24.55	7.70	0.21
40 min	77	9.50	47.70	28.40	8.67	0.07
50 min	77	10.30	51.00	31.36	9.26	0.01
1 hr	77	10.90	54.30	34.47	10.15	-0.01
1.5 hr	77	14.00	71.80	41.05	12.10	0.16
2 hr	77	16.40	82.30	47.51	14.05	0.15
3 hr	77	17.30	118.00	57.75	18.69	0.47
4 hr	77	26.10	138.00	65.80	22.45	0.62
6 hr	77	30.70	178.00	77.82	27.91	0.77
9 hr	77	33.00	259.00	91.69	36.56	1.41
12 hr	77	36.10	312.00	101.10	42.67	1.85
15 hr	77	41.00	348.00	108.34	45.26	2.20
18 hr	77	42.20	372.00	114.96	47.48	2.33
1 day	77	42.90	401.00	125.08	53.36	2.05

Table A. 9 Descriptive statistics for AMP data at Pohang station for 1954-1999

Duration	Basic Descriptive Statistics					
	Number of Data	Minimum (mm)	Maximum (mm)	Mean (mm)	Std. deviation (mm)	Skewness
10 min	46	2.90	24.50	10.37	4.35	0.92
20 min	46	5.30	29.60	15.23	5.70	0.77
30 min	46	7.70	40.30	19.74	7.72	0.77
40 min	46	10.20	46.50	23.28	8.75	0.71
50 min	46	10.80	53.00	25.93	9.59	0.71
1 hr	46	11.70	57.50	29.03	10.83	0.73
1.5 hr	46	18.00	66.00	35.52	11.94	0.72
2 hr	46	21.90	85.90	40.58	13.10	1.04
3 hr	46	27.50	123.00	49.54	16.21	1.95
4 hr	46	30.40	143.00	56.84	18.91	2.14
6 hr	46	35.10	163.00	68.72	23.07	1.91
9 hr	46	43.20	195.00	82.09	31.02	1.66
12 hr	46	50.50	205.00	92.29	36.64	1.53
15 hr	46	56.50	226.00	100.58	40.87	1.60
18 hr	46	56.80	265.00	107.93	43.83	1.63
1 day	46	61.10	348.00	121.72	52.48	2.04

Table A. 10 Descriptive statistics for AMP data at Yeosu station for 1952-1999

Duration	Basic Descriptive Statistics					
	Number of Data	Minimum (mm)	Maximum (mm)	Mean (mm)	Std. deviation (mm)	Skewness
10 min	48	4.50	26.00	13.84	4.10	0.65
20 min	48	6.00	40.00	21.15	6.73	0.53
30 min	48	8.00	50.00	27.42	9.12	0.49
40 min	48	10.00	60.00	32.77	11.44	0.64
50 min	48	11.00	69.00	36.54	13.50	0.75
1 hr	48	13.00	74.20	40.81	14.94	0.63
1.5 hr	48	19.00	92.50	48.78	17.27	0.68
2 hr	48	22.00	123.00	56.39	20.93	0.96
3 hr	48	33.00	168.00	70.13	26.80	1.30
4 hr	48	35.60	183.00	80.44	31.02	1.04
6 hr	48	37.70	219.00	95.14	36.78	1.04
9 hr	48	42.20	249.00	113.00	42.15	0.97
12 hr	48	42.20	283.00	125.98	46.98	1.12
15 hr	48	42.20	317.00	135.47	51.57	1.32
18 hr	48	42.20	322.00	142.87	54.36	1.22
1 day	48	69.60	331.00	156.38	60.20	1.11

Table A. 11 Descriptive statistics for AMP data at Chupungryong station for 1955-1999

Duration	Basic Descriptive Statistics					
	Number of Data	Minimum (mm)	Maximum (mm)	Mean (mm)	Std. deviation (mm)	Skewness
10 min	45	5.10	20.70	12.16	3.69	-0.04
20 min	45	8.00	28.60	17.15	5.03	0.45
30 min	45	10.50	39.00	21.80	6.55	0.44
40 min	45	14.30	42.00	25.36	7.53	0.41
50 min	45	16.20	48.50	28.54	8.66	0.45
1 hr	45	18.30	54.50	31.76	9.75	0.47
1.5 hr	45	19.50	81.20	37.84	13.13	1.14
2 hr	45	23.00	89.00	42.90	14.25	1.30
3 hr	45	27.00	103.00	50.25	15.66	1.42
4 hr	45	31.00	111.00	57.51	17.03	0.95
6 hr	45	36.40	123.00	69.12	21.07	0.66
9 hr	45	43.80	159.00	84.04	26.91	0.78
12 hr	45	50.10	167.00	93.55	28.60	0.77
15 hr	45	51.20	177.50	102.15	33.10	0.91
18 hr	45	52.80	205.50	109.47	37.24	1.05
1 day	45	65.50	255.50	122.78	44.92	1.10

Table A. 12 Descriptive statistics for AMP data at Ulsan station for 1954-1999

Duration	Basic Descriptive Statistics					
	Number of Data	Minimum (mm)	Maximum (mm)	Mean (mm)	Std. deviation (mm)	Skewness
10 min	46	4.20	23.00	12.67	4.31	0.13
20 min	46	7.50	43.00	19.31	7.82	0.94
30 min	46	8.50	56.00	24.58	10.81	0.89
40 min	46	9.10	68.50	28.98	13.23	1.02
50 min	46	10.60	75.00	32.38	14.91	1.06
1 hr	46	13.10	76.70	35.83	16.57	1.05
1.5 hr	46	18.60	100.00	44.94	21.66	0.92
2 hr	46	23.00	121.00	52.98	24.92	0.99
3 hr	46	26.10	150.00	64.97	30.61	1.10
4 hr	46	34.50	175.00	76.29	36.41	1.11
6 hr	46	42.50	232.00	95.55	44.40	1.11
9 hr	46	47.80	296.00	112.94	52.70	1.33
12 hr	46	48.30	352.00	125.31	59.28	1.70
15 hr	46	53.00	410.00	135.93	66.80	2.03
18 hr	46	55.60	434.00	143.37	72.24	2.16
1 day	46	59.80	458.00	154.93	76.34	2.30

Table A. 13 Descriptive statistics for AMP data at Cheongju station for 1967-1999

Duration	Basic Descriptive Statistics					
	Number of Data	Minimum (mm)	Maximum (mm)	Mean (mm)	Std. deviation (mm)	Skewness
10 min	33	7.00	29.00	15.48	4.97	0.28
20 min	33	8.50	42.10	22.73	7.55	0.31
30 min	33	9.70	47.20	27.92	9.00	0.01
40 min	33	11.50	53.50	32.62	10.61	-0.13
50 min	33	12.60	57.70	36.41	11.87	-0.19
1 hr	33	13.30	60.00	38.77	13.02	-0.10
1.5 hr	33	19.50	89.50	46.31	15.34	0.56
2 hr	33	24.50	102.00	50.73	17.32	0.96
3 hr	33	34.50	108.00	58.79	19.99	1.00
4 hr	33	40.50	173.00	68.67	26.51	2.17
6 hr	33	46.50	195.00	80.48	30.08	2.09
9 hr	33	54.60	213.00	96.19	36.09	1.77
12 hr	33	56.20	226.00	107.15	40.88	1.75
15 hr	33	56.90	282.00	115.92	48.08	1.79
18 hr	33	57.20	282.00	120.74	48.44	1.59
1 day	33	60.40	292.00	129.81	50.42	1.41

Appendix B

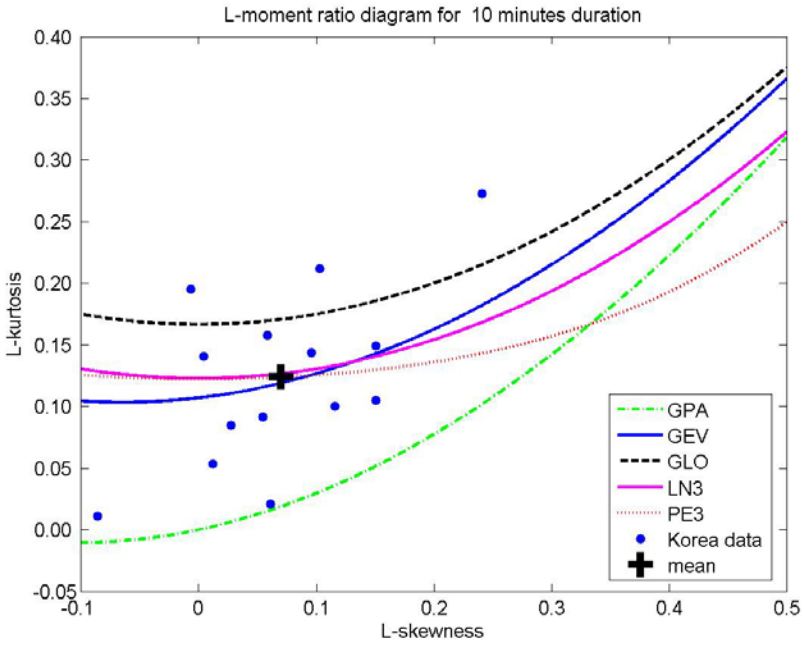

Figure B.1 L-moment ratio diagram for 10 minutes AMP in Korea

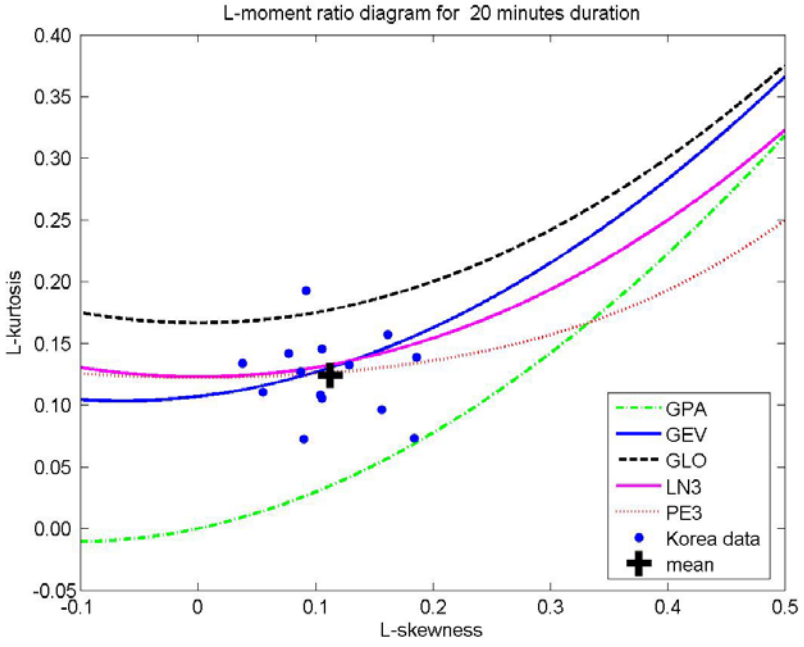

Figure B.2 L-moment ratio diagram for 20 minutes AMP in Korea

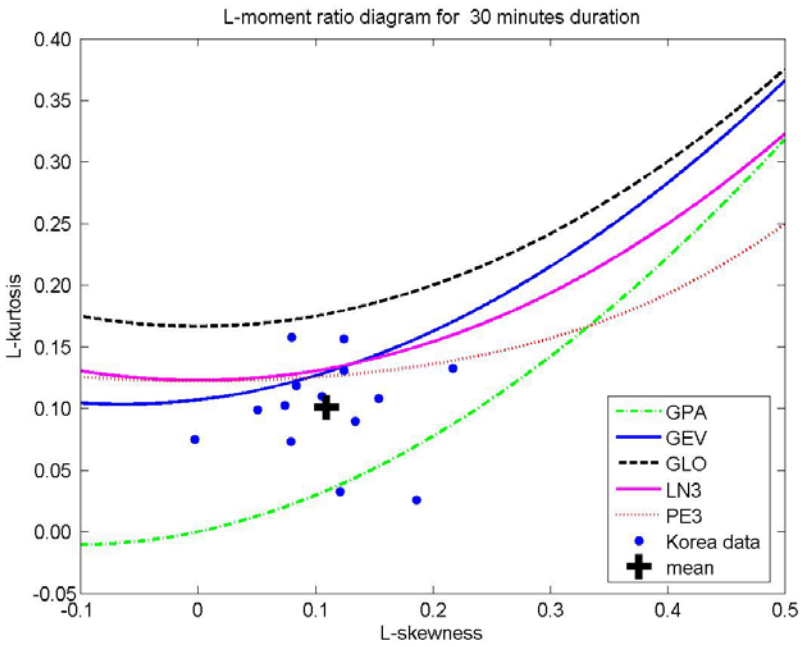

Figure B.3 L-moment ratio diagram for 30 minutes AMP in Korea

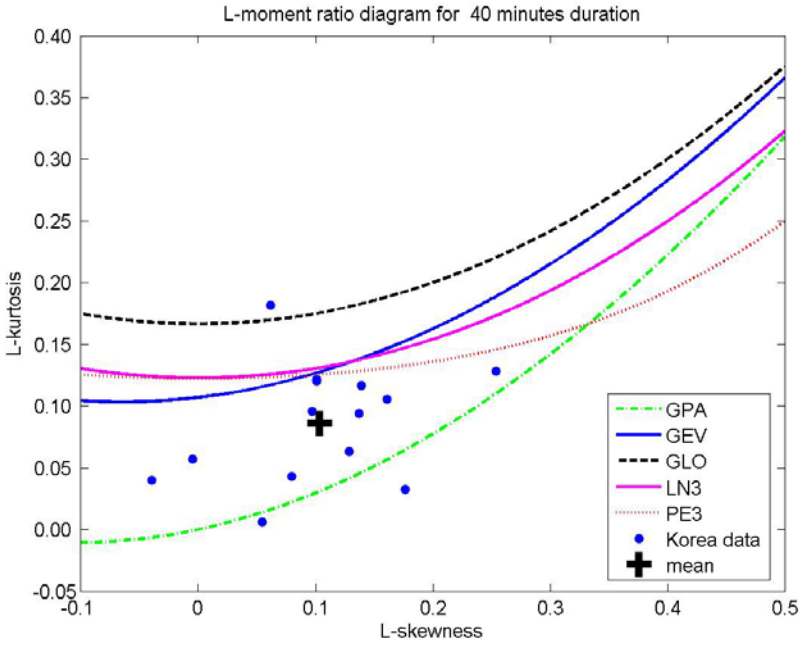

Figure B.4 L-moment ratio diagram for 40 minutes AMP in Korea

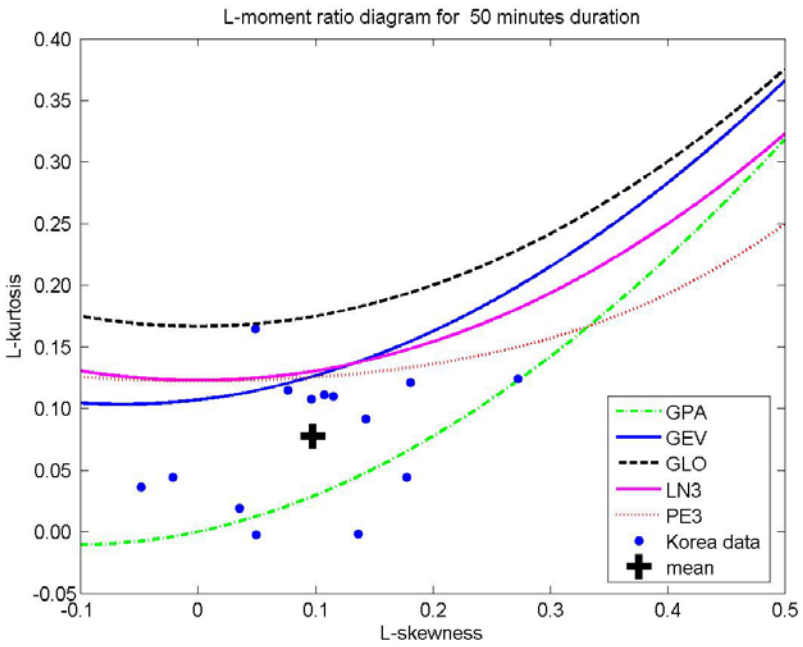

Figure B.5 L-moment ratio diagram for 50 minutes AMP in Korea

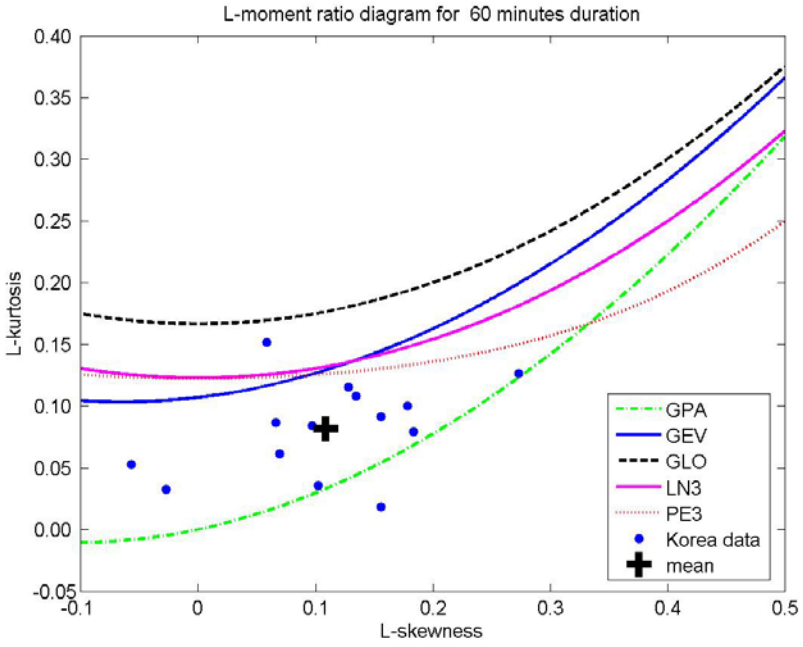

Figure B.6 L-moment ratio diagram for 60 minutes AMP in Korea

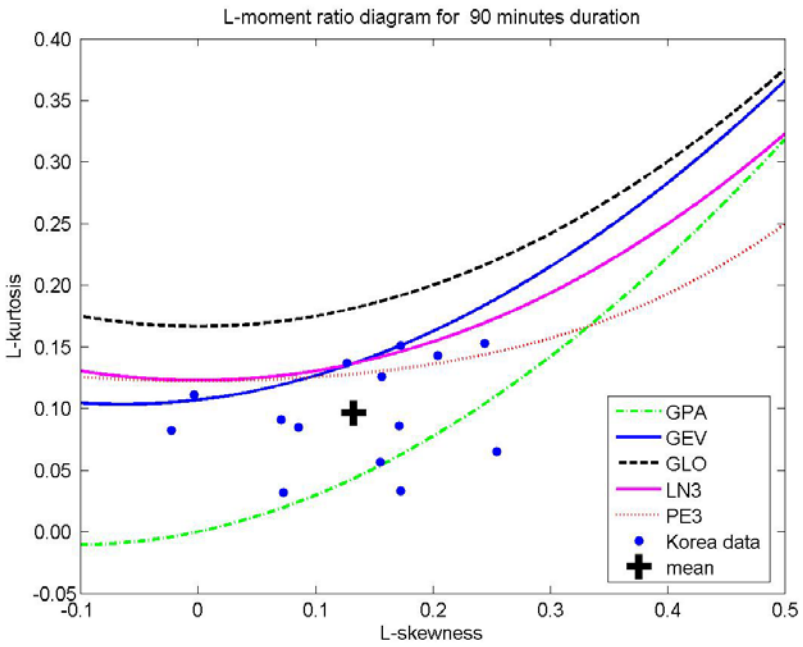

Figure B.7 L-moment ratio diagram for 90 minutes AMP in Korea

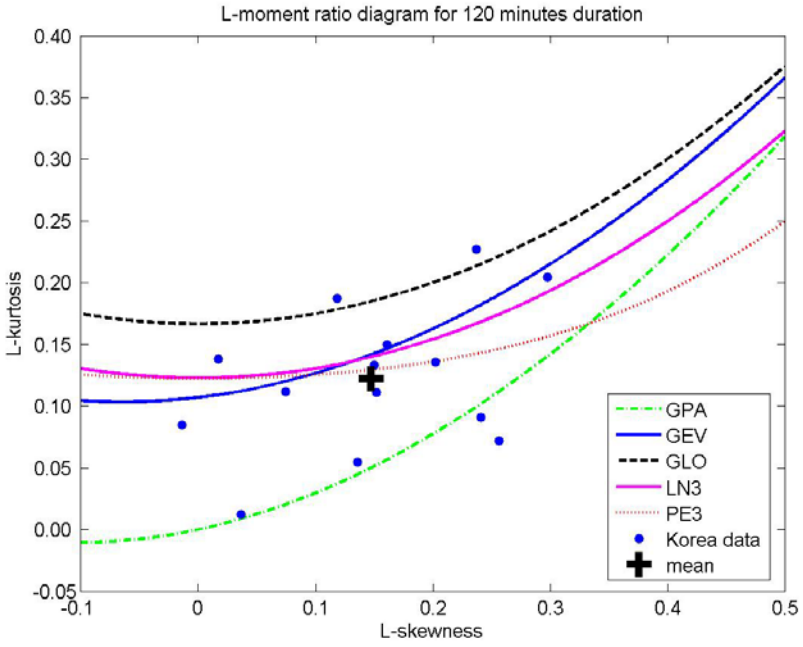

Figure B.8 L-moment ratio diagram for 120 minutes AMP in Korea

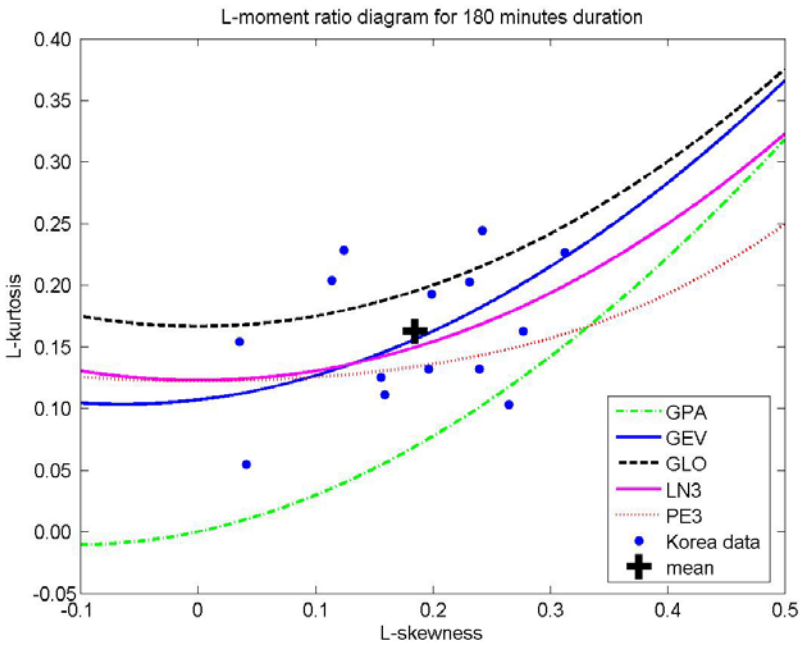

Figure B.9 L-moment ratio diagram for 180 minutes AMP in Korea

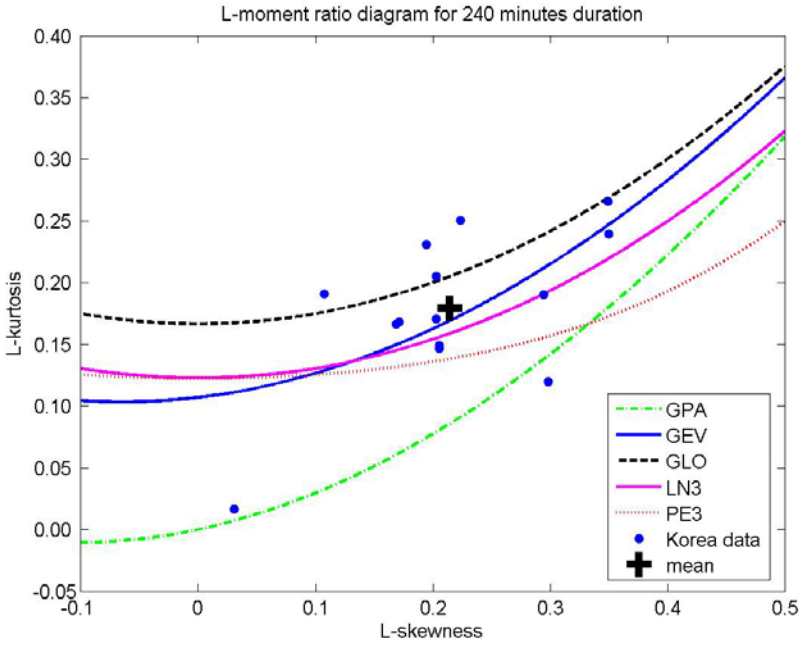

Figure B.10 L-moment ratio diagram for 240 minutes AMP in Korea

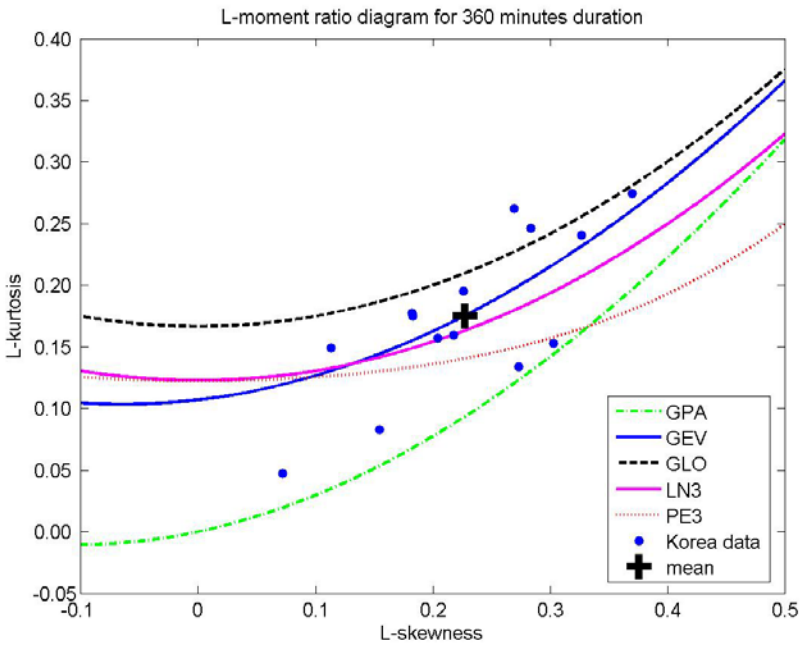

Figure B.11 L-moment ratio diagram for 360 minutes AMP in Korea

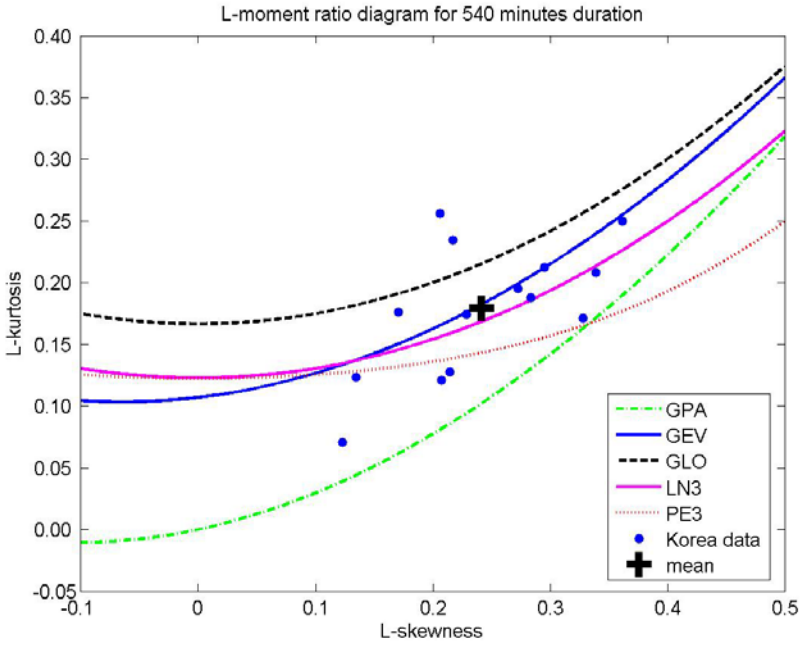

Figure B.12 L-moment ratio diagram for 540 minutes AMP in Korea

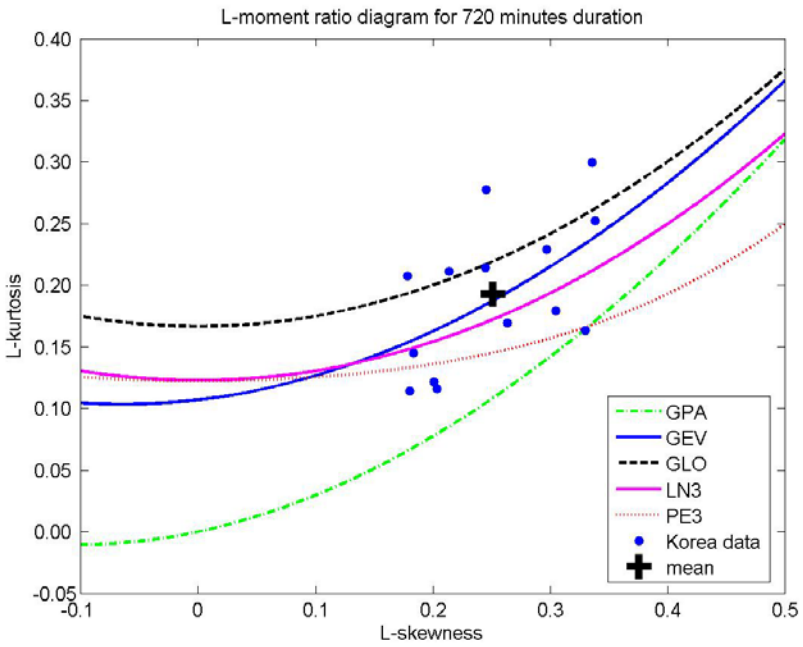

Figure B.13 L-moment ratio diagram for 720 minutes AMP in Korea

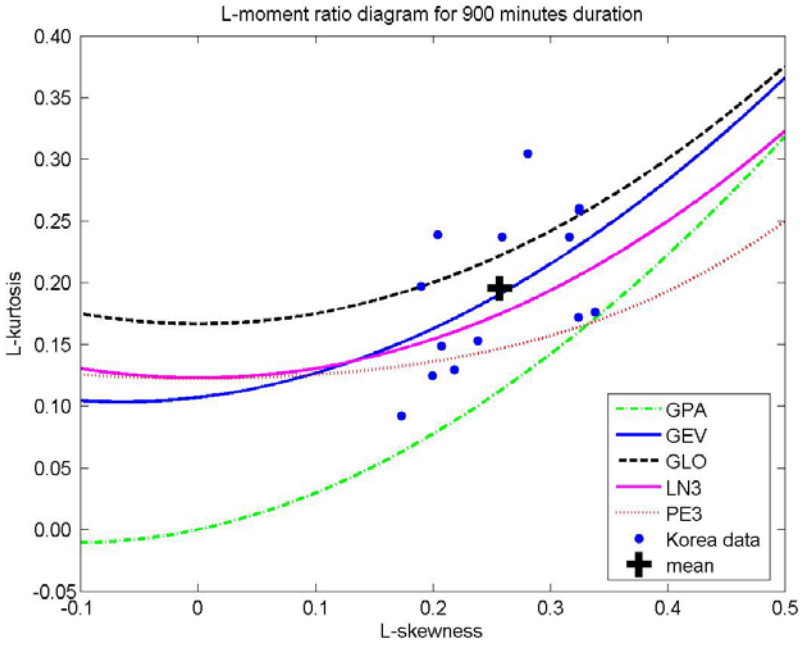

Figure B.14 L-moment ratio diagram for 900 minutes AMP in Korea

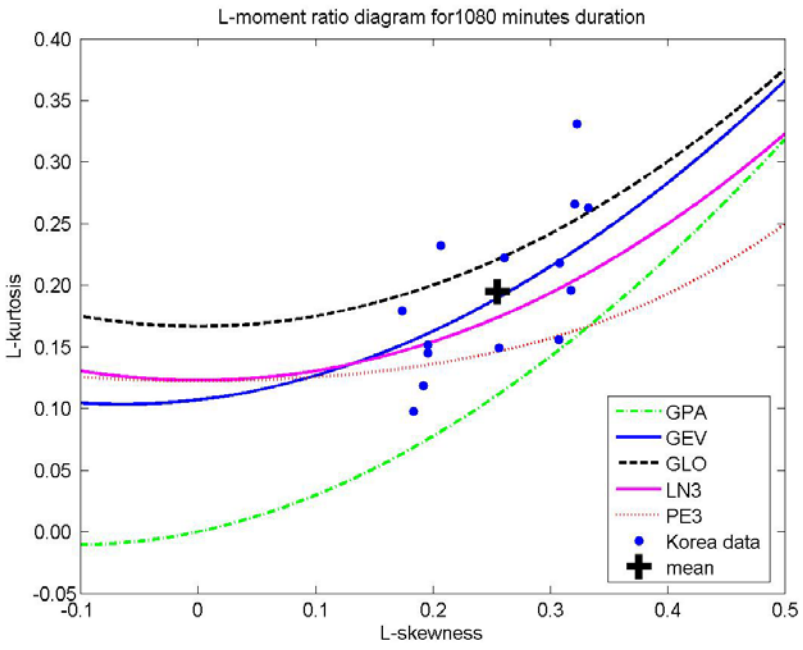

Figure B.15 L-moment ratio diagram for 1080 minutes AMP in Korea

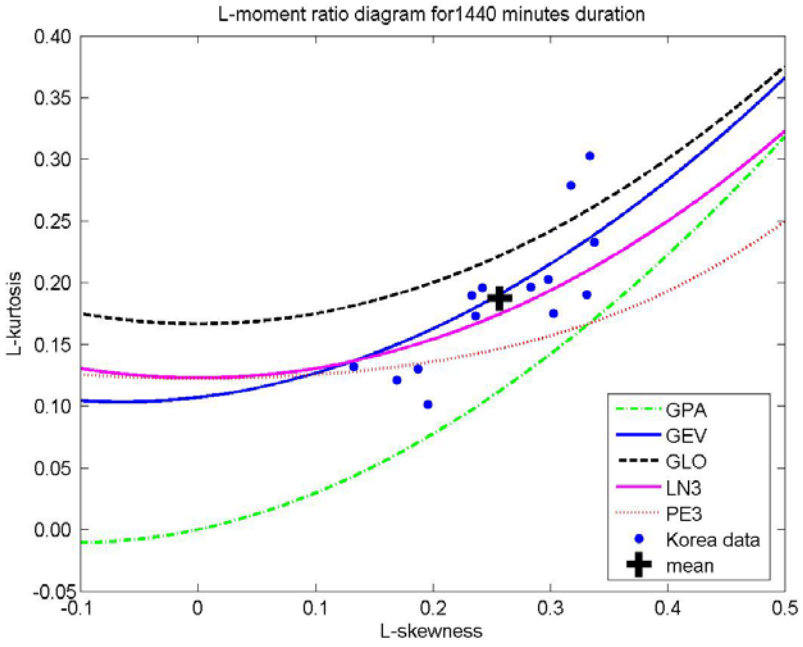

Figure B.16 L-moment ratio diagram for 1440 minutes AMP in Korea

Appendix C

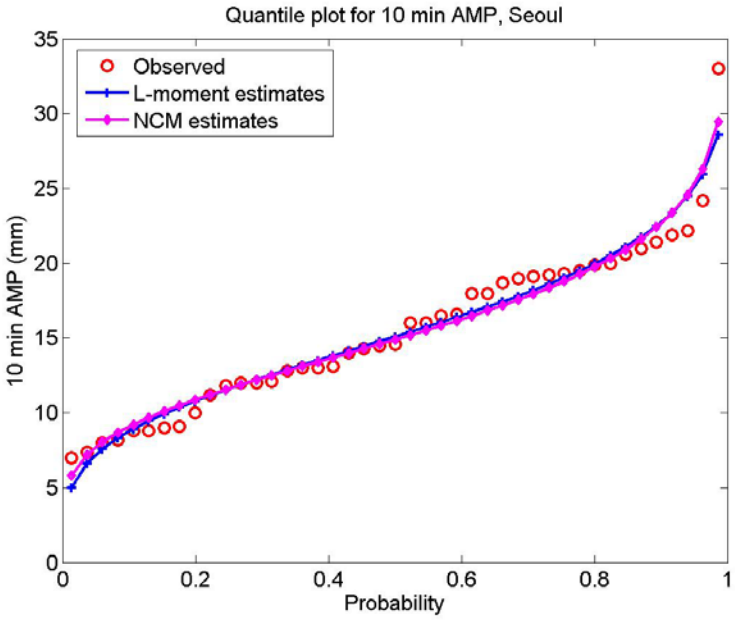

Figure C.1 Quantile plot of 10 minutes AMP, estimated by two parameter estimation methods and observed, at Seoul for 1957-1999 period.

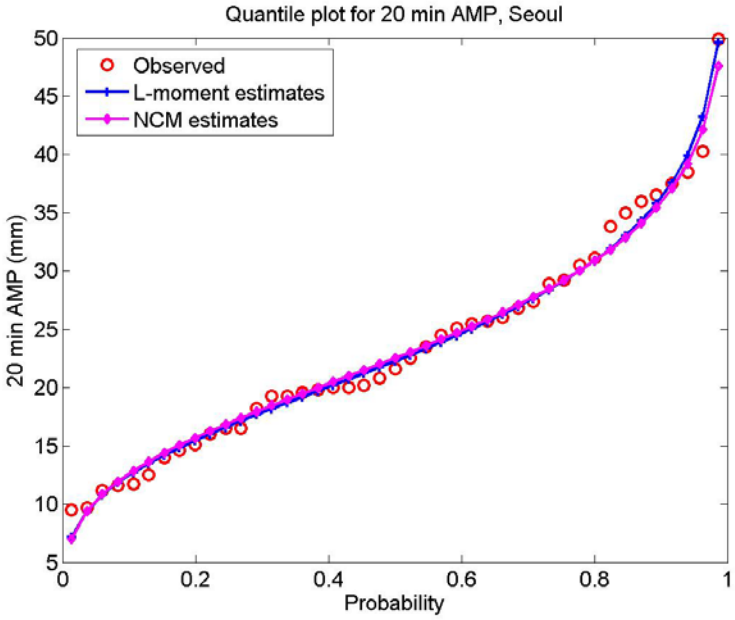

Figure C.2 Quantile plot of 20 minutes AMP, estimated by two parameter estimation methods and observed, at Seoul for 1957-1999 period.

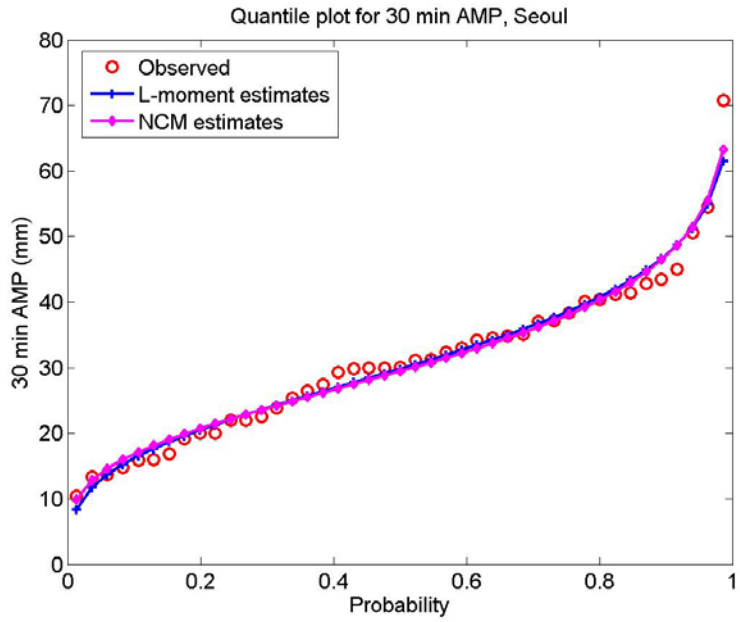

Figure C.3 Quantile plot of 30 minutes AMP, estimated by two parameter estimation methods and observed, at Seoul for 1957-1999 period.

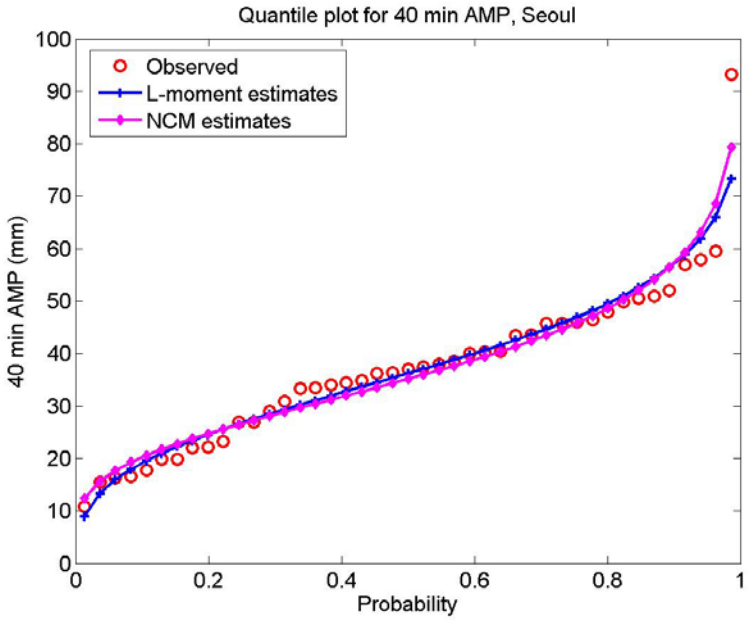

Figure C.4 Quantile plot of 40 minutes AMP, estimated by two parameter estimation methods and observed, at Seoul for 1957-1999 period.

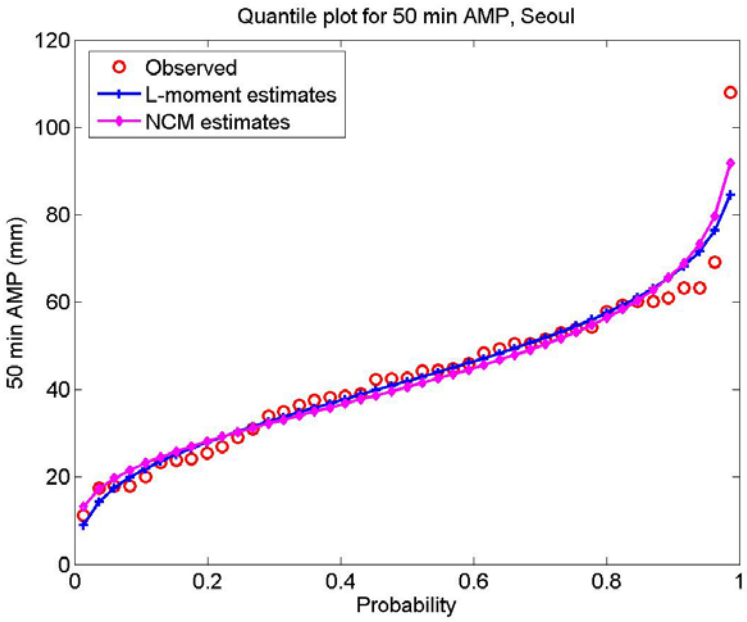

Figure C.5 ***Quantile plot of 50 minutes AMP, estimated by two parameter estimation methods and observed, at Seoul for 1957-1999 period.***

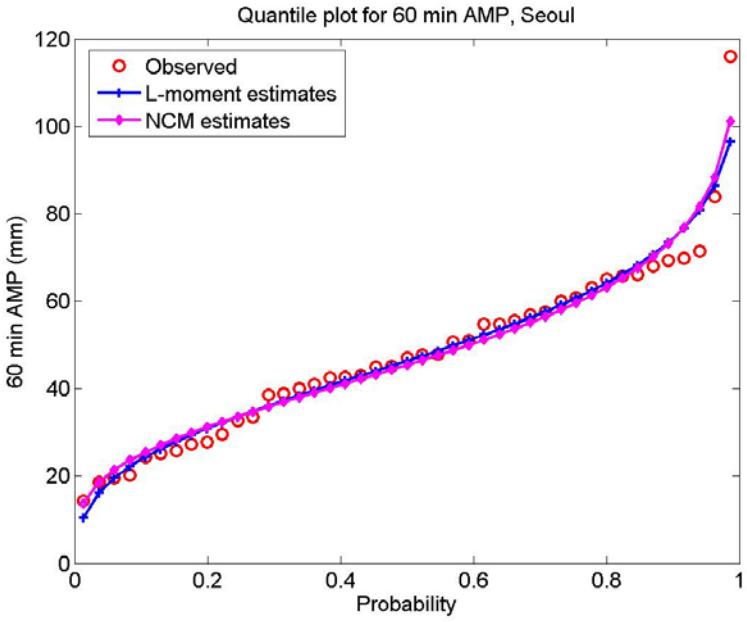

Figure C.6 ***Quantile plot of 60 minutes AMP, estimated by two parameter estimation methods and observed, at Seoul for 1957-1999 period.***

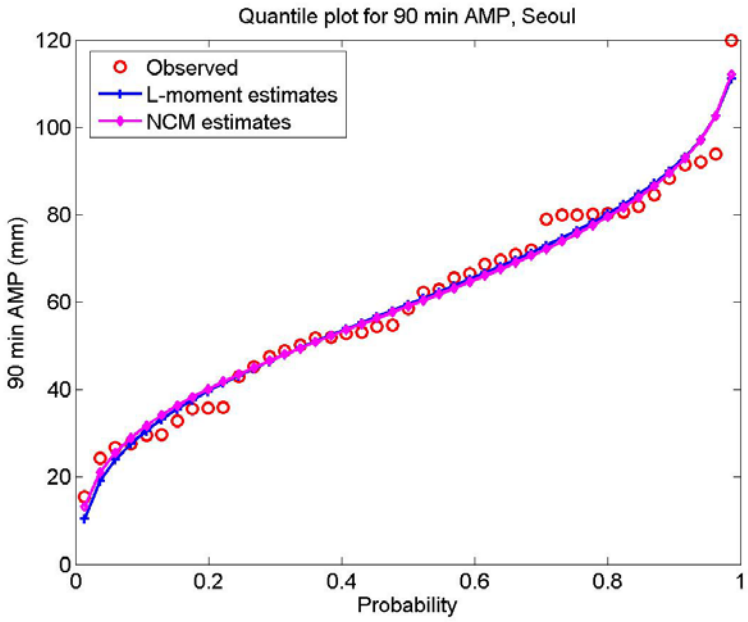

Figure C.7 Quantile plot of 90 minutes AMP, estimated by two parameter estimation methods and observed, at Seoul for 1957-1999 period.

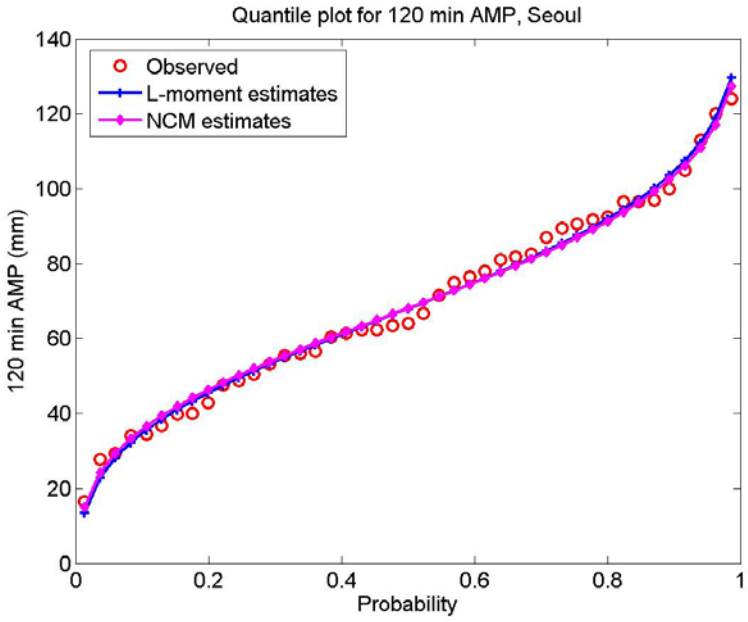

Figure C.8 Quantile plot of 120 minutes AMP, estimated by two parameter estimation methods and observed, at Seoul for 1957-1999 period.

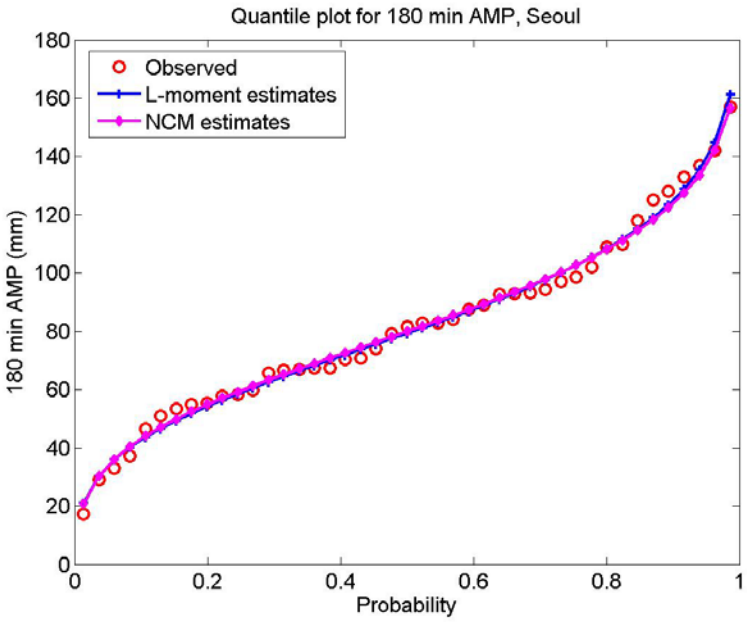

Figure C.9 Quantile plot of 180 minutes AMP, estimated by two parameter estimation methods and observed, at Seoul for 1957-1999 period.

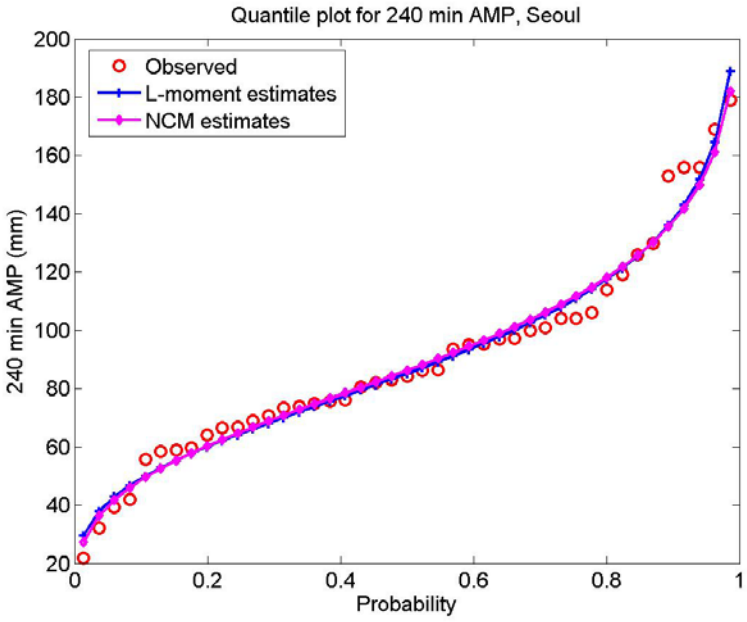

Figure C.10 Quantile plot of 240 minutes AMP, estimated by two parameter estimation methods and observed, at Seoul for 1957-1999 period.

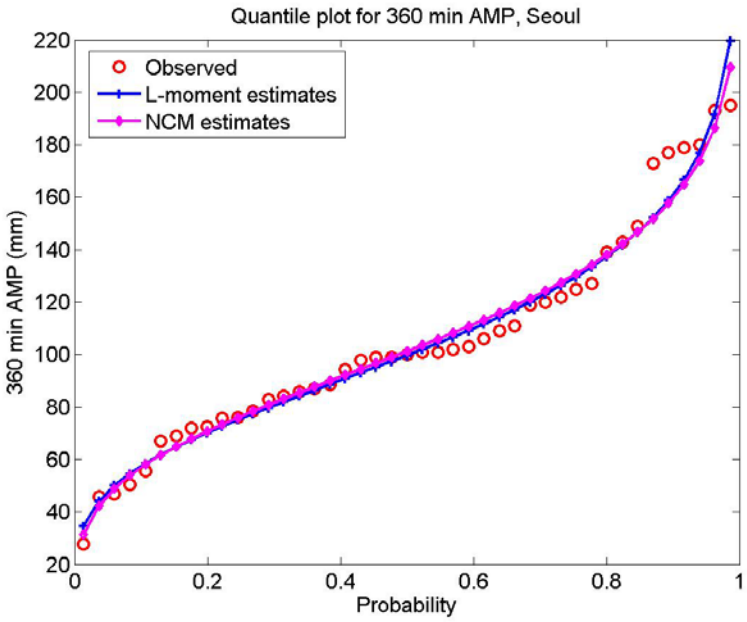

Figure C.11 Quantile plot of 360 minutes AMP, estimated by two parameter estimation methods and observed, at Seoul for 1957-1999 period.

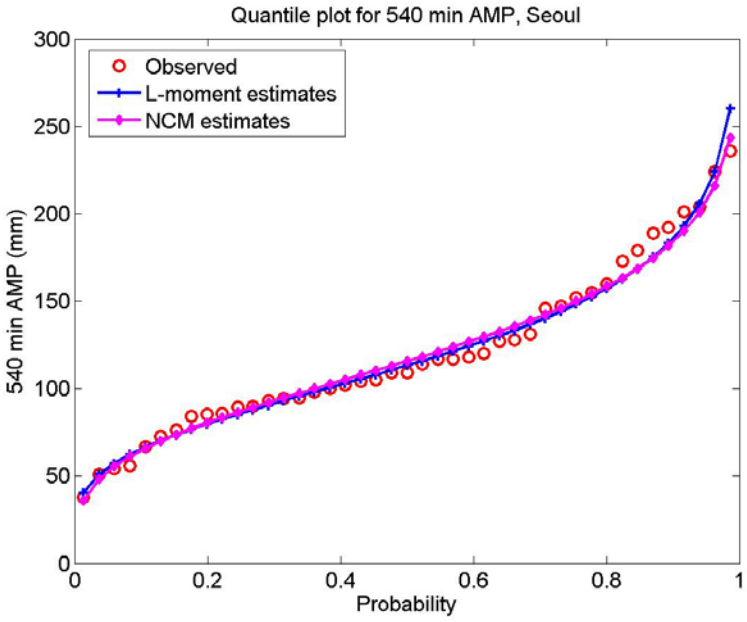

Figure C.12 Quantile plot of 540 minutes AMP, estimated by two parameter estimation methods and observed, at Seoul for 1957-1999 period.

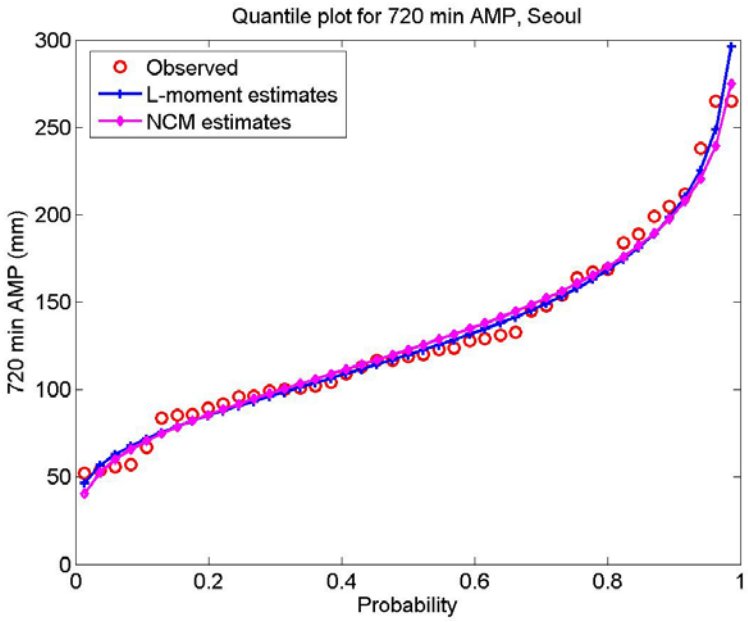

Figure C.13 Quantile plot of 720 minutes AMP, estimated by two parameter estimation methods and observed, at Seoul for 1957-1999 period.

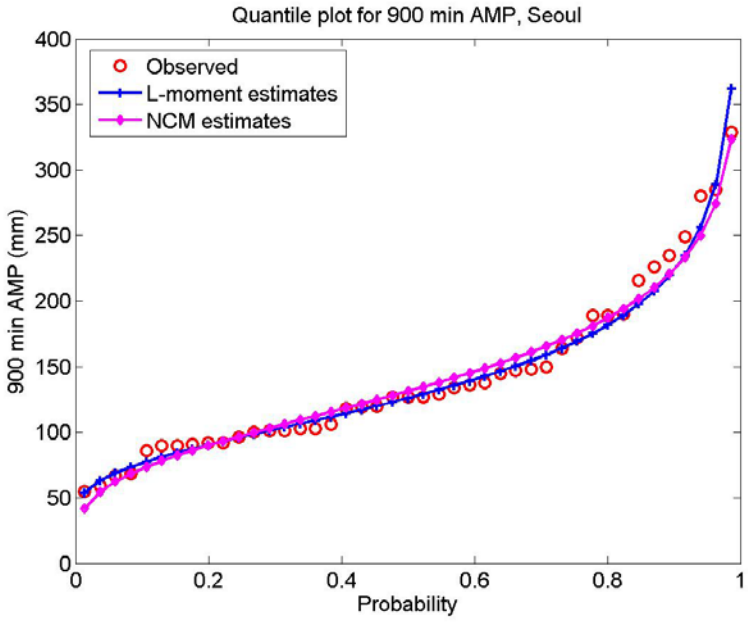

Figure C.14 Quantile plot of 900 minutes AMP, estimated by two parameter estimation methods and observed, at Seoul for 1957-1999 period.

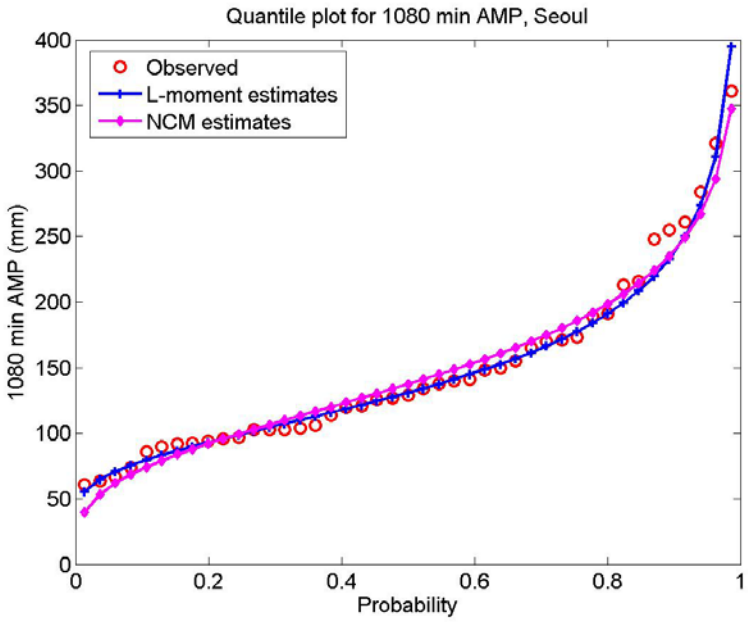

Figure C.15 Quantile plot of 1080 minutes AMP, estimated by two parameter estimation methods and observed, at Seoul for 1957-1999 period.

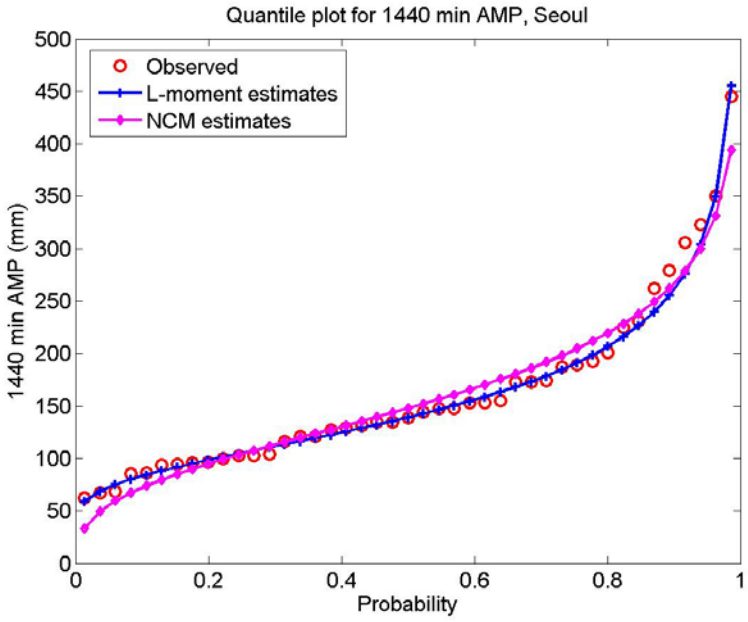

Figure C.16 Quantile plot of 1440 minutes AMP, estimated by two parameter estimation methods and observed, at Seoul for 1957-1999 period.

Appendix D

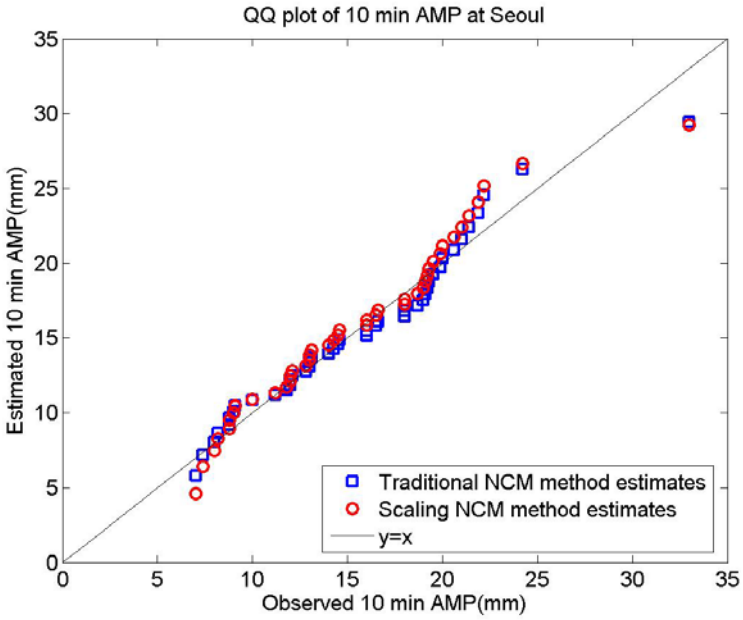

Figure D.1 Q-Q plot of estimated 10 min quantiles versus observed 10 min quantiles, Seoul station, 1957 – 1999 data period.

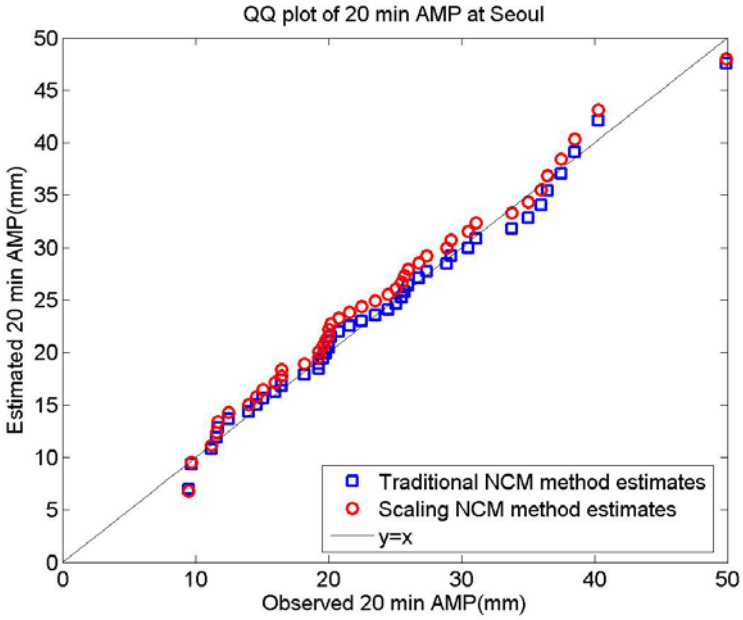

Figure D.2 Q-Q plot of estimated 20 min quantiles versus observed 20 min quantiles, Seoul station, 1957 – 1999 data period.

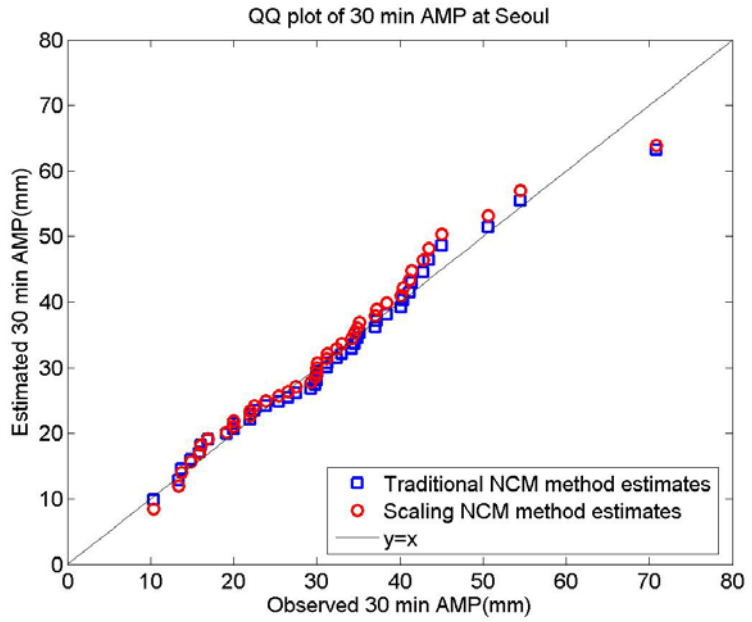

Figure D.3 ***Q-Q plot of estimated 30 min quantiles versus observed 30 min quantiles, Seoul station, 1957 – 1999 data period.***

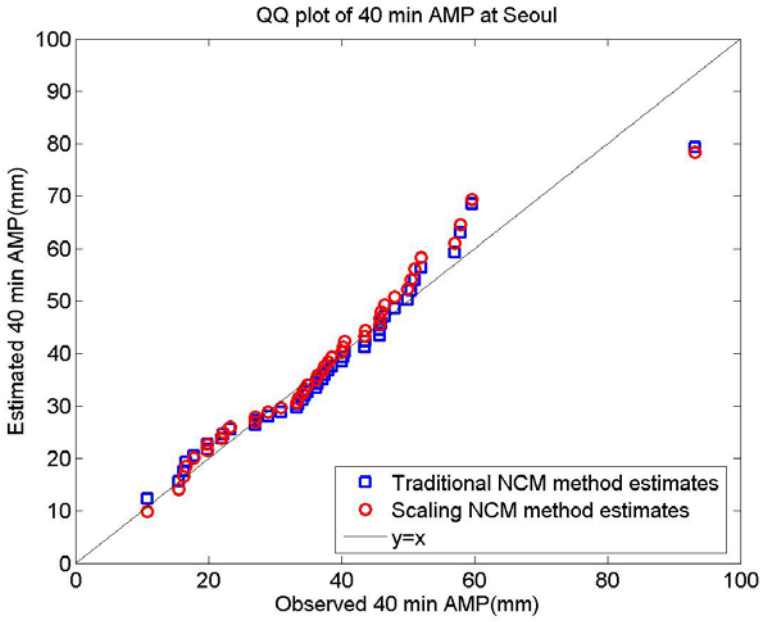

Figure D.4 ***Q-Q plot of estimated 40 min quantiles versus observed 40 min quantiles, Seoul station, 1957 – 1999 data period.***

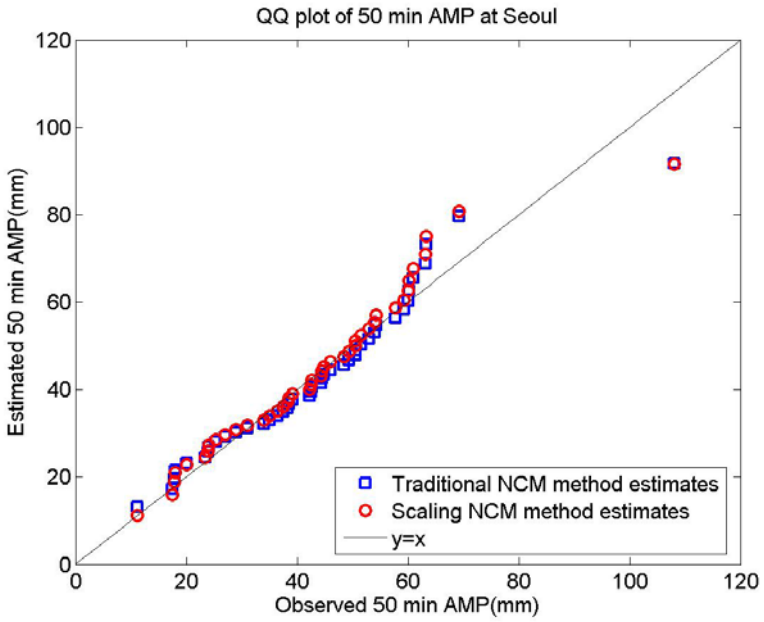

Figure D.5 Q-Q plot of estimated 50 min quantiles versus observed 50 min quantiles, Seoul station, 1957 – 1999 data period.

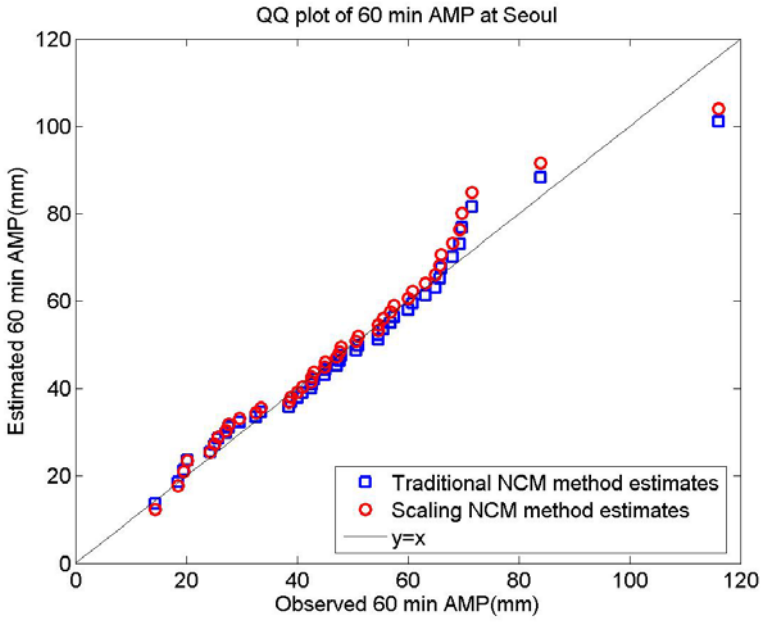

Figure D.6 Q-Q plot of estimated 60 min quantiles versus observed 60 min quantiles, Seoul station, 1957 – 1999 data period.

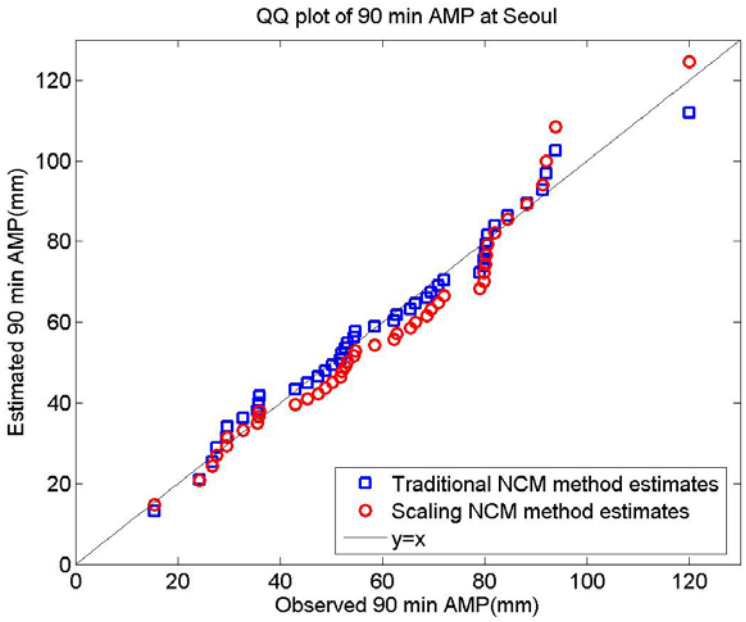

Figure D.7 Q-Q plot of estimated 90 min quantiles versus observed 90 min quantiles, Seoul station, 1957 – 1999 data period.

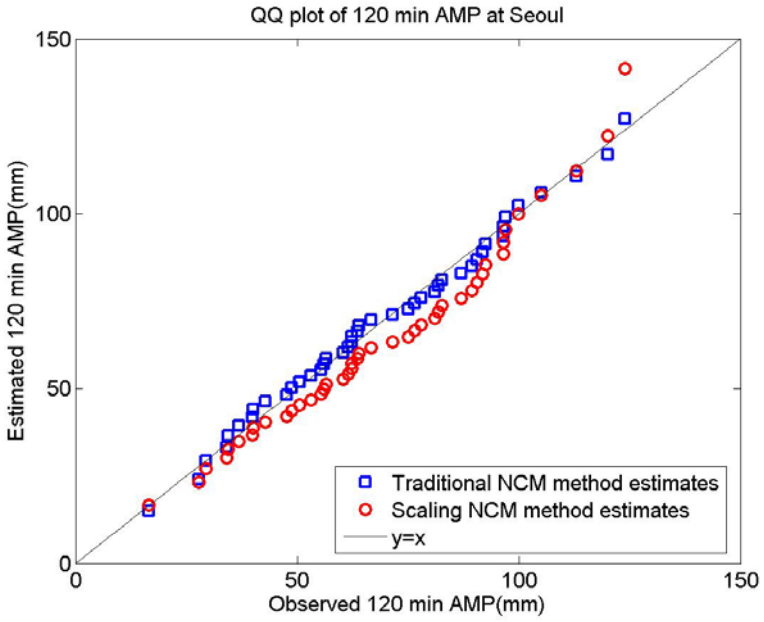

Figure D.8 Q-Q plot of estimated 120 min quantiles versus observed 120 min quantiles, Seoul station, 1957 – 1999 data period.

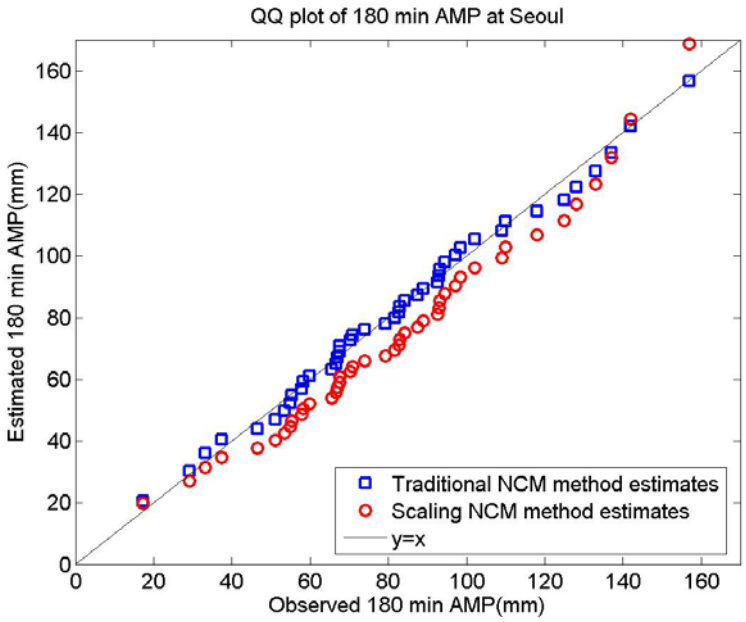

Figure D.9 Q-Q plot of estimated 180 min quantiles versus observed 180 min quantiles, Seoul station, 1957 – 1999 data period.

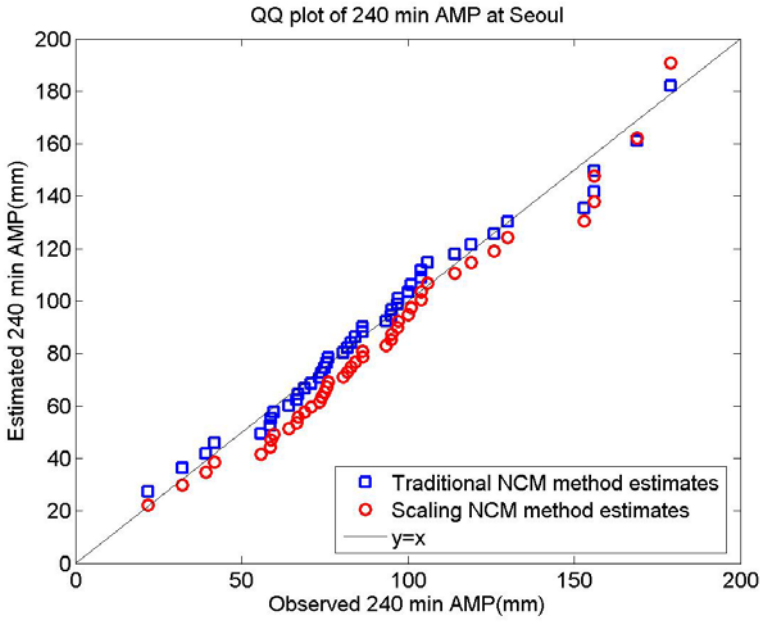

Figure D.10Q-Q plot of estimated 240 min quantiles versus observed 240 min quantiles, Seoul station, 1957 – 1999 data period.

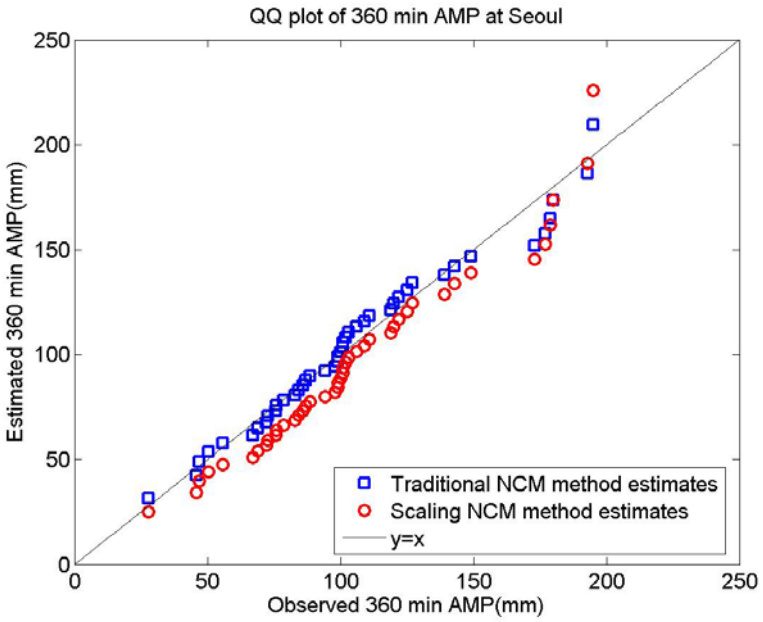

Figure D.11Q-Q plot of estimated 360 min quantiles versus observed 360 min quantiles, Seoul station, 1957 – 1999 data period.

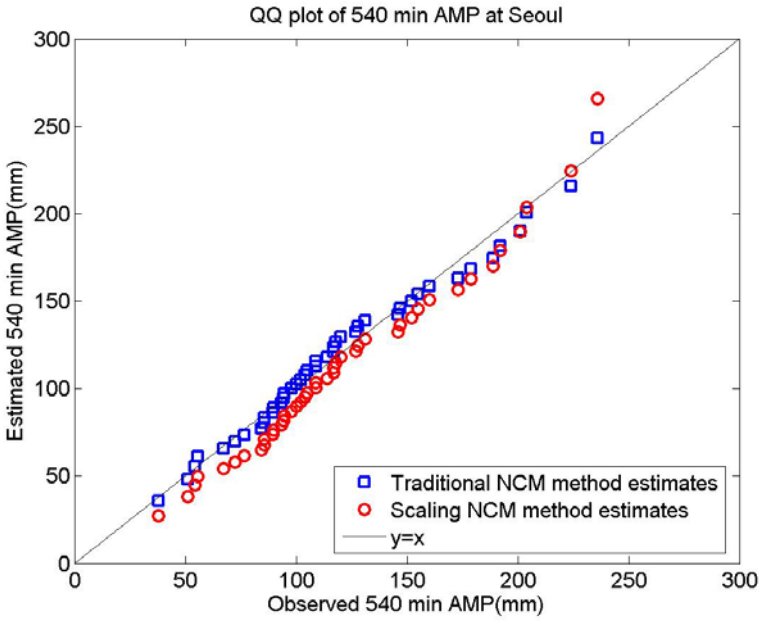

Figure D.12Q-Q plot of estimated 540 min quantiles versus observed 540 min quantiles, Seoul station, 1957 – 1999 data period.

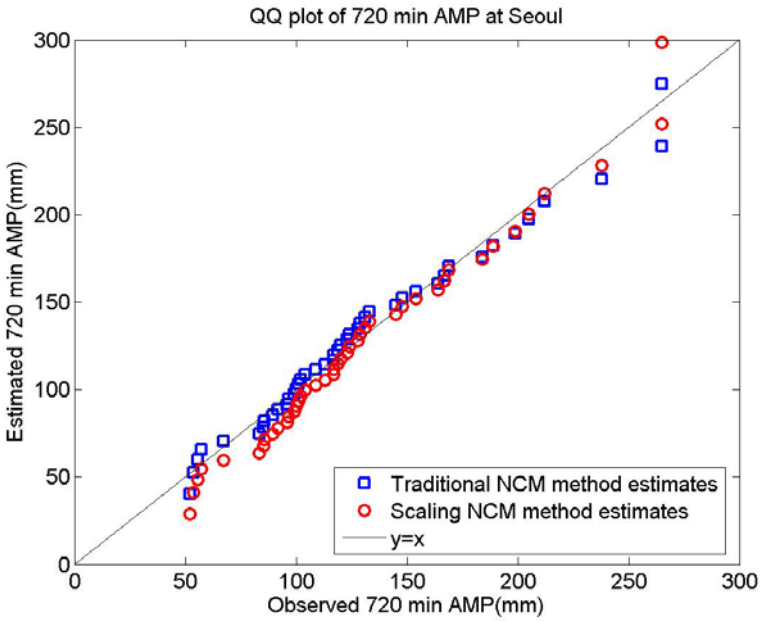

Figure D.13Q-Q plot of estimated 720 min quantiles versus observed 720 min quantiles, Seoul station, 1957 – 1999 data period.

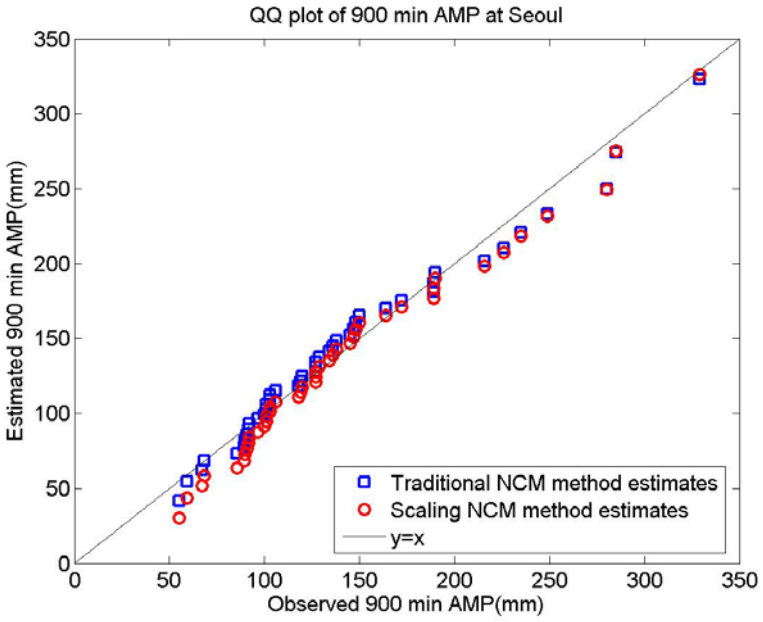

Figure D.14Q-Q plot of estimated 900 min quantiles versus observed 900 min quantiles, Seoul station, 1957 – 1999 data period.

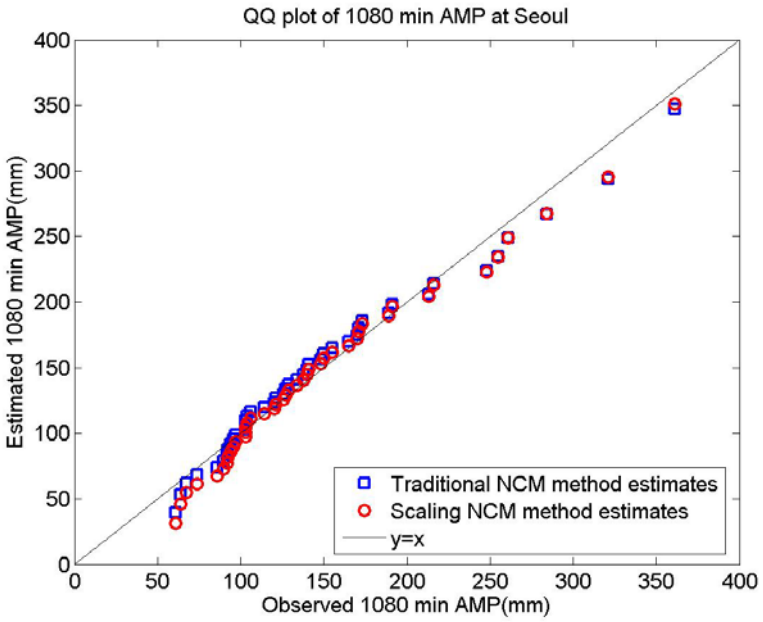

Figure D.15 Q-Q plot of estimated 1080 min quantiles versus observed 1080 min quantiles, Seoul station, 1957 – 1999 data period.

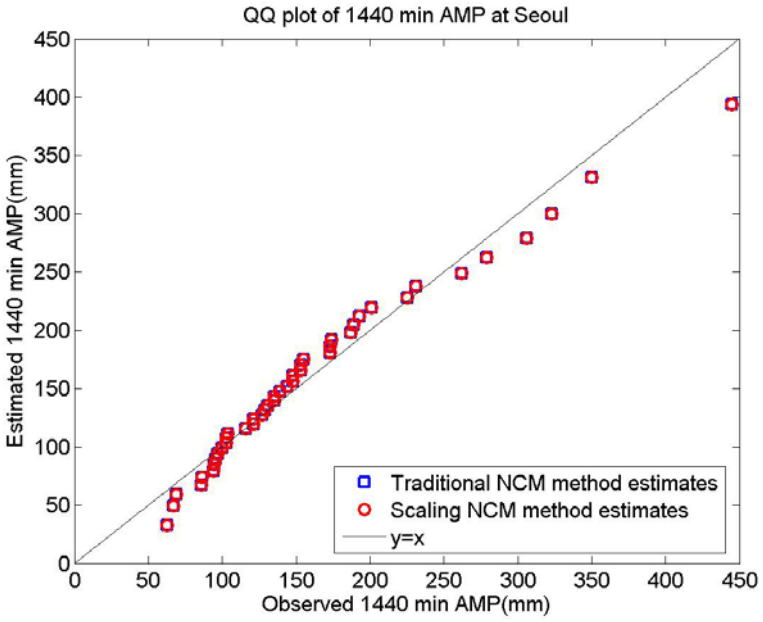

Figure D.16 Q-Q plot of estimated 1440 min quantiles versus observed 1440 min quantiles, Seoul station, 1957 – 1999 data period.

Appendix E

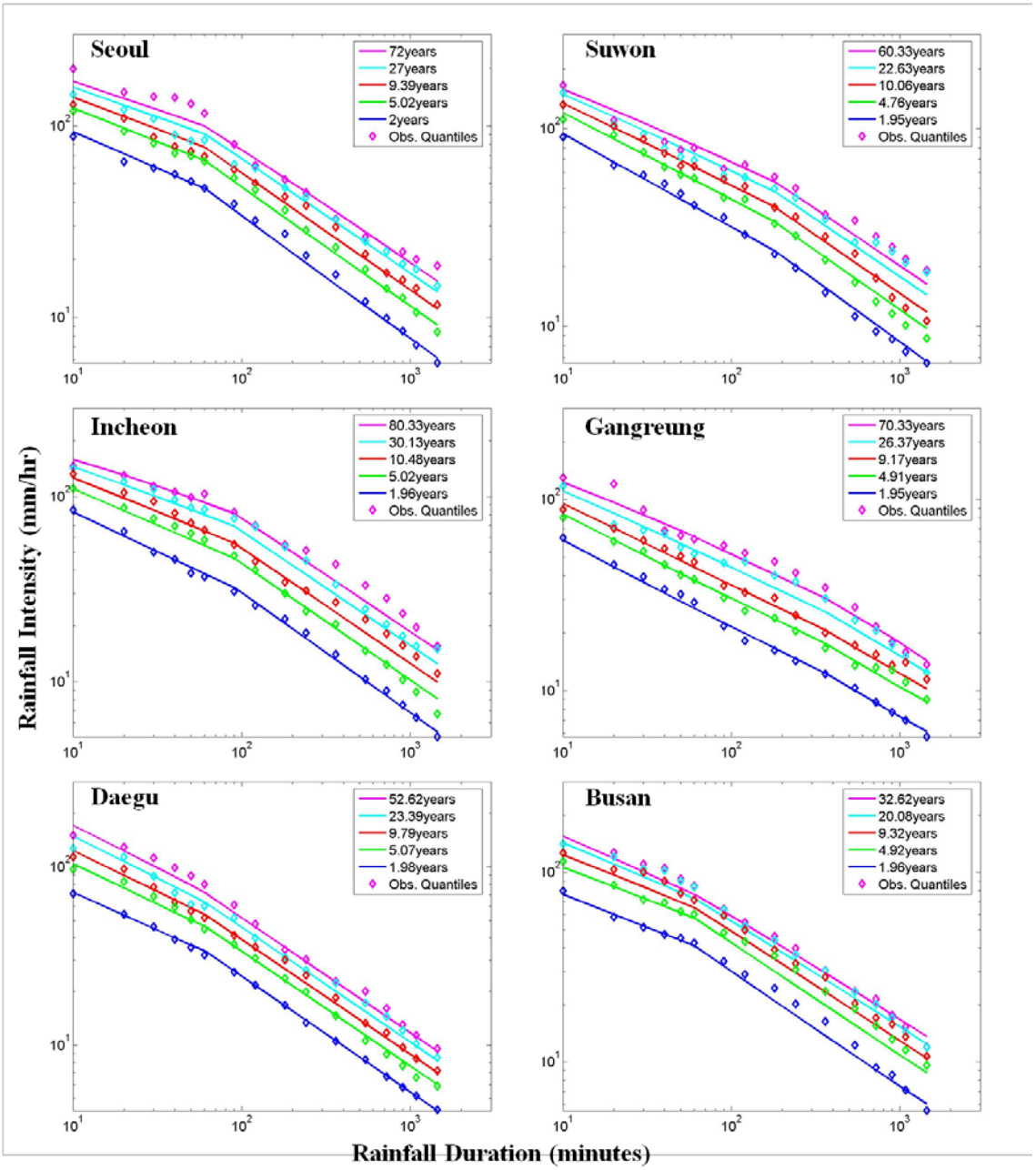
Seoul
72years
27years
9.39years
5.02years
2years
Obs. Quantiles
Suwon
60.33years
22.63years
10.06years
4.76years
1.95years
Obs. Quantiles
Incheon
80.33years
30.13years
10.48years
5.02years
1.96years
Obs. Quantiles
Gangreung
70.33years
26.37years
9.17years
4.91years
1.95years
Obs. Quantiles
Daegu
52.62years
23.39years
9.79years
5.07years
1.98years
Obs. Quantiles
Busan
32.62years
20.08years
9.32years
4.92years
1.96years
Obs. Quantiles
Rainfall Intensity (mm/hr)
Rainfall Duration (minutes)

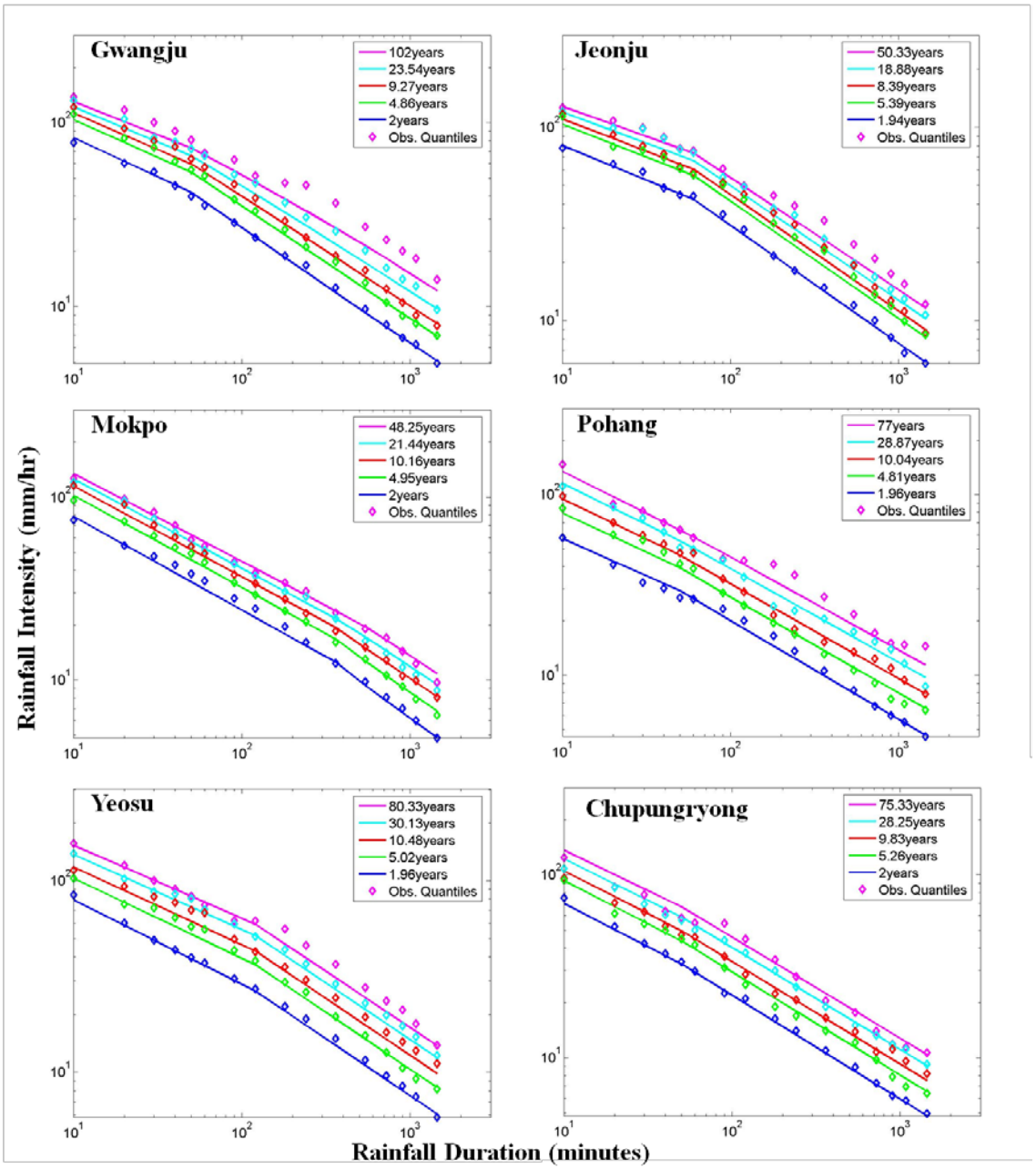

Figure E. 1 IDF curves drawn by scaling GEV method together with observed quantiles for stations in South Korea